

UNIVERSIDADE FEDERAL DO RIO GRANDE DO SUL
INSTITUTO DE CIÊNCIAS BÁSICAS DA SAÚDE
PROGRAMA DE PÓS-GRADUAÇÃO EM CIÊNCIAS BIOLÓGICAS:
FISIOLOGIA

Fernanda Staphenhorst França

**EFEITOS DE NANOPARTÍCULAS CONTENDO GALANTAMINA APÓS
LESÃO DA MEDULA ESPINAL EM RATOS**

Porto Alegre

2022

Fernanda Stapenhorst França

**EFEITOS DE NANOPARTÍCULAS CONTENDO GALANTAMINA APÓS
LESÃO DA MEDULA ESPINAL EM RATOS**

Tese apresentada ao Programa de Pós-Graduação em Ciências Biológicas: Fisiologia do Instituto de Ciências Básicas da Saúde da Universidade Federal do Rio Grande do Sul como requisito parcial para a obtenção do título de doutora em Fisiologia.

Orientadora: Profa. Dra. Patricia Pranke
Coorientadora: Profa. Dra. Laura Elena Sperling

Porto Alegre

2022

DEDICATÓRIA

Para meus pais, que sempre apoiaram minha carreira.

Para todos os futuros alunos do IPCT, que esta tese possa ajudar nos estudos da lesão da medula espinal.

AGRADECIMENTOS

Queria fazer meus agradecimentos tendo em vista toda a minha carreira acadêmica, considerando que o doutorado é o fim de uma longa jornada. Ainda tem muito caminho pela frente, mas é o fim de uma etapa que começou em 2010, na graduação.

Em primeiro lugar, gostaria de agradecer a minha família. Meus pais, que sempre me apoiaram nessa longa jornada acadêmica, desde a véspera do vestibular, quando eu chorei porque não queria fazer a prova, já que eu não ia passar (eu passei), durante a graduação, o mestrado, o limbo de crise existencial e durante todo o doutorado. Apoiaram quando eu quis fazer doutorado sanduíche, quando eu quis fazer doutorado pleno no exterior, quando eu decidi ficar, apoiaram as derrotas, as dificuldades, ficaram bravos e frustrados junto comigo durante todos os perrengues, fizeram questão de comemorar as pequenas vitórias e celebraram as grandes também. Por nunca terem me pressionado a ir pra outra carreira, por mais difícil e financeiramente ingrata que a carreira acadêmica seja. Por verem valor na minha jornada quando até eu tinha esquecido. Por me darem todos os recursos (financeiros, psicológicos, emocionais) que eu precisei durante essa caminhada.

À minha irmã, que da mesma forma sempre me apoiou, sempre fez de tudo pra eu alcançar o que eu queria, procurando oportunidades pra mim dentro e fora do Brasil, me incentivando a mandar os emails, a perguntar o que não era dito, racionalizando e pensando de forma prática os passos que eu precisava tomar para chegar em cada lugar, mesmo quando emocionalmente tudo parecia confuso. Por ser meu exemplo de estudante e de profissional, de desbravadora de oportunidades, de disciplina e de sempre fazer o que precisa ser feito para se chegar onde se quer. Por ter sempre comemorado comigo as vitórias, por trazer leveza e humor mesmo nos momentos difíceis, por me levar com ela nas aventuras dela. Ao Lourenço, que desde o começo desse caminho passou de melhor amigo pra família, que esteve junto comigo desde o vestibular até ao fim do doutorado, comemorou comigo cada passo e me consolou nas derrotas.

À toda a minha família, por sempre ter me apoiado nessa jornada e por sempre terem torcido por mim e valorizado o meu trabalho. Por todo apoio emocional nos momentos difíceis da família, que não foram poucos, mas sempre nos mantivemos unidos.

Aos que acompanharam o começo dessa trajetória mas que não estão mais aqui, à Dinda Cláudia e ao Vô Milton que sempre incentivaram o caminho da área da saúde, compartilharam recursos e, talvez o mais valioso, histórias de vida. À dinda Carina que também apoiou todos os passos, sempre acompanhando o meu caminho com muito amor, carinho e

alegria. À todos pelos momentos de alegria que me proporcionaram não só nesses últimos 12 anos, mas toda a minha vida. Imagino que vocês estariam orgulhosos de eu estar terminando essa etapa.

Ao Juliano e à Michele, meus amigos desde a graduação que de formas diferentes acabaram tendo uma jornada muito parecida com a minha. Por compartilharem comigo cada surto, cada crise existencial profissional, cada conquista, cada título. Ter vocês como referência de colegas profissionais me ajudou muito a não sair do meu caminho e sentir que eu tava fazendo a coisa certa.

Ao Artur, que foi um dos meus maiores apoiadores no último ano, que participou de perto dos surtos e das crises de fim de doutorado, que sempre fez questão de valorizar e me mostrar o valor do que eu estava fazendo, que apoiou meus projetos pro futuro e por sempre ter acreditado no meu potencial.

Especificamente dos últimos 4 anos, agradeço à Professora Patricia, pela confiança depositada em mim para tocar meu trabalho, por me dar liberdade nos meus experimentos e por apoiar meus projetos. À Laura, por tudo que ela me ensinou, tanto tecnicamente, profissionalmente e academicamente. Por todo apoio técnico e emocional durante esses 4 anos, por acreditar e confiar em mim, por todas as reuniões e conselhos.

Ao Marcelo, meu *lab buddy* durante todo esse tempo, pela amizade, conselhos, surtos, rolês, discussões acadêmicas e não acadêmicas, por me ajudar nos meus experimentos, pelas ideias de projeto, por ajudar na resolução de problemas (que não foram poucos), por me ensinar tanto e por aprender comigo. Ao João, da mesma forma pela amizade, pela parceria e pelas discussões científicas, pelas milhares de ideias novas e por me ajudar a pensar fora da caixa.

Ao Luiz, por ajudar a resolver todas as demandas administrativas, de compras e arrumando soluções para o laboratório, além de me ajudar nos experimentos e na produção das nanopartículas. Ao Cristian, por todo apoio técnico e emocional, por me ajudar e me ensinar tanto. A todos os ICs que passaram pelo lab, pela amizade, por me permitirem ter a experiência de orientação acadêmica e por confiarem em mim para orientar vocês, por toda ajuda técnica e apoio emocional do meu doutorado. A todos os demais colegas do IPCT, pelas discussões, pelo apoio e por toda ajuda.

À UFRGS, por ter me formado e me dado os recursos durante os últimos 12 anos. A todos os funcionários do ICBS e do CREAL, por não medirem esforços para auxiliar os alunos.

Ao CNPq, pela bolsa de doutorado.

A todos que participaram de alguma forma nesses últimos 12 anos, muito obrigada!

RESUMO

Distúrbios do sistema nervoso central apresentam dificuldades de tratamento devido à baixa capacidade regenerativa das células deste sistema. Dentre eles, a lesão da medula espinal (LME) é uma condição que leva a grandes impactos na vida do paciente acometido, como situações de paraplegia, e não há tratamentos eficazes até o presente momento. A galantamina é um fármaco utilizado na doença de Alzheimer. Estudo prévio realizado pelo grupo demonstrou a eficácia em promover melhora funcional em um modelo de LME em ratos. Entretanto, administrações sistêmicas de medicamentos produzem mais efeitos colaterais e levam a menor biodisponibilidade do fármaco no tecido-alvo. Assim, o objetivo deste trabalho foi produzir e avaliar o potencial terapêutico de nanopartículas contendo galantamina para LME. As partículas de poli(ácido lático-co-glicólico) (PLGA) e galantamina foram produzidas por *electrospraying* e caracterizadas por microscopia eletrônica de varredura e por espalhamento de luz dinâmico para avaliação do tamanho, potencial zeta e índice de poldispersão (Pdl). A liberação de galantamina das partículas foi avaliada por 35 dias através de cromatografia líquida de alta eficiência (HPLC). O potencial neuroprotetor das partículas foi avaliado *in vitro* em uma cultura de células PC12. *In vivo*, utilizou-se um modelo de contusão de LME em ratos e as formulações farmacêuticas foram aplicadas no local da lesão. Os animais foram separados em 5 grupos: Sham, lesão, galantamina, partículas de PLGA e partículas de PLGA contendo galantamina (PG). Os efeitos desse tratamento foram avaliados após 3 e 42 dias, quando os parâmetros oxidativos e inflamatórios das medulas espinais foram avaliados, assim como os parâmetros histológicos, após 42 dias. Ainda, a locomoção dos animais foi avaliada semanalmente, por 6 semanas. As partículas poliméricas apresentaram morfologia bicôncava e tamanho adequado, assim como potencial zeta e Pdl também adequados para administração local. A galantamina apresentou uma liberação no perfil de *burst*, mas manteve uma liberação controlada ao longo de 35 dias. *In vitro*, apenas o tratamento com galantamina livre reduziu a perda de viabilidade das células expostas a peróxido de hidrogênio e nenhuma das formulações farmacêuticas promoveu a redução da produção de espécies reativas de oxigênio (EROs) após a exposição. Por outro lado, em estudo *in vivo*, o único grupo que apresentou melhoras significativas na função motora após 42 dias foi o grupo tratado com PG. Três dias após a lesão, a administração de galantamina diminuiu os níveis de peroxidação lipídica, ao passo que PG diminuiu os níveis de EROs e IL-1 β , além dos níveis de peroxidação lipídica. Além disso, ao analisar os efeitos dos tratamentos em 42 dias após a lesão, o grupo no qual administrou-se apenas a galantamina apresentou diminuição dos níveis de EROs, enquanto o grupo PG diminuiu tanto EROs quanto IL-1 β . Assim, o tratamento com PG demonstrou melhoras inflamatórias e oxidativas, bem como melhora funcional após LME.

Palavras-chave: Lesão da medula espinal; galantamina; nanopartículas

ABSTRACT

Central nervous system disorders are particularly difficult to treat due to the limited regenerative capacity of the cells from this system. Among them, spinal cord injury (SCI) is a condition that provokes great impact on the patient's life, such as paraplegy, and currently there are no effective treatments for this disorder. Galantamine is a drug used for Alzheimer's disease. A previous study from the group demonstrated its efficacy in promoting functional improvements in a rat model of SCI. However, systemic drug administration can cause side effects and lead to decreased drug bioavailability at the target tissue. Hence, the aim of this study has been to produce and evaluate the therapeutic potential of galantamine nanoparticles for SCI. Poly(lactic acid-co-glycolic acid) (PLGA) and galantamine particles were produced using electrospraying and characterized by scanning electron microscopy and dynamic light scattering for assessment of size, zeta potential and polydispersity index (PDI). Galantamine release from the particles was evaluated for 35 days using High Performance Liquid Chromatography (HPLC). The particles' neuroprotective potential was assessed *in vitro* in PC12 cell culture. A contusion model of SCI in rats was used *in vivo*, and the pharmaceutical formulations were applied at the lesion site. The animals were divided into 5 groups: sham, injury, galantamine, PLGA particles and PLGA particles containing galantamine (PG). The treatment effects were evaluated after 3 and 42 days, when oxidative and inflammatory parameters were assessed, as well as histological parameters after 42 days. In addition, the animals' locomotion was evaluated weekly for 6 weeks. The particles presented a biconcave shape and adequate size, as well as adequate zeta potential and PDI for local administration. Galantamine was released in a burst profile, but maintained a controlled release for 35 days. *In vitro*, only galantamine reduced the viability loss in the cells exposed to hydrogen peroxide, and no pharmaceutical formulation reduced reactive oxygen species (ROS) production after the exposure. *In vivo*, on the other hand, the only group that presented significant improvements in motor function was in the PG treatment. Three days after the injury, the administration of galantamine resulted in a decrease in lipid peroxidation levels, whereas the use of PG improved levels of reactive oxygen species (ROS) and IL-1 β , in addition to lipid peroxidation levels. Furthermore, when analyzing the treatment effects 42 days after the injury, galantamine treatment was able to reduce ROS, while PG reduced both ROS and IL-1 β . Therefore, PG treatment showed not only inflammatory and oxidant improvements, but also significant functional recovery after SCI.

Key-words: Spinal cord injury; galantamine; nanoparticles

SUMÁRIO

| | |
|---|-----------|
| 1. REVISÃO BIBLIOGRÁFICA | 8 |
| 1.1. ANATOMIA E FISILOGIA DA MEDULA ESPINAL | 8 |
| 1.1.1. Substância cinzenta | 10 |
| 1.1.2. Substância branca | 12 |
| 1.1.3. Células gliais na medula espinal | 14 |
| 1.2. LESÃO DA MEDULA ESPINAL | 15 |
| 1.2.1. Inflamação | 16 |
| 1.2.2. Estresse oxidativo | 19 |
| 1.2.3. Cicatriz glial | 20 |
| 1.3. GALANTAMINA | 21 |
| 1.4. NANOTECNOLOGIA | 24 |
| 1.5. ELETROPULVERIZAÇÃO | 26 |
| 1.6. NANOTECNOLOGIA E LESÃO DA MEDULA ESPINAL | 27 |
| 2. HIPÓTESE | 28 |
| 3. JUSTIFICATIVA | 28 |
| 4. OBJETIVOS | 28 |
| 5. RESULTADOS | 30 |
| Artigo 1. | 30 |
| Artigo 2. | 50 |
| 6. DISCUSSÃO | 64 |
| 6.1. CARACTERIZAÇÃO DAS NANOPARTÍCULAS | 64 |
| 6.2. EFEITOS IN VITRO | 65 |
| 6.3. EFEITOS IN VIVO | 66 |
| 6.3.1. Recuperação funcional | 66 |
| 6.3.2. Estresse oxidativo | 66 |
| 6.3.3. Inflamação | 67 |
| 7. CONCLUSÕES | 68 |
| 8. PERSPECTIVAS | 68 |
| 9. REFERÊNCIAS | 69 |
| ANEXO I - Artigo de revisão | 75 |

1. REVISÃO BIBLIOGRÁFICA

1.1. ANATOMIA E FISIOLOGIA DA MEDULA ESPINAL

A medula espinal constitui uma importante parte do sistema nervoso central (SNC), e localiza-se no canal espinal da coluna vertebral. A estrutura da medula pode ser observada na Figura 1. Assim como o encéfalo, a medula espinal é envolta por três membranas protetoras, as meninges: a dura mãe, mais externa; a aracnóide, que é intermediária; e a pia-mãter, que é a membrana mais interna, fazendo contato com a medula espinal. Entre a pia-mãter e a aracnóide há o espaço subaracnóide, por onde passam os vasos sanguíneos que irrigam a medula e o qual é preenchido por fluido cerebroespinal (FCE). Funcionalmente, a medula espinal pode ser dividida em 31 segmentos e cada um emite um par de nervos espinais. Assim, há 8 segmentos cervicais, 12 segmentos torácicos, 5 segmentos lombares, 5 segmentos sacrais e 1 segmento coccígeo. Como a medula espinal é mais curta do que o canal vertebral, terminando no nível de L1/2 em adultos, e considerando que cada nervo espinal precisa sair em um forame intervertebral, parte das raízes dos nervos formam a cauda equina no canal vertebral, abaixo de onde termina a medula espinal. Ainda, a porção terminal da medula espinal é chamada de cone medular. Os nervos espinais são formados pela união da raiz dorsal com a raiz ventral, que se unem antes da saída do nervo espinal pelos forames intervertebrais. Ainda, existem duas regiões medulares em que há um alargamento da medula: um entre as vértebras C4 e T1, chamado de alargamento cervical, e um entre as vértebras L2 e S3, chamado de alargamento lombar. O alargamento cervical forma o plexo braquial, o qual inerva os membros superiores, ao passo que o alargamento lombar corresponde ao plexo lombar, que inerva os membros inferiores (BRODAL, 2010; CHANDAR; FREEMAN, 2014).

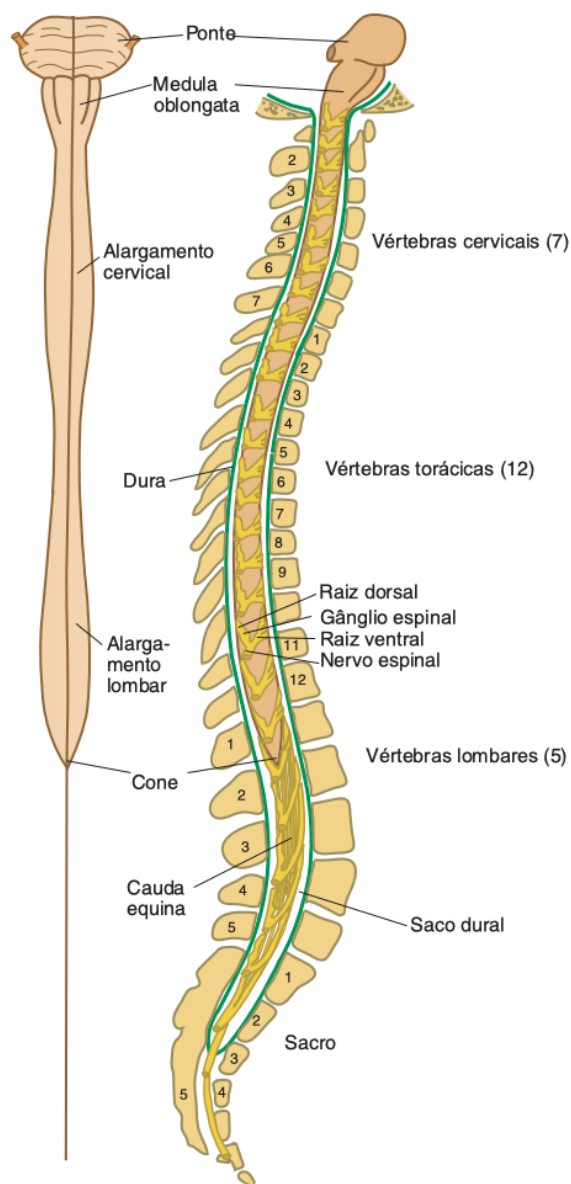


Figura 1 - Estrutura da medula espinhal A medula espinhal pode ser dividida em 31 segmentos, sendo 7 segmentos cervicais, 12 torácicos, 5 lombares, 5 sacrais e 1 coccígeo. Observa-se também na região terminal da medula a presença do cone espinhal e da cauda equina. Fonte: Adaptado de Brodal (2010, p. 75).

Internamente, a medula espinhal é organizada em substância branca e substância cinzenta. Ao contrário do cérebro, na medula espinhal a substância branca envolve externamente a substância cinzenta. Assim, em um corte transversal, observa-se no centro da medula uma

região em formato de H, correspondente à substância cinzenta (CHAMBERS; HUANG; MATTHEWS, 2014).

1.1.1. Substância cinzenta

As diferentes regiões desta forma de H são chamadas de cornos ventrais e dorsais. A substância cinzenta é composta pelo corpo celular de todos os neurônios da medula espinal, que podem ser:

- Motoneurônios, ou neurônios motores;
- neurônios pré-ganglionares autonômicos;
- interneurônios;
- neurônios de projeção.

Os neurônios motores podem ser subdivididos em motoneurônios alfa, que inervam fibras musculares extrafusais, produzindo força e gerando movimento, e motoneurônios gama, que inervam fibras musculares intrafusais, estando envolvidos na propriocepção. Os corpos celulares dessas células localizam-se nos cornos ventrais da substância cinzenta, e seus axônios deixam a medula espinal através das raízes ventrais. A atividade dos motoneurônios alfa, também chamados de neurônios motores inferiores, é modulada pelos interneurônios e por neurônios motores superiores, os quais se originam no córtex motor cerebral (CHANDAR; FREEMAN, 2014).

Os neurônios pré-ganglionares autonômicos podem ser simpáticos ou parassimpáticos. No caso dos neurônios pré-ganglionares simpáticos, seus corpos celulares localizam-se nos cornos laterais da substância cinzenta, entre os segmentos T1 e L2, projetando-se para os neurônios pós-ganglionares localizados nos gânglios simpáticos adjacentes à medula espinal. Já os corpos celulares dos neurônios pré-ganglionares parassimpáticos localizam-se nos cornos laterais entre os segmentos S2 e S4, tendo suas projeções para os gânglios parassimpáticos nas vísceras. Os axônios de ambos tipos de neurônios pré-ganglionares deixam a medula espinal pelas raízes ventrais (CHANDAR; FREEMAN, 2014).

Os neurônios da substância cinzenta são organizados em diferentes regiões laminares de acordo com a densidade e tamanho neuronal, que podem ser observadas na Figura 2. Essas regiões foram identificadas e descritas por Rexed, que definiu 6 lâminas (I - VI) no corno dorsal, 3 lâminas laterais e ventrais (VII - IX) e 1 lâmina ao redor do canal central (X) (REXED, 1952).

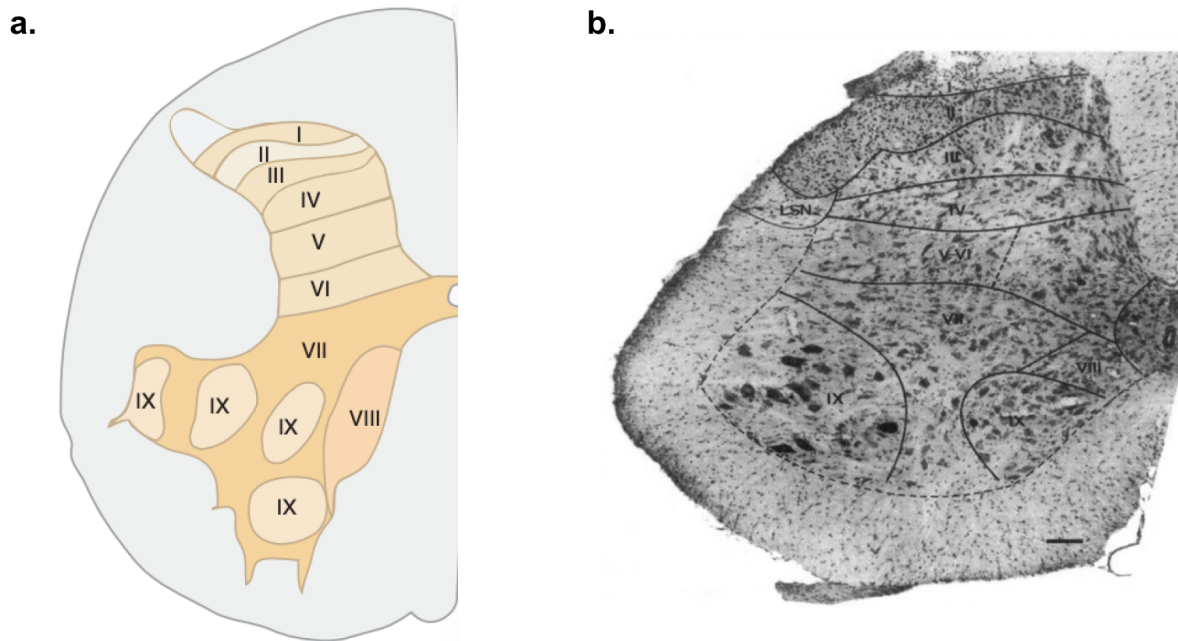


Figura 2 - Lâminas da substância cinzenta Desenho esquemático das lâminas da substância cinzenta; b. Delimitação histológica. Fonte: Adaptado de Brodal (2010, p.79) e Nogradi (2006, p. 3).

A lâmina I apresenta uma baixa densidade neuronal e é composta por neurônios de tamanhos variados que recebem informação de fibras aferentes nociceptoras $A\delta$. Na lâmina II, há uma alta densidade neuronal, consistindo de pequenos neurônios, os quais recebem informações de fibras aferentes não mielinizadas do tipo C relativo a estímulos nocivos e de temperatura. As lâminas III e IV formam o núcleo próprio e caracterizam-se por uma baixa densidade neuronal e neurônios de tamanhos intermediários. Essas células recebem informações de aferentes mielinizados de mecanorreceptores da pele relativo ao toque, à temperatura e a estímulo nocivo. As lâminas V e VI apresentam neurônios triangulares e fusiformes, e recebem informações de axônios sensoriais do fuso muscular, órgão tendinoso de Golgi e articulações, bem como de fibras sensíveis a estímulos nocivos e temperatura. Ainda, os interneurônios dessas regiões fazem sinapses com neurônios motores superiores de vias descendentes (CHANDAR; FREEMAN, 2014; NÓGRÁDI, 2006).

Nos cornos laterais e ventrais, a organização das lâminas é menos delimitada. De forma geral, o corno ventral está relacionado com eferentes que fazem o controle do movimento, ao passo que o corno lateral contém os neurônios autonômicos. Assim, a lâmina VII, que se encontra no corno lateral, é composta, nas regiões entre T1-L2 e S2-S4, neurônios pré-ganglionares simpáticos e parassimpáticos, respectivamente. Já na parte medial da lâmina VII, entre T1-L2, há um grupo de neurônios chamado de núcleo de Clarke, os quais recebem informações de aferentes proprioceptivos, e seus axônios formam o trato espinocerebelar. Na região medial da lâmina VII também há o núcleo intermediário, formado por interneurônios que recebem informações de aferentes musculares e cutâneos, e estão relacionados a diversos reflexos. Nesta lâmina também estão presentes interneurônios que inibem motoneurônios, participando do reflexo de estiramento (CHANDAR; FREEMAN, 2014; NÓGRÁDI, 2006).

A lâmina VIII é composta de interneurônios de diversos tamanhos, os quais estão envolvidos na coordenação de atividades motoras. Já a lâmina IX é onde estão localizados os neurônios motores que inervam os músculos esqueléticos. Por fim, a lâmina X é localizada ao redor do canal central, e as funções dos neurônios desta região ainda não estão elucidadas (CHANDAR; FREEMAN, 2014).

1.1.2. Substância branca

A substância branca é composta por axônios mielinizados ascendentes e descendentes, chamados de tratos. Os tratos ascendentes são compostos de axônios sensoriais, ao passo que os tratos descendentes são compostos de axônios motores (CHAMBERS; HUANG; MATTHEWS, 2014). A localização dos tratos ascendentes e descendentes podem ser visualizados na Figura 3. Um dos principais tratos descendentes é o trato corticoespinal (TCE), que é a via primária de neurônios somáticos motores. Essa via origina-se no córtex motor, onde neurônios motores superiores estão localizados e descendem para a medula espinal. Nas pirâmides medulares, aproximadamente 90% das fibras decussam e descendem pelo TCE lateral, fazendo sinapses na medula com interneurônios ou diretamente com neurônios motores inferiores, ao passo que os 10% das fibras que não decussam descendem ipsilateralmente pelo TCE anterior ou ventral (CHAMBERS; HUANG; MATTHEWS, 2014; CHANDAR; FREEMAN, 2014).

Outros importantes tratos descendentes são o trato rubroespinal, reticuloespinal e vestibuloespinal. O trato rubroespinal se origina no núcleo rubro do mesencéfalo e tem como função a influência em interneurônios que regulam a atividade de motoneurônios alfa de músculos flexores das extremidades superiores. O trato reticuloespinal medial projeta para

interneurônios que controlam motoneurônios alfa envolvidos com músculos axiais e proximais relativos a manutenção do equilíbrio e da postura. Esse trato é ativado em antecipação a alguma alteração no equilíbrio. Outro trato importante relacionado à postura e equilíbrio é o trato vestibuloespinal lateral, que age reativamente a perturbações do equilíbrio, como ao tropeçar (CHANDAR; FREEMAN, 2014).

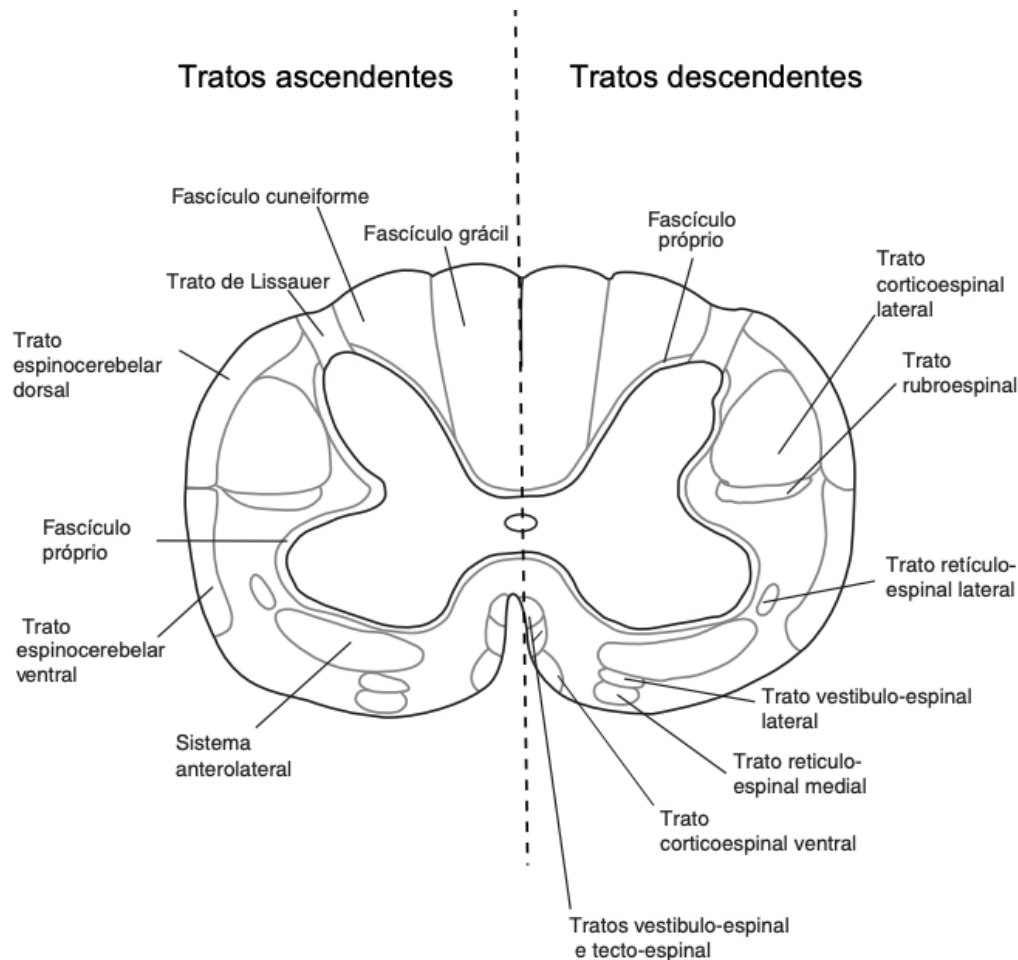


Figura 3 - Tratos espinais ascendentes e descendentes Localização dos tratos espinais. Do lado esquerdo, estão representados os tratos ascendentes, e do lado direito os tratos descendentes. Fonte: Adaptado de Chandar (2014, p. 256).

Dentre os principais tratos ascendentes, há a via coluna dorsal-lemnisco medial. A coluna dorsal compreende os fascículos grácil e cuneiforme, os quais são compostos de processos centrais de axônios de neurônios somatossensoriais provenientes de mecanorreceptores da pele, músculos, tendões e articulações. Da coluna dorsal, esses

neurônios projetam-se contralateralmente até o tálamo dorsal através do lemnisco medial. Essa via é importante, visto que leva informações somatossensoriais de toque fino, discriminação de dois pontos, vibração, estereognosia e propriocepção consciente. Outra importante via ascendente é o sistema anterolateral, ou trato espinotalâmico, a qual leva informações de estímulos nocivos, temperatura e ao tato protopático. Por fim, os tratos espinocerebelares levam informações de propriocepção inconsciente dos fusos musculares, órgão tendinoso de Golgi e articulações até o cerebelo (CHANDAR; FREEMAN, 2014).

1.1.3. Células gliais na medula espinal

Além dos neurônios, a medula espinal também conta com células gliais, que possuem papéis fundamentais em condições fisiológicas e patológicas. Estas células possuem diferentes origens embrionárias, sendo astrócitos, oligodendrócitos e células ependimais de origem neuroepitelial e a microglia de origem mielóide (ESCARTIN et al., 2021).

Os astrócitos são as células gliais mais abundantes do SNC e possuem diversos papéis essenciais para a função neuronal, promovendo a formação de sinapses, regulando e tamponando as concentrações extracelulares de íons e neurotransmissores, regulando as pressões osmóticas, fornecendo suporte metabólico e energético, modulando a neuroplasticidade e fazendo a manutenção da barreira hematoencefálica e hematoespinal (KRONSCHLÄGER et al., 2021; SUN; JAKOBS, 2012). Além disso, os astrócitos são considerados células imunocompetentes, detectando sinais de lesão ou de patógenos e respondendo através da secreção de citocinas (COLOMBO; FARINA, 2016).

No SNC, a bainha de mielina que envolve os axônios é formada pelos oligodendrócitos, ao passo que no Sistema Nervoso Periférico (SNP) essa estrutura é formada pelas células de Schwann. Essa estrutura é formada quando os oligodendrócitos se enrolam ao redor do axônio, formando várias camadas formadas quase exclusivamente de membrana celular. O citoplasma dessas células é comprimido, e algumas proteínas de membrana ligam os lados externos opostos da membrana, enquanto outra proteína de membrana, a proteína básica da mielina, liga os lados citoplasmáticos da membrana. Essa membrana celular que forma a mielina possui uma composição única de lipídios e proteínas, com alto conteúdo de colesterol e de glicolipídeos (BRODAL, 2010).

As células ependimais formam o epitélio colunar que reveste o canal central da medula espinal, sendo uma interface entre a cavidade contendo FCE e o parênquima. Assim, essas células possuem um importante papel no controle da passagem bidirecional de células imunes e solutos entre o FCE e o interstício (MACDONALD et al., 2021). Ainda, a membrana apical

dessas células apresenta cílios que ajudam a movimentar o FCE, ao passo que a membrana lateral possui junções de oclusão, de forma a controlar a difusão do FCE (MORENO-MANZANO, 2020).

Por fim, a microglia possui origem mielóide. Até recentemente, acreditava-se que a microglia tinha origem hematopoiética, porém, um estudo de 2010 estabeleceu que, diferentemente de macrófagos, a microglia origina-se de progenitores do neuroepitélio do saco vitelino (GINHOUX et al., 2010). Durante o desenvolvimento, a microglia tem papel de regular sinapses e, no SNC adulto em repouso, a microglia escaneia o ambiente em busca de sinais de lesão ou de infecção. Quando há uma lesão no SNC, a microglia é ativada, secretando citocinas inflamatórias, realizando fagocitose de debris e células mortas, recrutando células imunes e apresentando antígenos (BROCKIE; HONG; FEHLINGS, 2021). Ainda, a microglia apresenta receptores imunes e receptores de reconhecimento de padrões, monitorando a atividade neuronal e modulando a plasticidade e a densidade dendrítica (ZHANG et al., 2022).

1.2. LESÃO DA MEDULA ESPINAL

A lesão da medula espinal é uma síndrome neurológica altamente debilitante para a qual não há tratamentos eficazes atualmente. Essa condição acarreta em graves sintomas e grandes impactos na vida dos pacientes acometidos, podendo levar à paraplegia. Além disso, a LME leva a diversas comorbidades, como disfunções respiratórias, cardiovasculares, metabólicas, entre outras (GUEST et al., 2022). No Brasil, a incidência de LME é de 40 novos casos por ano por milhão de habitantes, resultando em cerca de 6 a 8 mil novos casos por ano. Destes, 80% das vítimas são homens, onde a faixa etária mais prevalente é de 10 a 30 anos (MINISTÉRIO DA SAÚDE, 2013). Apesar disso, ainda não existem tratamentos eficazes disponíveis. Atualmente, o tratamento baseia-se em cirurgia de descompressão da medula e administração de esteróides, como a metilprednisolona. Entretanto, esses tratamentos levam apenas a melhoras modestas (AHUJA et al., 2017a). Portanto, faz-se necessária a busca por novos tratamentos que sejam mais eficazes.

A LME pode ser traumática, quando um impacto físico externo leva ao dano na medula, ou pode ser causada por outras condições, como tumores, doenças neurodegenerativas e infecções. No caso da lesão traumática, o dano físico pode ser uma força de compressão, contusão ou transecção, entre outros. Essa força física leva a uma lesão primária, lesionando as células locais e rompendo a vasculatura, alterando a permeabilidade da barreira hematoespinal (BHE). A partir disso, uma cascata de eventos patofisiológicos inicia,

caracterizando a lesão secundária (AHUJA et al., 2017a). As diferentes fases da lesão e seus principais eventos podem ser observados na Figura 4.

A fase aguda da lesão secundária dura até 48h, e inicia com lesão isquêmica devido à destruição da microvasculatura, bem como eventos hemorrágicos que levam a um influxo de células inflamatórias. Com isso, a medula espinal incha, aumentando a compressão. Nesse período, há ainda liberação de glutamato pelos neurônios e astrócitos que estão morrendo, levando à excitotoxicidade glutamatérgica e propagando ainda mais a morte celular (AHUJA et al., 2017b). De 48h a 14 dias, caracteriza-se a fase subaguda da lesão secundária, marcada pela perda de homeostase iônica, o que leva à morte de neurônios e células gliais pelo desbalanço dos níveis de cálcio intracelular. Ainda, a inflamação propaga-se devido a mediadores que são liberados com o aumento da morte neuronal. Além disso, o metabolismo de células inflamatórias, juntamente com o desbalanço iônico e o aumento na concentração de glutamato, levam a disfunção mitocondrial e produção de espécies reativas de oxigênio (EROs) e radicais livres. Essas moléculas, por sua vez, levam a uma série de danos celulares, como a peroxidação lipídica. Nessa fase, inicia o processo de astrogliose e a formação da cicatriz glial (AHUJA et al., 2017b; ANJUM et al., 2020).

Por fim, após duas semanas, inicia a fase crônica da lesão, em que há a formação de uma cavidade cística no local da lesão, contendo líquido extracelular, tecido conjuntivo e macrófagos. Na borda dessa cavidade, há a proliferação de astrócitos reativos, continuando a formação da cicatriz glial, a qual contém uma matriz extracelular altamente inibitória que restringe a regeneração axonal. Nessa fase, também há uma tentativa de regeneração e remielinização, com migração de progenitores de oligodendrócitos que se associam com axônios lesionados (AHUJA et al., 2017b; ANJUM et al., 2020).

Dois aspectos centrais da lesão secundária são a inflamação e o estresse oxidativo, que levam a grande parte do dano (AHUJA et al., 2017b). Ainda, a cicatriz glial é a principal barreira para a regeneração axonal. Considerando a importância desses processos patofisiológicos no desenvolvimento e progressão da lesão, o uso de estratégias terapêuticas que visem mitigar esses danos podem ser promissores.

1.2.1. Inflamação

A partir da lesão primária e ruptura da microcirculação da medula, alterações na oxigenação e nos níveis de metabólitos extracelulares levam à rápida ativação da microglia. A microglia ativada irá, então, liberar mediadores inflamatórios para recrutar neutrófilos, monócitos e linfócitos. Após 4 horas da lesão, neutrófilos já são observados próximos à microvasculatura,

estando presentes no parênquima medular de 8 a 24h após a lesão (JONES; MCDANIEL; POPOVICH, 2005). Já os monócitos circulantes infiltram a medula de 2 a 3 dias após a lesão, período em que há um segundo evento de aumento da permeabilidade da barreira hematoespinal (DONNELLY; POPOVICH, 2008). Esses monócitos, então, diferenciam-se em macrófagos, tornando-se indistinguíveis da microglia residente, em 1 semana. De 2 a 4 semanas após a lesão, há uma diminuição de marcadores de ativação de macrófagos, entretanto, macrófagos presentes em *rafts* lipídicos persistem no local da lesão por anos (JONES; MCDANIEL; POPOVICH, 2005).

Durante a fase aguda da lesão, as células inflamatórias possuem o papel de remover tecidos danificados, debris de mielina e coordenar respostas regenerativas (GENSEL; ZHANG, 2015). Entretanto, os macrófagos, neutrófilos e microglia produzem citocinas inflamatórias, radicais livres e outros mediadores que levam a toxicidade de neurônios e células gliais. Níveis elevados de citocinas inflamatórias IL-1 β , TNF- α e IL-6 levam a morte de neurônios e oligodendrócitos, aumentam a infiltração de leucócitos e prejudicam o crescimento axonal (DONNELLY; POPOVICH, 2008).

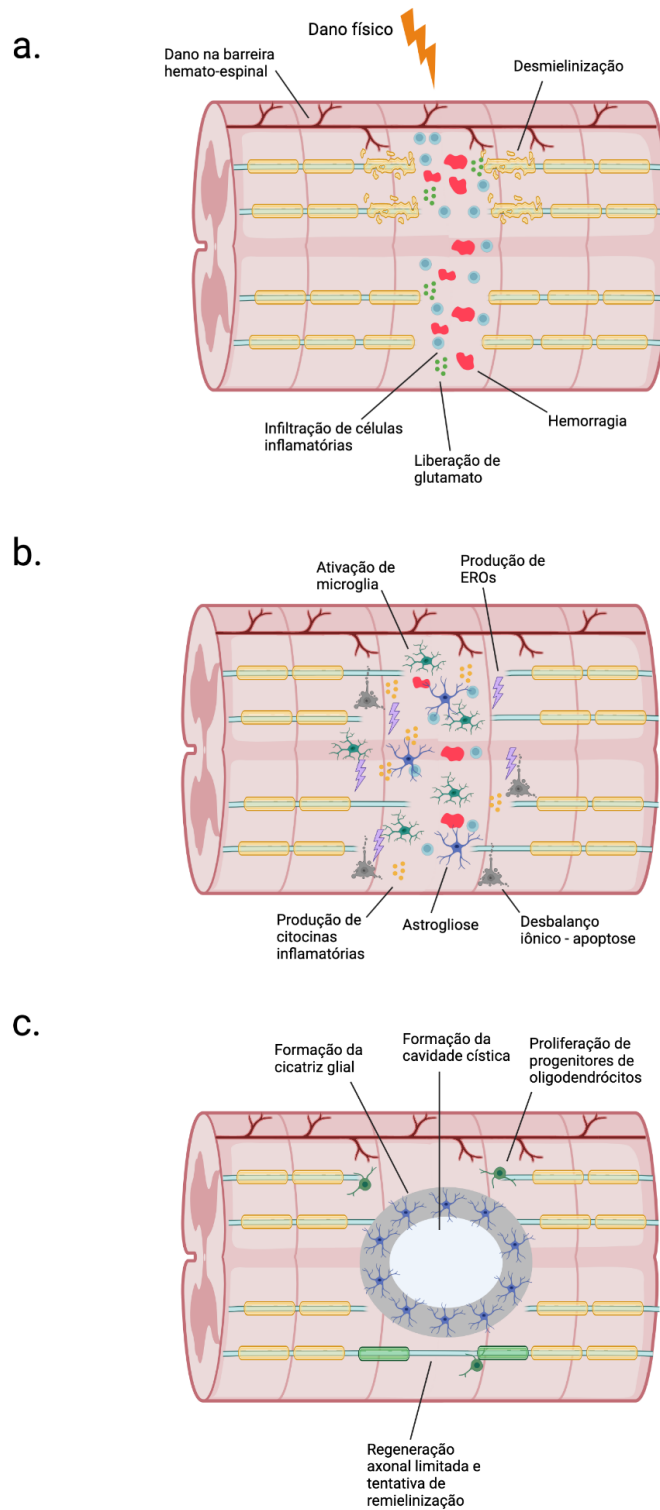


Figura 4 - Fases da LME a. Fase aguda, que ocorre de 0 a 48h após a lesão; b. Fase sub-aguda, de 48h a 14 dias; c. Fase crônica, que inicia 14 dias após a lesão e pode durar indefinidamente. Fonte: Elaborada pelo autor utilizando o Biorender

1.2.2. Estresse oxidativo

O estresse oxidativo acontece quando há um desbalanço entre a produção de radicais livres e a capacidade antioxidante em um tecido. Uma das principais classes de moléculas oxidantes são as espécies reativas de oxigênio (EROs), que incluem os radicais livres superóxido e radical hidroxil, bem como as moléculas não radicais peróxido de hidrogênio e oxigênio singlete (FATIMA et al., 2015). Essas moléculas são produzidas fisiologicamente no metabolismo celular, porém, quando produzidas em excesso, as EROs reagem e danificam moléculas biológicas como lipídios, proteínas e DNA (JIA et al., 2012). Para compensar a produção de EROs, as células possuem mecanismos antioxidantes enzimáticos e não enzimáticos. As principais enzimas antioxidantes são a superóxido dismutase, catalase, glutatona redutase e glutatona peroxidase, ao passo que as defesas não enzimáticas incluem glutatona, vitaminas C e E, β -caroteno e ácido úrico (JIA et al., 2012).

Na lesão da medula espinal, EROs são produzidas de diversas fontes. O processo inflamatório decorrente da lesão primária é uma delas, onde neutrófilos e macrófagos apresentam um aumento no consumo de oxigênio, gerando superóxido (TAOKA et al., 1995). Ainda, a excitotoxicidade glutamatérgica e o desbalanço iônico contribuem para o dano mitocondrial, que também leva a uma maior produção de EROs (JIA et al., 2012). Por fim, outras fontes de EROs são a cascata do ácido araquidônico, oxidação de amins biogênicas e atividade da xantina oxidase (HALL, 2011).

Uma das principais consequências do estresse oxidativo na lesão da medula espinal é a peroxidação lipídica. Nesse processo, EROs reagem com ácidos graxos poliinsaturados de membrana, como o ácido araquidônico, ácido linoleico, ácido eicosapentaenóico ou ácido docosahexaenóico, formando um radical lipídico ($L\bullet$) e gerando uma quebra na integridade de membrana. Em seguida, o $L\bullet$ reage com o oxigênio, formando o radical lipídico peroxil ($LOO\bullet$), que retira um átomo de hidrogênio de um ácido graxo poliinsaturado adjacente, formando um hidroperóxido lipídico ($LOOH$) e um segundo $L\bullet$, gerando portanto uma propagação de reações em cadeia. No fim desse processo, são formados malondialdeído (MDA) e 4-hidroxinonenal (4-HNE) (HALL, 2011). De fato, 4-HNE e substâncias reativas de ácido tiobarbitúrico (TBARS) já foram detectados 1 hora após a lesão, com acúmulo máximo de 4-HNE em 2 dias (BALDWIN et al., 1998).

O estresse oxidativo na LME leva a uma propagação do dano secundário, visto que o dano oxidativo a membranas exacerba a disfunção na homeostase iônica já presente devido à despolarização mecânica e liberação de aminoácidos excitatórios. As EROs levam a um

aumento das concentrações de cálcio e sódio intracelular, onde a peroxidação lipídica inativa a bomba de cálcio do retículo endoplasmático e a bomba de sódio e potássio. Com isso, há também a exacerbação da disfunção mitocondrial e da excitotoxicidade glutamatérgica, e já foi observado que o acúmulo de 4-HNE em membranas sinaptossomais da medula espinal está associado com um prejuízo na recaptação de glutamato da fenda sináptica (HALL, 2011; SPRINGER et al., 2002).

A importância da peroxidação lipídica e outros danos oxidativos são evidenciados por diversos estudos com antioxidantes na lesão da medula espinal que demonstraram melhoras na patofisiologia da lesão, conforme revisado por Hall e colaboradores (HALL, 2011).

1.2.3. Cicatriz glial

De 7 a 10 dias após a lesão, os astrócitos próximos ao local da lesão proliferam e organizam-se ao redor do tecido lesionado, formando a cicatriz glial (ANJUM et al., 2020). Esses astrócitos sofrem transformações morfológicas, superexpressando proteínas de citoesqueleto, como a proteína ácida fibrilar glial (GFAP, do inglês *glial fibrillar acidic protein*), vimentina e nestina, hipertrofiando e retraindo seus processos celulares. Outras células também são recrutadas na formação da cicatriz glial, como:

- astrócitos distantes que migram em direção ao tecido danificado;
- astrócitos com características de células-tronco que geram novos astrócitos;
- células endimais, que são induzidas com a lesão e geram células que se diferenciam em astrócitos;
- células NG2 positivas, como células progenitoras de oligodendrócitos (OPCs, do inglês *oligodendrocytes progenitor cells*), pericitos, macrófagos e microglia (YUAN; HE, 2013).

No epicentro da lesão é gerada uma cicatriz fibrótica, formada por fibroblastos e pericitos e, principalmente, componentes de matriz extracelular, que são secretados pelos fibroblastos e pelos astrócitos. Dentre eles, os proteoglicanos de sulfato de condroitina (CSPG, do inglês *chondroitin sulfate proteoglycans*), como neurocan, versican e brevican, são componentes inibitórios da regeneração axonal, já tendo sido demonstrado que essas moléculas inibem o crescimento de dendritos *in vivo* e *in vitro*, bem como inibem a proliferação e diferenciação de OPCs *in vitro* (YUAN; HE, 2013).

Assim, a cicatriz glial é formada por uma rede de moléculas que formam um impedimento físico e químico para a regeneração axonal. Entretanto, nos estágios iniciais da lesão, a cicatriz glial tem o papel de conter o dano, separando o tecido saudável do tecido danificado, diminuindo o dano da BHE e limitando a extensão da resposta inflamatória. Estudos

demonstram que interferências na ativação de astrócitos no momento da lesão pioram o desfecho da LME, com comprometimento da reconstrução da BHE, presença de edema vasogênico, inflamação e danos teciduais dispersos (FAULKNER, 2004). Dessa forma, a modulação dos astrócitos na formação da cicatriz glial nos estágios mais avançados da lesão pode ser uma estratégia terapêutica, tendo em mente a importância da cicatriz glial nos estágios iniciais.

1.3. GALANTAMINA

Considerando o caráter multifatorial da fisiopatologia da LME e da importância da inflamação e do estresse oxidativo em orquestrar as demais respostas patológicas, a galantamina surge como uma possibilidade de tratamento para a LME. Esse fármaco é um alcalóide fitoquímico originalmente extraído da *Galanthus nivalis* que, nos anos 1950, era utilizada para tratar poliomielite e miastenia grave, sendo comercializada com o nome de Nivalin. Atualmente, a galantamina é sintetizada quimicamente, e o hidrobrometo de galantamina é comercializado com o nome de Razadyne™, e é aprovada pelo *Food and Drug Administration* (FDA) para o tratamento de demência leve a moderada na doença de Alzheimer (METZ; PAVLOV, 2021).

A galantamina foi inicialmente caracterizada como um inibidor competitivo e reversível da acetilcolinesterase e, posteriormente, foi observado que ela também atua como um modulador alostérico do receptor nicotínico $\alpha 7$ (nAChR $\alpha 7$). Assim, a galantamina age estimulando a liberação de acetilcolina, aumentando sua concentração e, ao mesmo tempo, prolongando a ação da acetilcolina na fenda sináptica ao inibir a acetilcolinesterase (VILLARROYA et al., 2007). Esses mecanismos fazem com que a galantamina seja utilizada tanto em condições que necessitam melhoras no tônus muscular quanto em condições em que disfunções colinérgicas levam a danos cognitivos (METZ; PAVLOV, 2021).

Ainda, sabe-se que o nAChR $\alpha 7$ tem um importante papel na via colinérgica anti-inflamatória. Essa via foi originalmente descrita ao observar-se que a estimulação do nervo vago levava a uma diminuição dos níveis sistêmicos de TNF em ratos expostos a lipopolissacarídeo (LPS), uma molécula produzida por bactérias gram-negativas (BOROVIKOVA et al., 2000). Posteriormente, foi observado que este efeito ocorria através do nAChR $\alpha 7$ especialmente de macrófagos (WANG et al., 2003). A ativação do nAChR $\alpha 7$ em monócitos, macrófagos e células gliais leva à inibição da via do NF-kB, diminuindo a produção de citocinas

inflamatórias, EROs e, inclusive, levando a uma polarização de macrófagos e microglia de um fenótipo pró-inflamatório para um fenótipo anti-inflamatório (HAN et al., 2014; PATEL et al., 2017; SUGANO et al., 1998; WANG et al., 2003; ZHANG et al., 2017). Devido à atuação da galantamina no nAChR $\alpha 7$, esse medicamento possui importantes efeitos anti-inflamatórios sistêmicos e centrais. A administração de galantamina juntamente com huperzina A, outro inibidor da acetilcolinesterase, levou à diminuição da inflamação sistêmica e aumento de sobrevivência de camundongos com endotoxemia (PAVLOV et al., 2009). Esses efeitos anti-inflamatórios sistêmicos também foram observados em modelos de colite (JI et al., 2014), lupus eritematoso sistêmico (PHAM; WANG; MATHIS, 2018), entre outros. Além disso, a galantamina também age centralmente, diminuindo a neuroinflamação (LIU et al., 2018b).

A galantamina possui propriedades antioxidantes por sequestrar oxigênio, devido à presença do grupamento enol da molécula. Esse efeito é potencializado na mudança para hidrobrometo de galantamina (TSVETKOVA et al., 2013). Em uma cultura primária de neurônios de ratos, a galantamina diminuiu a produção de EROs e a peroxidação lipídica, bem como preveniu a redução dos níveis de glutatona após a exposição ao peptídeo β -amilóide (MELO et al., 2009). Assim, a galantamina apresenta diversos mecanismos de neuroproteção, mostrando-se relevante em diversas patologias, como Alzheimer, Parkinson, esquizofrenia, lesão cerebral traumática e, inclusive, LME (METZ; PAVLOV, 2021). Os estudos clínicos que utilizaram galantamina para distúrbios do sistema nervoso estão listados na Tabela 1. Em um trabalho anterior do grupo de pesquisa, a galantamina foi administrada intraperitonealmente por 5 dias em ratos que sofreram uma LME por contusão, e observou-se uma diminuição no tamanho da lesão e melhora funcional do movimento dos membros posteriores (SPERLING et al., 2019).

Tabela 1. Estudos clínicos com galantamina em desordens do sistema nervoso

| Doença | Efeitos | Referência |
|----------------------------------|--|--------------------------------------|
| Poliomielite | Alívio sintomático | (REVELLI; GRASO, 1962) |
| Doença de Alzheimer | Melhora de sintomas cognitivos, funcionais e comportamentais | (TARIOT et al., 2000) |
| | Melhora nos escores Sub-escala cognitiva da Escala de Avaliação da Doença de Alzheimer, Escala da impressão global da mudança e Escala de deterioração progressiva | (WILKINSON; MURRAY; GROUP, 2001) |
| Acidente vascular cerebral (AVC) | Menor fardo do cuidador | (KAUFER et al., 2005) |
| | Menor risco de AVC isquêmico em pacientes com demência sem histórico de AVC isquêmico | (LIN et al., 2016) |
| Doença de Parkinson | Menor risco de AVC isquêmico e morte em pacientes com demência | (TAN et al., 2018) |
| | Melhora dos sintomas mentais globais na maioria dos pacientes (piora em alguns), alívio de alucinações, melhora de função cognitiva | (AARSLAND; HUTCHINSON; LARSEN, 2003) |
| Esquizofrenia | Melhora em escores de função cognitiva; melhora de alucinações, ansiedade, distúrbios do sono e apatia; melhora na marcha e diminuição de <i>freezing</i> e quedas; menores níveis de perturbação nos familiares e melhoras nas atividades diárias | (LIU et al., 2018a) |
| | Benefícios diferenciais para aspectos de velocidade de processamento e memória verbal | (BUCHANAN et al., 2008) |
| Esquizofrenia | Melhora de memória e atenção em pacientes estabilizados com risperidona | (SCHUBERT; YOUNG; HICKS, 2006) |
| | Benefícios na alogia, mas não em outros sintomas | (CONLEY et al., 2009) |

| | | |
|------------------------------|--|-------------------------|
| | Em combinação com CDP-colina, houve melhora nos índices de marcha e na inibição dos estímulos testados | (CHOUÉIRY et al., 2019) |
| | Melhora de déficits cognitivos | (KOOLA et al., 2020) |
| Lesão cerebral traumática | Melhora de déficits cognitivos, aumento da vigilância | (TENOVUO, 2005) |
| Desordem do espectro autista | Melhora na irritabilidade e nas sub-escalas de letargia e de retirada social, sem diferenças significantes nos efeitos colaterais em comparação com o placebo. | (GHALEIHA et al., 2014) |
| Doença de Huntington | Melhora de sintomas psiquiátricos e motores | (PETRIKIS et al., 2004) |

Adaptada de Metz e Pavlov, 2021.

1.4. NANOTECNOLOGIA

Um dos desafios da administração sistêmica de fármacos é a diminuição da biodisponibilidade da droga no tecido-alvo e aumento de efeitos colaterais. Essa via de administração leva a uma alta concentração plasmática da droga no momento da aplicação, que logo diminui para níveis sub-terapêuticos, necessitando da complacência do paciente para a repetição da administração de novas doses (SU et al., 2021). Nesse contexto, a nanotecnologia vem como alternativa para novos sistemas de liberação de drogas (DDS, do inglês, *drug delivery systems*), como as nanopartículas. A nanotecnologia pode ser definida como a manipulação da matéria em níveis atômicos e moleculares e, na área biológica, sistemas na faixa de 1 a 1000nm são considerados parte da nanotecnologia (PARK, 2007). DDS que apresentem uma liberação controlada e sustentada possuem as vantagens de menor frequência de administração, menos efeitos colaterais, melhor atividade farmacológica e efeitos terapêuticos mais prolongados (PRAJAPATI; JANI; KAPADIA, 2015). Uma opção que vem sendo muito utilizada é a utilização de nanopartículas poliméricas, que podem ser nanocápsulas ou nanoesferas. No caso das nanocápsulas, o fármaco de interesse fica retido no centro da partícula, envolto por uma casca polimérica. Já nas nanoesferas, o fármaco pode estar distribuído tanto na casca como no centro da partícula, como demonstrado na Figura 5 (EL-SAY; EL-SAWY, 2017).

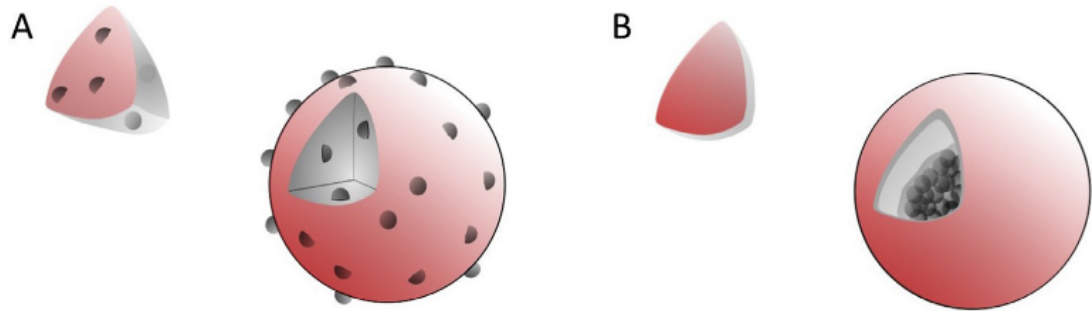


Figura 5 - Nanopartículas Nanoesferas são caracterizadas pela distribuição do fármaco na casca e no centro da partícula; b. Nanocápsulas retêm o fármaco dentro da partícula. Fonte: El-Say (2017, p. 676).

Para formular essas partículas, podem ser utilizados polímeros biodegradáveis, que podem ter origem sintética ou natural. Dentre os polímeros sintéticos, destacam-se os poliésteres, como poli(ácido glicólico) (PGA), poli(ácido lático) (PLA), poli(ácido lático-co-glicólico) (PLGA) e policaprolactona (PCL), ao passo que dentre os polímeros naturais, temos a quitosana, o ácido hialurônico, o alginato, a gelatina, entre outros. Os poliésteres são polímeros sintéticos biocompatíveis e biodegradáveis, sendo degradados pela clivagem de suas ligações éster. O PLGA é um polímero extensamente estudado e muito utilizado para formulações de DDS e *scaffolds* na engenharia de tecidos por ser aprovado pelo FDA (*Food and Drug Administration*) para diversas aplicações clínicas e pelo fato de que sua taxa de degradação e suas propriedades mecânicas podem ser moduladas alterando a razão de ácido lático/ácido glicólico (PARK; YE; PARK, 2005; PRAJAPATI; JANI; KAPADIA, 2015). Polímeros com maior conteúdo de ácido lático levam a uma diminuição da taxa de degradação e liberação mais lenta do fármaco na nanopartícula (PRAJAPATI; JANI; KAPADIA, 2015). O PLGA é degradado pelo processo de erosão homogênea, em que a água penetra a matriz polimérica e inicia a cisão em cadeia. Como a água penetra mais rapidamente do que o processo de erosão da matriz, a degradação polimérica ocorre homoganeamente através da matriz (EDLUND, U, 2002). Assim, os produtos da degradação do PLGA são ácido glicólico e ácido lático, os quais são metabolizados em água e CO₂ pelo ciclo de Krebs e eliminados pela respiração (PARK; YE; PARK, 2005).

Entre os diversos métodos de produção de nanopartículas poliméricas pode-se citar a polimerização interfacial, a polimerização in situ, a separação de fases, a emulsão e a eletropulverização.

1.5. ELETROPULVERIZAÇÃO

A eletropulverização apresenta como vantagens a possibilidade de regular diversos parâmetros experimentais para atingir diferentes tamanhos e morfologias de partículas, além de apresentar uma alta taxa de encapsulamento (SU et al., 2021). Nessa técnica, utiliza-se uma emulsão composta pelo fármaco de interesse e uma solução polimérica, onde o polímero é dissolvido em um solvente orgânico como acetonitrila, acetona, etc. Essa solução é então carregada em uma seringa, cujo êmbolo é pressionado por uma bomba, de forma a extrair a solução de maneira controlada por uma agulha. Nessa agulha, é aplicada uma voltagem positiva e, opostamente à agulha, há uma placa coletora onde é aplicada uma voltagem negativa, ilustrado na Figura 6. Assim, a eletropulverização baseia-se no princípio que uma força elétrica aplicada em uma gota saindo de um capilar é capaz de deformar a interface da gota. Essa força elétrica gera uma força eletrostática dentro da gota que compete com a tensão superficial, superando-a e gerando gotas micro e nanométricas que são ejetadas da gota primária e atraídas pela placa coletora. No caminho, o solvente orgânico é evaporado, sendo coletadas as nanopartículas poliméricas contendo o fármaco (BOCK; DARGAVILLE; WOODRUFF, 2012).

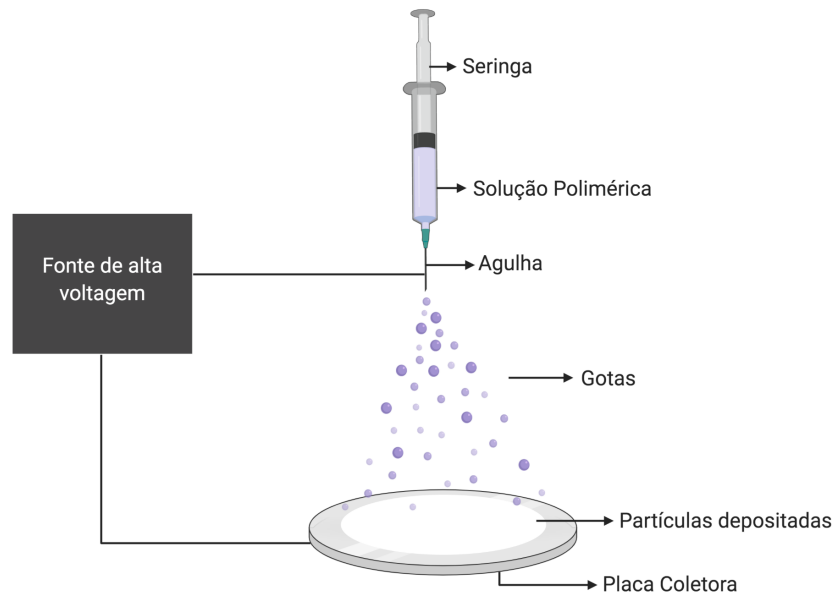


Figura 6 - Eletropulverização A técnica de eletropulverização baseia-se no uso de uma fonte de alta voltagem sendo aplicada na gota de solução polimérica que é extruída por uma agulha. Esse processo altera as propriedades eletrostáticas da gota, formando gotas micro e nanométricas que, ao terem o solvente evaporado e serem depositadas na placa coletora, formam nanopartículas. Fonte: elaborada pelo autor utilizando o Biorender.

1.6. NANOTECNOLOGIA E LESÃO DA MEDULA ESPINAL

Diversas estratégias utilizando nanotecnologia, para o tratamento da LME, já vêm sendo utilizadas em testes pré-clínicos. O uso de micelas poliméricas como tratamento para LME já foi testado para a liberação de Rolipram (MACKS et al., 2018) e minociclina (WANG et al., 2019b). Ambas abordagens demonstraram melhoras após a LME, onde o Rolipram levou à diminuição da apoptose e da inflamação, ao passo que as micelas contendo minociclina diminuiram o tamanho da lesão e promoveram uma recuperação da função motora dos animais.

As nanopartículas poliméricas também foram utilizadas em diversos estudos como estratégia terapêutica para LME. Em um desses estudos, avaliou-se o uso de nanopartículas compostas de quitosana-glicol modificada com ácido ferúlico, observando-se uma melhora locomotora em ratos após LME por contusão (WU et al., 2014). Ainda, o uso de nanopartículas contendo metilprednisolona também foi estudado. Esse fármaco é uma das formas de tratamento atualmente utilizada em pacientes de LME, mas apresenta grandes efeitos colaterais e baixa eficácia terapêutica. Quando administrada localmente na forma de nanopartículas, a metilprednisolona foi mais eficaz do que quando administrada sistemicamente, apresentando um menor volume de lesão e maior melhora locomotora (KIM; CALDWELL; BELLAMKONDA, 2009).

Outra abordagem promissora é o uso de nanofibras eletrofiadas. Em um estudo prévio do grupo de pesquisa, foram avaliadas nanofibras contendo o fator de crescimento de fibroblastos (FGF-2) em um modelo de LME por hemiseção. Observou-se que esse biomaterial promoveu uma melhora locomotora dos animais após 4 semanas e diminuiu a expressão de GFAP, indicando uma melhora na cicatriz glial (REIS et al., 2018).

2. HIPÓTESE

A partir dos dados da literatura, as hipóteses testadas no presente estudo foram: a) que é possível produzir nanopartículas de PLGA contendo galantamina pela técnica de eletropulverização; b) que estas partículas são capazes de prevenir a morte celular e a produção de EROs em um modelo neuronal *in vitro* após a exposição à peróxido de hidrogênio; c) que estas partículas, quando aplicadas *in vivo* em um modelo de LME por contusão em ratos, são capazes de diminuir a inflamação e o estresse oxidativo, bem como gerar uma melhora locomotora dos animais.

3. JUSTIFICATIVA

Milhares de pessoas sofrem uma lesão da medula espinal por ano no mundo e esta condição representa uma importante causa de morbidade e mortalidade. Já foi demonstrado que a galantamina é uma promissora estratégia terapêutica para a LME e a sua administração, na forma de nanopartículas, pode maximizar os benefícios desse medicamento. Por fim, os efeitos da galantamina em parâmetros oxidativos e inflamatórios após a LME ainda não foram estudados, bem como não há estudos, até o momento, que utilizem nanopartículas de galantamina em um modelo animal de LME.

4. OBJETIVOS

Objetivo geral

O objetivo deste estudo é investigar os efeitos do implante de nanopartículas de PLGA com a galantamina na produção de citocinas inflamatórias, no estresse oxidativo e na recuperação motora em modelo de lesão da medula espinal em ratos.

Objetivos específicos

1. Produzir e caracterizar partículas de PLGA contendo galantamina;
2. Avaliar a cinética de liberação da galantamina;

3. Avaliar os efeitos das partículas de galantamina na prevenção de perda de viabilidade e na produção de EROs em um modelo neuronal *in vitro* após a exposição ao peróxido de hidrogênio;
4. Implantar as partículas de galantamina em modelo animal de LME, provocada por contusão;
5. Avaliar a atividade locomotora dos animais por 42 dias;
6. Avaliar os efeitos antiinflamatórios e antioxidantes do tratamento com as nanopartículas de galantamina, 3 e 42 dias após a LME.

5. RESULTADOS

Artigo 1.

Galantamine-PLGA nanoparticles decrease oxidative stress and inflammation in a model of acute spinal cord injury

Fernanda Stapenhorst Franca^{1,2}, Laura Sperling^{1,2}, Marcelo Garrido^{1,2}, Luiz Sommer^{1,2}, Cristian Teixeira^{1,2}, Gabriele Didó^{1,2}, João Pedro Prestes^{1,2}, Tiago Oliveira³, Patrick Turck⁴, Adriane Bello Klein⁴, Patricia Pranke^{1,2,5}

¹Hematology and Stem Cell Laboratory, Faculty of Pharmacy, Universidade Federal do Rio Grande do Sul; ²Stem Cell Laboratory, Fundamental Health Science Institute, Universidade Federal do Rio Grande do Sul; ³Pharmacosciences Department, Federal University of Health Sciences of Porto Alegre, Porto Alegre, RS, Brazil; ⁴Laboratory of Cardiovascular Physiology and Reactive Oxygen Species, Institute of Basic Health Sciences, Universidade Federal do Rio Grande do Sul; ⁵Instituto de Pesquisa com Células-tronco (IPCT). Porto Alegre, RS, Brazil.

Artigo em revisão final no periódico Biomedical Materials (Fator de impacto 4.103)

Abstract

Spinal cord injury (SCI) is a debilitating condition with no effective treatment. Inflammation and oxidative stress play an important role in SCI pathophysiology. Previous studies from our group have indicated that galantamine improves recovery after SCI. Biodegradable polymer carriers are a good therapeutic approach due to their ability to sustain the release of the encapsulated drugs. Hence, the aim of this study has been to produce galantamine nanoparticles and to evaluate its therapeutic effects *in vitro* and during acute SCI. Galantamine was mixed in a 4% PLGA solution and electrosprayed to produce the nanoparticles containing galantamine (PG). The material was characterized according to its size, zeta potential and polydispersity index. Galantamine release was assessed for 35 days by HPLC. PC12 cells exposed to hydrogen peroxide were treated with the particles and assessed for viability and reactive oxygen species (ROS) production. The particles were also administered in a rat model of contusion spinal cord injury and the anti-inflammatory and antioxidant effects of the treatment were analyzed after 3 days. The particles presented a biconcave morphology with and without galantamine. The PLGA particles alone presented a diameter of 3451.62 nm, zeta potential of -50.05 mV and a 0.715

PdI, whereas the PG particles had a diameter of 568.27 nm, a zeta potential of -23.59 mV and PdI of 0.586. Galantamine was released from the PG particles in a burst profile and was detected for up to 35 days. *In vitro*, galantamine alone was able to preserve cell viability after exposure to hydrogen peroxide, but no treatment showed a decrease in ROS production. *In vivo*, only the PG treatment decreased ROS production and IL-1 β levels 3 days after the injury, and both the PG and galantamine were able to decrease lipid peroxidation levels. Thus, although galantamine alone showed oxidant improvements after SCI, only the PG was able to improve both inflammation and oxidative parameters. Hence, PG could be a promising treatment strategy for SCI.

Introduction

The central nervous system (CNS) has a very limited regeneration capacity, hence CNS injuries, such as stroke, traumatic brain injury and spinal cord injury (SCI) lead to debilitating conditions and neurological dysfunctions (1). Specifically, the extent of function loss in SCI is dictated by the level of spinal injury, leading to loss of motor, sensory and autonomic nervous system functions at the affected areas (2). Despite affecting millions of people worldwide, due to the limited CNS regeneration, there are no effective treatments for SCI to date. Inflammation and oxidative stress play important roles in the pathophysiology of SCI, where inflammatory cells release cytokines and produce reactive oxygen species (ROS), leading to significant cell death (3).

Considering that targeting a single mechanism of injury in a complex condition such as SCI is unlikely to elicit significant regeneration, using a drug that can address multiple pathophysiological pathways seems to be a more promising approach. Galantamine has been shown to have neuroprotective, anti-inflammatory and antioxidant activities, due to its activity as an acetylcholinesterase inhibitor, and has been evaluated in pre-clinical studies for several neurological conditions, such as Alzheimer's disease, Parkinson's disease, schizophrenia, traumatic brain injury and spinal cord injury (4). Specifically, in spinal cord injury, intraperitoneal administration of galantamine led to improved motor functional recovery and decreased lesion size in rats (5).

Traditional drug administration routes require high plasmatic drug concentrations in order to have the proper therapeutic dose at the target tissue, leading to increased side effects, and present a short time of action, calling for repeated drug administration. These inconveniences can be overcome with the use of controlled release drug delivery systems that maintains therapeutic concentrations to be released over time (6). Nanotechnology based drug delivery

systems have been widely studied in SCI in order to achieve this goal, increasing drug bioavailability at the lesion site (7). Nanoparticles can range from 1 to 1000nm and have been successfully used in the treatment of several diseases (8). Polymeric nanoparticles are a common type of nanoparticles that have the advantage of being biocompatible and which present a low toxicity for the CNS, as well as presenting good stability and controlled drug release (9,10). One of the main polymers used for nanoparticles with sustained drug release is poly(lactic-co-glycolic acid) (PLGA), due to its biocompatibility, biodegradability and to the fact that it has been approved by several regulatory agencies for human use. Furthermore, by adjusting the PLGA properties and the lactide:glycolide ratio can alter the drug release profile, making it possible to tailor the particle production according to the necessity (11). In SCI, previous works have shown that PLGA particles containing drugs such as methylprednisolone and flavopiridol administered directly at the lesion site presented improvements in functional recovery of injured rats (12,13).

Polymeric particles can be produced by several methods, such as emulsion, nanoprecipitation, coacervation and spray drying, but most of these techniques lead to low encapsulation efficiency and drug inactivation (14). Electro spraying, however, is a technique that has the tendency of presenting high encapsulation efficiency and which preserves the functionality of the active components (15). In this method, a high voltage is applied in a nozzle containing the polymeric solution, which is extruded at a constant rate using a syringe pump. The high voltage causes the droplet to break up into micro- or nanoparticles, the solvent is evaporated and the dry particles are collected. Because the solvent is evaporated, the particles present low toxicity and good biocompatibility (16).

In the present work, PLGA nanoparticles containing galantamine were produced and characterized according to their morphology, size, zeta potential and polydispersity index. The galantamine release profile was assessed and the neuroprotective effects of the particles were analyzed in vitro using PC12 cells as a neural model. In addition, the particles were implanted in situ in a rat model of SCI and the treatment effects in inflammation and oxidative stress were evaluated 3 days after the injury. This novel method of galantamine delivery could be beneficial in reducing secondary damage in SCI, leading to better long-term outcomes.

Methods

1. Particle production and characterization
 - 1.1. Electro spraying

The particles were produced using a PLGA solution made with 4% PLGA 75:25 (Purasorb®) dissolved in acetonitrile (Sigma–Aldrich®). For the galantamine-loaded microparticles (PG), 20 mg/mL of galantamine hydrobromide (ChemCruz™) were incorporated in the 4% PLGA solution to reach a final concentration of 2.5%. The solutions were electrosprayed using a voltage of +24/-2kV for the PLGA only particles and +25/-4kV for the PG. The solutions were extruded through 0.6mm needles, with a flow rate of 0.1 - 0.5 mL/h, and controlled humidity of 30% and temperature of 30°C. The distance between the needle and the collector plate was 9 cm. Prior to the use of the particles in cell culture or in the animals, the samples were sterilized in UV light for 30 minutes.

1.2. Scanning Electron Microscopy

Particle morphology and structure were analyzed through scanning electron microscopy (SEM) (JEOL JSM-6060). The particles were sputter coated with a thin layer of gold before observation. The acceleration voltage was adjusted to 10 kV and magnification was from 2000 to 10,000x.

1.3. Particle size, polydispersity index and zeta potential

Particle diameter, polydispersity index (PDI) and Zeta potential were analyzed by dynamic light scattering using ZetaSizer equipment (Malvern®). The particles were suspended in NaCl 1mM and analyzed using the refractive index of 1.46 of PLGA 75:25.

1.4. Drug release

The galantamine release from the PG particles was determined after 1, 3, 6, 12, 24 and 72h, 1 week and weekly up to 4 weeks. The particles were solubilized in PBS and at each time point, 1 mL of the supernatant was collected and 1mL of fresh PBS was added to each tube. Aliquots of 1 µL of supernatant were injected in a rapid and simple method based on ultra-high-performance liquid chromatography-tandem mass spectrometry (UHPLC-MS/MS). A Nexera UFLC system coupled to a LCMS-8045 triple quadrupole mass spectrometer (Shimadzu, Japan) was used for the analysis. Separation was performed on a 75 × 2.0 mm i.d., 2.2 µm, Shim-pack XR-ODS II column (Shimadzu, Kyoto, Japan) eluted with water (A) and acetonitrile (B) both containing 0.1% formic acid as mobile phases. A gradient mode was applied as described: 0.0 – 2.5 min, 5 – 100% of B; 2.5 – 3.0 min, 100% of B; 3.0 – 3.5 min, 100 – 5% of B; and 3.5 – 8.0 min, 5% of B. The flow rate was maintained at 0.35 mL/min at 40° C. Mass spectra were obtained with the following conditions: positive ion acquisition mode; capillary voltage, 4500 V; desolvation line temperature, 250 °C; heating block temperature, 400 °C; drying gas, 10 L/min; nebulizing gas, 3

L/min; and mass range, m/z , 50 – 300. Collision-induced dissociation was obtained with 270 kPa argon pressure and with a collision energy of 35 eV. The time-dependent galantamine release was monitored by the signal of m/z 288.00 → 198.00 and m/z 288.00 → 213.00. Calculations were corrected to express the cumulative drug release.

2. Cell culture

PC12 cells (ATCC - CRL-1721) were cultivated in DMEM high-glucose medium, supplemented with 10% fetal bovine serum, 5% horse serum and 1% penicillin-streptomycin. The cells were maintained at 37°C in a humidified atmosphere containing 5% CO₂. For the viability assay, the cells were seeded in 96 well plates at a density of 5.26 x 10⁴ cells/mL. For the DCF assay, the cells were seeded in 48 well plates at a density of 6x10⁴ cells/mL. 24 hours after seeding, the cells were treated with 200µM of H₂O₂ and either PLGA particles (PLGA concentration of 5µg/mL), PG (PLGA and estimated galantamine concentration of 5µg/mL) or galantamine (5µg/mL). Viability, live/dead and DCF assays were carried out 24 hours after treatment.

3. Viability assay

Cell viability was assessed by colorimetric assay using 3-(4,5-dimethylthiazol-2-yl)-2,5-diphenyltetrazolium bromide (thiazolyl blue; MTT Sigma), following incubation. The plates were read at 540/620 nm on a spectrophotometer (Thermo Scientific). The results are expressed as a percentage of the controls.

4. Live/Dead assay

Cell viability was also assessed using Live/Dead assay kit (*Life Technologies*®) according to the manufacturer's protocol. Briefly, PC12 cells were washed with PBS and incubated with calcein-AM and ethidium bromide for 15 minutes at 37°C. Calcein-AM has a green fluorescence and indicates the presence of live cells, whereas ethidium bromide has a red fluorescence, indicating the presence of dead cells. Samples were visualized using fluorescence microscopy (Leica Dmi8 - Leica Microsystems) and images were acquired for qualitative and quantitative analysis. For quantification, 3 images of different areas for each group were acquired. Images were analyzed using ImageJ (U. S. National Institutes of Health, Bethesda, Maryland, USA, <https://imagej.nih.gov/ij/>), where stained cells were counted and the average of live and dead cells was calculated.

5. Animals

The experimental protocols were approved by the Institutional Animal Care and Use Committee of the Universidade Federal do Rio Grande do Sul (Porto Alegre, Brazil - CEUA project number 35781). A total of 42 adult male Wistar rats (8-9 weeks old, 250–300 g) raised at the animal facility of the Federal University of Rio Grande do Sul were used in this study. The rats were housed in groups of two to four at a 12-hour light/dark cycle with food and water available *ad libitum*. All surgical procedures were performed under general anesthesia with 75 mg/kg intraperitoneal ketamine mixed with 5 mg/kg xylazine, administering a 50% supplemental single dose of ketamine whenever necessary. The spinal cord was exposed through laminectomy at T-10, and a 10g rod was dropped from a height of 12.50 cm directly onto the cord using the NYU MASCIS (New York University, Multicenter Animal Spinal Cord Injury Study) impactor (17–19). After the contusion, the treatments were applied at the lesion site in an intraparenchymal manner in the spinal cord. Following this, the muscles and skin were sutured and the animals were kept at 37°C with the aid of a thermal pad. Antibiotics (Baytril, 10 mg/kg) were administered intraperitoneally immediately after surgery and on a daily basis. The analgesic tramadol was administered subcutaneously after surgery, and at 8 and 16 hours post-surgery. The bladders were manually emptied, twice daily.

6. Spinal cord tissue preparation

Three days after the injury, the animals were euthanized with a lethal dose of ketamine and xylazine and the spinal cords were collected. The spinal cord tissue was weighed and homogenized using 20 mmol/L phenyl methyl sulphonyl fluoride (PMSF) and 1.15% w/v KCl in a Potter-Elvehjem homogenizer. The suspension was centrifuged at 1000 g for 20 minutes at 4–5°C and the supernatants were collected.

7. Protein concentration

Total proteins were quantified using the Lowry method (20). Bovine serum albumin was used as the standard and this was also used to express the results.

8. ROS levels quantification

ROS levels in the PC12 cells and in the spinal cord tissue were measured by quantifying the fluorescence of the oxidation of 2',7'-dichlorofluorescein diacetate (DCFH-DA) (Sigma-Aldrich, USA) by the ROS present in the sample. For the *in vitro* experiments, after the incubation time,

the cells were trypsinized and collected. The samples were incubated with DCFH-DA for 1 hour. A standard curve with known concentrations of 2',7'- dichlorofluorescein (DCF) was used. The samples were excited at 488 nm; emission was collected with a 525-nm long-pass filter and expressed as nmol/mg protein (21).

9. Lipid peroxidation analysis

The formation of TBARS during an acid-heating reaction was measured as previously described (22) and it was used as an index of lipid peroxidation. Briefly, the samples were incubated with 0.8% thiobarbituric acid (TBA) for 1 hour at 100°C and then centrifuged at 3500 rpm for 10 minutes. The amount of malondialdehyde (MDA), present as thiobarbituric acid reactive substances (TBARS) formed in the supernatant, was measured at 535 nm. The results are expressed as nmol per milligram of protein.

10. Sulfhydryls

The sulfhydryl content represents a non-enzymatic antioxidant defense, which is inversely correlated with oxidative damage to proteins. For this assay, 0.1 mM of 5,5'-dithiobis-2-nitrobenzoic acid (DTNB) was incubated with the samples for 30 minutes at room temperature, as described by Aksenov and Markesberry (23). The formation of TNB was measured spectrophotometrically at 412 nm and the results were expressed in nmol/mg protein.

11. Inflammatory cytokines

The levels of pro-inflammatory cytokines IL-1 β and IL-6 in the spinal cord tissue were measured using commercial Enzyme-linked immunosorbent assay (ELISA) kits (Boster), in accordance with the manufacturer's instructions.

12. Statistical analysis

Statistical analysis was performed using Prism9. Size, zeta potential and Pdl differences were compared by Student t-test. One-way analysis of variance (ANOVA) with Dunnett's multiple comparisons test was performed for statistical significance of MTT assay for cell viability. For comparison of the amount of live and dead cells, *in vitro* and *in vivo* ROS production, lipid peroxidation levels, antioxidant non-enzymatic defense, IL-1 β and IL-6 levels, one-way ANOVA with Tuckey's multiple comparisons was performed. Data are shown as mean \pm standard deviation. $p < 0.05$ was considered statistically significant. All the experiments were realized in triplicate.

Results

1. Characterization of the particles

The particle morphology was assessed with SEM. The PLGA particles presented a round to biconcave shape with a smooth surface (Figure 1). The addition of galantamine decreased the stability of the particle production, showing the presence of fibers, but the round to biconcave shape and smooth surface was maintained.

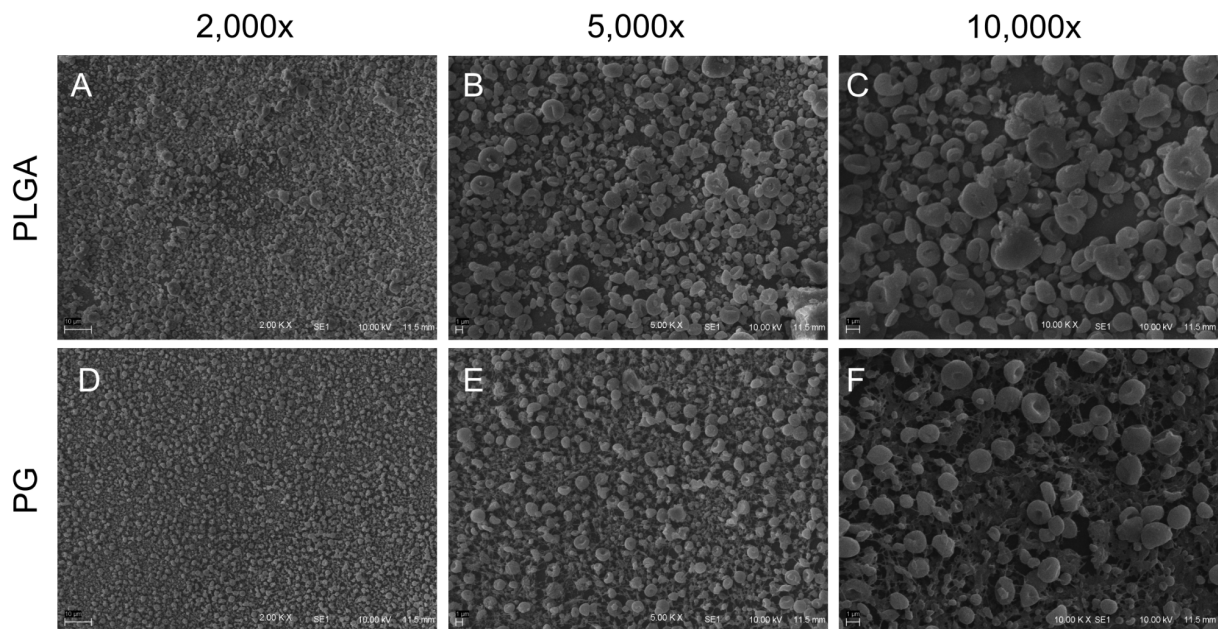


Figure 1. SEM analysis of PLGA particles (A - C) and PLGA particles containing galantamine (PG) (D - F). Magnifications were 2,000x (A and D), 5,000x (B and E) and 10,000x (C and F). Scale bar 10 μm (2,000x) and 1 μm (5,000 and 10,000x).

The PLGA particles presented an average diameter of 3247.58 nm, and the addition of galantamine significantly decreased the particle diameter to 568.27nm (Table 1). The PLGA particles had a zeta potential of -50.05 mV, indicating good stability, and the PG particles presented a significant decrease in potential, to a value of -23.59 mV. The polydispersity index of the PLGA particles was 0.715 ± 0.20 , while the PG particles had values of 0.586 ± 0.10 .

Table 1. Particle size, zeta potential and polydispersity index (Pdl)

| Sample | Diameter (nm) | Zeta potential (mV) | Pdl |
|---------|-------------------|---------------------|--------------|
| PLGA 4% | 3451.62 ± 1158.72 | -50.05 ± 11.89 | 0.715 ± 0.20 |
| PG | 568.27 ± 199.21* | -23.59 ± 5.27* | 0.586 ± 0.10 |

PLGA 4% - particles made of 4% poly(acid lactic-co-glycolic acid), PG - PLGA particles containing galantamine. Results are expressed as mean ± standard deviation. *p < 0.05 Student t-test (n = 4).

The galantamine release profile was assessed by HPLC. The encapsulation efficiency was 12.47% ± 8.29. As seen in Figure 2, the analysis showed a burst release in the first 6 hours, maintaining a relatively steady release for 35 days. At 35 days, out of 3.11 µg of encapsulated galantamine, approximately 1 µg was released.

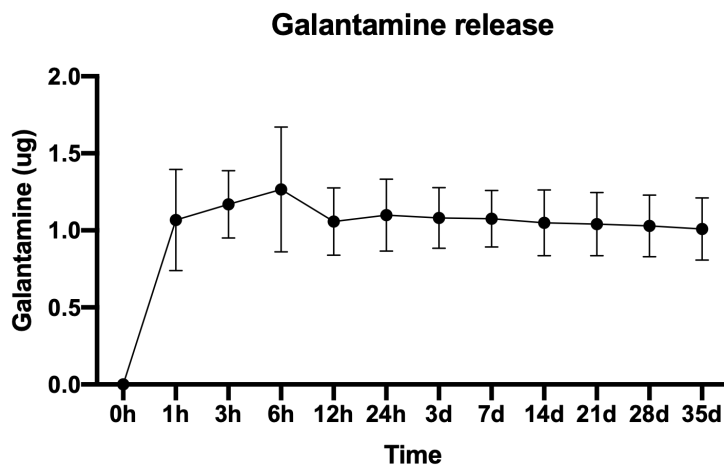


Figure 2. Release of galantamine from PG particles was analyzed by HPLC at different timepoints. Results are expressed as mean ± standard deviation. n = 3.

2. *In vitro* particle activity

In order to assess the neuroprotective potential of the particles and galantamine, the PC12 cells were pre-treated with hydrogen peroxide, following treatment with galantamine, PLGA particles or PG particles. Figure 3 shows that galantamine increased cell viability when compared to cells treated only with hydrogen peroxide, but neither treatment reduced the

production of ROS following peroxide treatment. Furthermore, galantamine, PLGA and PG particles did not alter cell viability on their own (Figure 3).

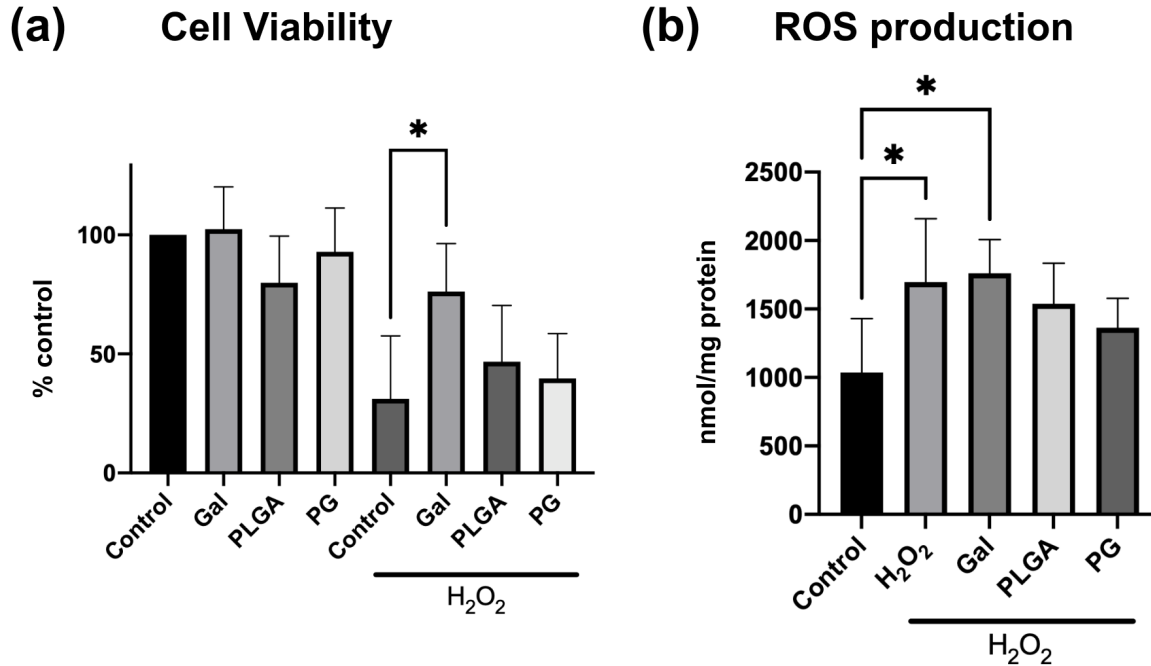


Figure 3. *In vitro* particle and galantamine effect on PC12 cells after H₂O₂ exposure. (a) Cell viability determined by MTT assay. **p* < 0.05, One-way ANOVA with Dunnett's multiple comparisons test (*n* = 5-6). (b) ROS production by DCF oxidation. **p* < 0.05 One-way ANOVA with Tuckey's multiple comparisons test (*n* = 3-6). Results are expressed as mean ± standard deviation. Control - cells only, Gal - cells treated with 5µg/ml galantamine, PLGA - cells treated with PLGA particles to a final concentration of 5µg/ml of PLGA, PG - cells treated with PLGA particles containing galantamine to a final concentration of 5µg/ml of galantamine. The H₂O₂ groups were co-treated with 200µM H₂O₂.

Further, the presence of live and dead cells was analyzed after treatment (Figures 4 and 5). The addition of H₂O₂ seems to decrease the number of live cells in all treatment groups, but there were no statistical differences in the percentage of live and dead cells in any treatment group. However, galantamine treatment after exposure to H₂O₂ showed a tendency of a decreased percentage of dead cells, corroborating with the MTT result.

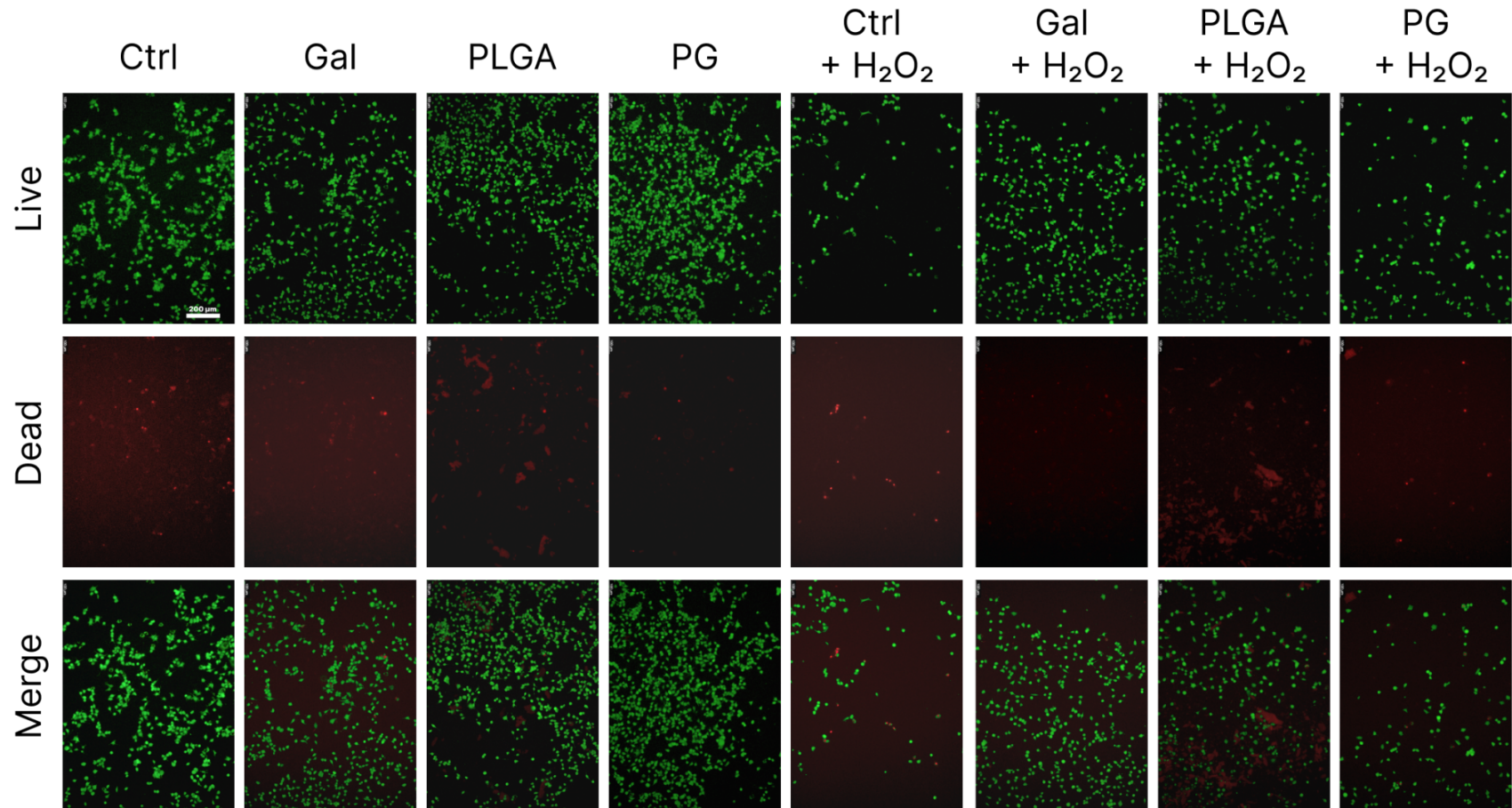


Figure 4. Effects of particles and galantamine treatment to PC12 cells evaluated by live/dead assay. Control - cells only, Gal - cells treated with 5μg/mL galantamine, PLGA - cells treated with PLGA particles to a final concentration of 5μg/mL of PLGA, PG - cells treated with PLGA particles containing galantamine to a final concentration of 5μg/mL of galantamine. The H₂O₂ groups were co-treated with 200μM H₂O₂.

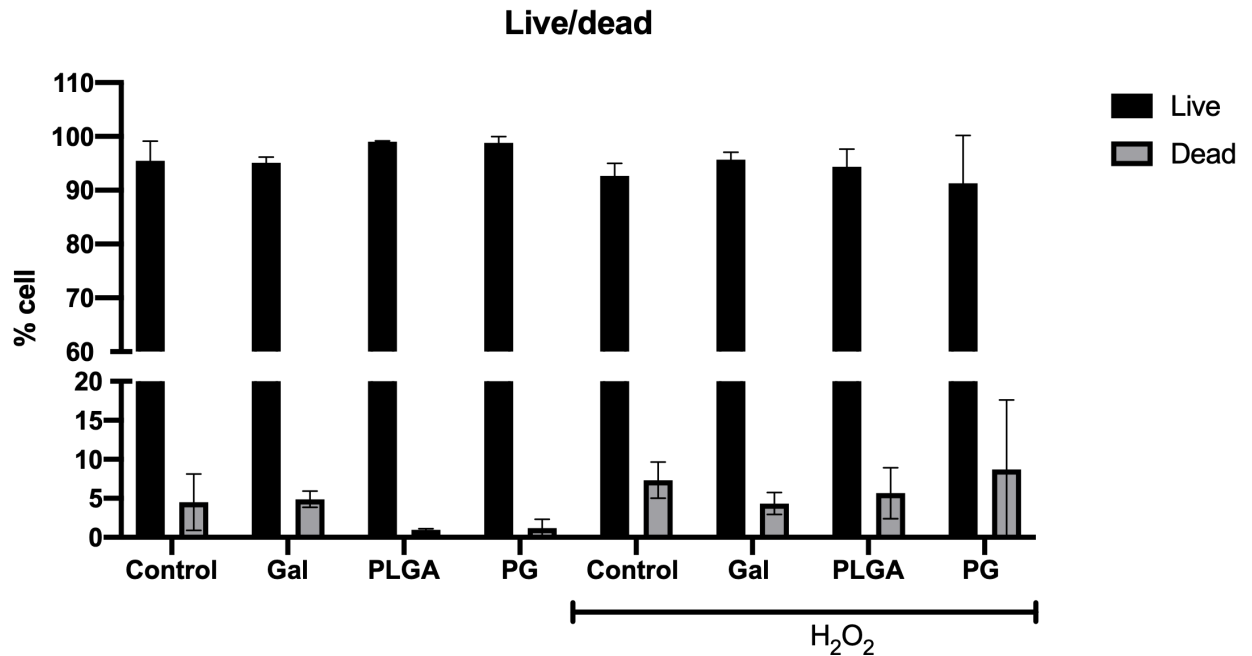


Figure 5. Quantification of live/dead assay using ImageJ. Control - cells only, Gal - cells treated with 5 μ g/mL galantamine, PLGA - cells treated with PLGA particles to a final concentration of 5 μ g/ml of PLGA, PG - cells treated with PLGA particles containing galantamine to a final concentration of 5 μ g/ml of galantamine. The H₂O₂ groups were co-treated with 200 μ M H₂O₂. One-way ANOVA with Tuckey's multiple comparison test of live cells between the treatment groups and dead cells between the treatment groups (n = 3). Results are expressed as mean \pm standard deviation.

3. Oxidative stress

The therapeutic potential of galantamine and PG was assessed in a contusion spinal cord injury model in rats, and its effects on oxidative stress and inflammation were evaluated 3 days after the injury, which corresponds to the subacute phase.

The group that received the PG particles showed a significant decrease in ROS production, and it was the only treatment able to reduce this production compared to the injury group. Moreover, the animals that were treated with galantamine and PG showed a significant reduction in lipid peroxidation levels compared to the injury group. However, neither the galantamine nor PG treatments increased the antioxidant defense, and galantamine seemed to significantly decrease the sulfhydryl content compared to the sham animals (Figure 6).

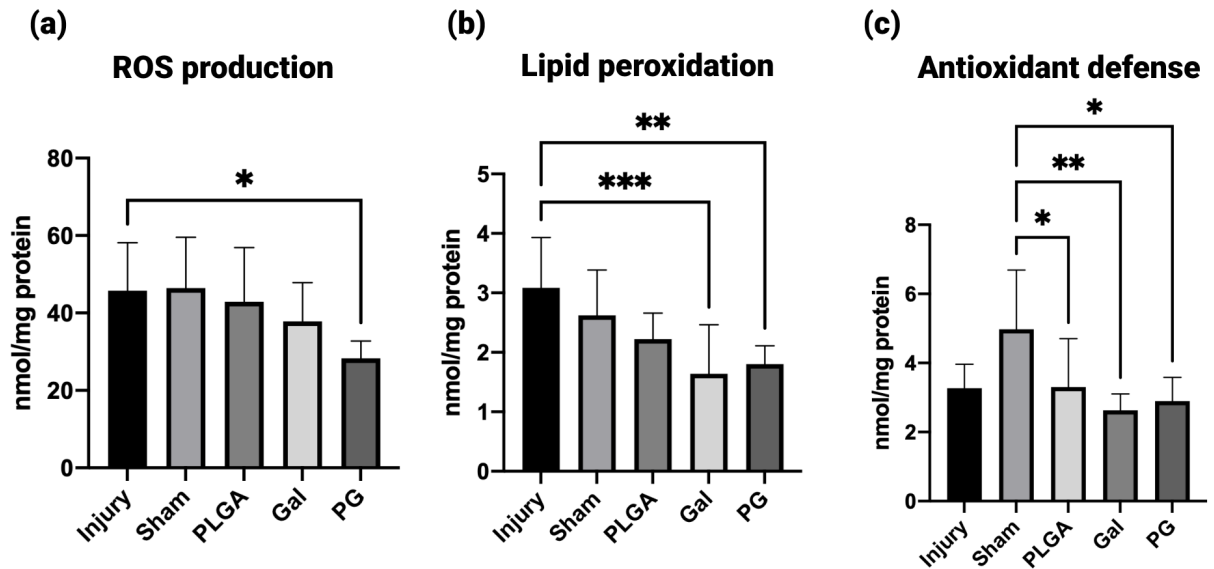


Figure 6. Oxidative stress analysis in spinal cord tissue 3 days after injury. (a) ROS production analyzed by DCF oxidation (b) Lipid peroxidation levels assessed by TBARS (c) Sulfhydryls analysis of antioxidant defense. Injury - animals with spinal cord injury (n = 9), Sham - animals that went through laminectomy (n = 8); PLGA - animals with SCI treated with PLGA particles (n = 8); Gal - animals with SCI treated with galantamine (n = 9); PG - animals with SCI treated with PLGA particles containing galantamine (n = 8). * $p < 0.05$; ** $p < 0.01$; *** $p < 0.005$. One-way ANOVA with Tuckey's multiple comparison test. Results are expressed as mean \pm standard deviation.

4. Inflammation

When assessing inflammation, the PG group presented significantly lower levels of IL-1 β when compared to the injury group. Interestingly, the PLGA group was the only treatment that significantly reduced IL-6 levels, presenting levels even lower than the sham group (Figure 7).

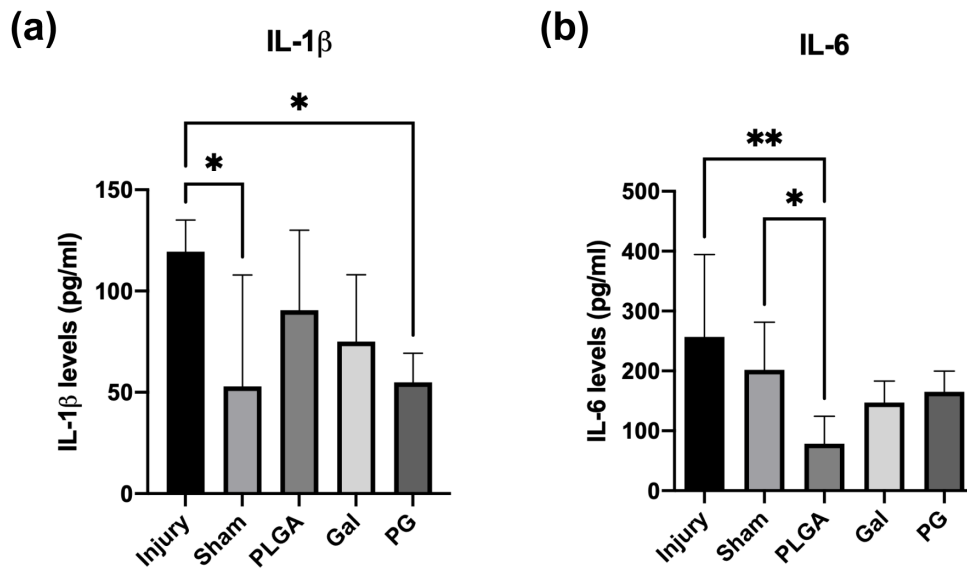


Figure 7. Dosage of Inflammatory cytokines analyzed by ELISA in spinal cord tissue 3 days after injury. (a) IL-1 β levels and (b) IL-6 levels Injury - animals with spinal cord injury (n = 8), Sham - animals that went through laminectomy (n = 7); PLGA - animals with SCI treated with PLGA particles (n = 8); Gal - animals with SCI treated with galantamine (n = 7); PG - animals with SCI treated with PLGA particles containing galantamine (n = 7). *p < 0.05; **p < 0.01. One-way ANOVA with Tuckey's multiple comparison test. Results are expressed as mean \pm standard deviation.

Discussion

Spinal cord injury is a complex neurological condition where several pathological processes are involved, making it difficult for a treatment to address all the molecular and cellular events that comprise this condition. Galantamine has been shown to have neuroprotective, anti-inflammatory and antioxidant effects in several neurological diseases (4), and has been demonstrated to improve functional recovery and decrease the lesion size 42 days after the injury (5). Polymeric nanoparticles drug delivery systems have the advantage of presenting a controlled drug release, leading to decreased side effects and increased bioavailability at the target tissue (24). Furthermore, due to the small size, they can be administered in several locations using a syringe needle. Using biodegradable materials, the drug is released as the polymer is being naturally degraded by the organism, and the degradation by-products are metabolized into water and CO₂ (25). Various other approaches for modulating neuroinflammation have been used, such as nanopolymers and liposomes for drug delivery and stem cell therapy (26–28).

Hence, in this work, we have aimed to investigate the molecular effects of this treatment 3 days after injury, where inflammation and oxidative stress play an important role in the physiopathology of SCI. Here, galantamine was administered directly at the lesion site, either in a solution form or in a nanoparticle drug delivery system.

The production of PLGA-galantamine particles by emulsion electrospray resulted in more irregular shaped and less stable production when compared to the PLGA particles alone. Rougher and more irregularly shaped particles were also produced by Yao and colleagues using water dissolved BSA in comparison to PLGA particles alone. In their work, it was demonstrated that the aqueous phase had a significant effect in particle morphology, where increasing the volume of the aqueous phase resulted in increased particle irregularity and decreased particle mean diameter (14). Because galantamine was dissolved in water prior to addition to the PLGA solution, there was an alteration in the electrostatics that can lead to these morphology differences.

In the present work, the addition of galantamine decreased particle size by 6-fold. Particle size is an important parameter, influencing *in vivo* distribution, drug release and stability of the particles. It has been demonstrated that smaller particles have higher cellular uptake and blood-brain barrier permeability, as well as faster drug release (24). However, the addition of galantamine also decreased the particles zeta potential, and the literature shows that particles with zeta potentials more than +25mV and less than -25mV present more stability, due to the decreased chance of aggregation (29). Still, the PG particles had a mean zeta potential of -23.59mV, which can still be considered acceptable. In addition, despite the decreased zeta potential, the PG particles presented a lower Pdl than the PLGA particles, demonstrating increased homogeneity of particle size distribution (30). The differences found here between PLGA particles and PG can be explained by the addition of water to the solution. It has been demonstrated that increasing the aqueous volume in particles produced by emulsion electrospray can lead to decreased mean particle diameter, since the particles can collapse in the drying process, which also explain the difference in Pdl (14). Collectively, these data demonstrate that the particles produced were suitable for *in vivo* administration.

Electrospraying is a method for producing particles that tends to present high encapsulation efficiency. However, for emulsion electrospray, the interface between the organic and aqueous phases can interfere in the encapsulation efficiency. In the present work, approximately 12% of galantamine was encapsulated. In the work from Yao and colleagues, it was observed that increasing the aqueous phase volume ratio led to more drug distribution at the surface of the particle, which could be lost while collecting the particles, hence presenting a

decreased encapsulation efficiency (14). This could explain the low encapsulation efficiency encountered in the galantamine particles, as there was a volume ratio of the aqueous drug phase to the organic PLGA phase of 25:1000. Considering that possibly most of the galantamine was distributed in the particle surface, this also explains the release profile, where burst release was attributed to the drug molecules being close to the particle surface (31). In SCI, inflammation starts within minutes after injury, and studies have identified the presence of IL-1 β and TNF- α starting after 5 and 15 minutes after injury, produced mainly by microglia and astrocytes (32). Hence, galantamine burst release during the first hour can be beneficial, acting during the first phases of inflammation and oxidative stress. Furthermore, in this work, galantamine was detected for up to 35 days, demonstrating that it could have long term therapeutic effects.

The therapeutic effect of galantamine particles and galantamine alone has been assessed in the present study both *in vitro* and *in vivo*. The *in vitro* analysis showed the neuroprotective effect of galantamine before exposure to hydrogen peroxide in the MTT assay. The live/dead analysis did not show significant differences in any of the treatment groups, although there was a tendency of a decreased number of dead cells in the group treated with galantamine after H₂O₂ exposure. This effect was also seen in SK-N-SH cells exposed to hydrogen peroxide for 2 hours, where pretreatment with galantamine led to increased cell viability. This study has shown that galantamine exerts an antioxidant effect by several mechanisms, such as decreasing reactive oxygen and nitrogen species, prevention of membrane disturbances and loss of mitochondrial membrane potential, increasing acetylcholine availability and allosteric activation of nAChR $\alpha 7$ (33). However, here, ROS production did not change with the galantamine or PG treatment, which could be due to a longer exposure to hydrogen peroxide. It is important to note that in this experimental setting of 24 hour treatment, the PG did not present any significant effect after hydrogen peroxide exposure. Although most of the galantamine is released in the first six hours, considering the low encapsulation efficiency, the galantamine concentration when administered freely was much higher than in the PG.

In vivo, the intraparenchymal administration of galantamine and PG particles at the lesion site was evaluated 3 days after the injury. This time point is usually considered to be the acute to early subacute phase (34–36), which is characterized by inflammatory infiltration, with a peak of neutrophils and the beginning of monocyte infiltration and high levels of ROS, IL-1 β and IL-6 (3). Contrary to the *in vitro* results, only the nanoparticles were able to significantly reduce the production of ROS, whereas both forms decreased lipid peroxidation. Neither treatment forms, however, significantly altered the sulfhydryl content, which corresponds to the antioxidant

defense. Several studies have reported galantamine antioxidant effects, and it has been shown that it decreased oxidative stress when administered orally in a pre-plaque stage mice model of Alzheimer's disease (37). Furthermore, intraperitoneal galantamine administration prior to hypoxia exposure of neonatal rats increased neuron survival and catalase activity, but did not alter ROS levels (38). Considering the galantamine release profile of the PG particles, the 3-day period after the administration of the treatment presented a sustained release of the drug, which could still have been acting as a ROS scavenger at this time point. Conversely, galantamine administered freely could be rapidly degraded. Indeed, plasma half-life of galantamine administered IV is 3.5 hours in rat males (39). Hence, although the first hours after the injury are critical for the development of secondary injury, having a drug delivery system that continuously releases galantamine at the injury site seems to have beneficial effects on oxidative parameters at the acute phase of SCI. This is also true for IL-1 β levels, where the PG presented a significant decrease in these cytokine levels, demonstrating decreased inflammation. Galantamine anti-inflammatory activity has already been described in the literature, due to its $\alpha 7$ nAChR allosteric activation mechanism and AChE inhibition. Intraperitoneal administration of galantamine prior to LPS intracerebroventricular injection significantly reduced the expression of IL-1 β , IL-6 and TNF- α and prevented cognitive deficits in mice, showing the important role of galantamine in neuroinflammation (40). In addition, in a newborn rat model of hypoxia-ischemia, pre-treatment with galantamine significantly reduced IL-1 β protein levels (41).

Interestingly, animals treated with PLGA particles alone presented a significant decrease in IL-6 levels, whereas the presence of galantamine did not significantly alter the levels of this cytokine. PLGA is rapidly degraded in the organism into lactic acid and glycolic acid (42), and the PLGA used in this study had a 75:25 ratio of acid lactic to acid glycolic. It has been reported that lactic acid produced by tumor cells has a critical role in M2 polarization of tumor-associated macrophages, and the role of a hypoxia-lactate axis in inflammation and in macrophage polarization has recently risen (43,44). Thus, it is possible that due to PLGA degradation into lactate, the PLGA particles alone exerted an anti-inflammatory effect. This could also potentiate the anti-inflammatory effect of galantamine in the PG particles treatment.

Conclusion and future perspectives

In the present study, we have demonstrated the anti-inflammatory and antioxidant effect of galantamine in the acute phase of spinal cord injury. The administration of galantamine in the form of nanoparticles showed beneficial effects in comparison to administering galantamine freely at the injury site, with significant reduction of ROS production, lipid peroxidation and IL-1 β

levels. Galantamine showed substantial promise as a neuroprotective agent during acute SCI. However, the long-term effects of this treatment remain to be elucidated, including the possible locomotor effects. Since many times the efficacy of the treatment is dependent on the timing of the drug administration, further studies are necessary to determine the functional window and the most effective dosage. Another critical question to be addressed is the dosage.

Acknowledgements

Funding sources: CNPq, FINEP, FAPERGS, IPCT, MCTIC

References

1. Uyeda A, Muramatsu R. Molecular Mechanisms of Central Nervous System Axonal Regeneration and Remyelination: A Review. *Int J Mol Sci.* 2020 Oct 30;21(21):8116.
2. Kjell J, Olson L. Rat models of spinal cord injury: from pathology to potential therapies. *Dis Model Mech.* 2016 Oct 1;9(10):1125–37.
3. Donnelly DJ, Popovich PG. Inflammation and its role in neuroprotection, axonal regeneration and functional recovery after spinal cord injury. *Exp Neurol.* 2008 Feb;209(2):378–88.
4. Metz CN, Pavlov VA. Treating disorders across the lifespan by modulating cholinergic signaling with galantamine. *J Neurochem.* 2021 Sep;158(6):1359–80.
5. Sperling LE, Pires Reis K, Nicola F, Euzebio Teixeira C, Gulielmin Didó G, Garrido dos Santos M, et al. Galantamine improves functional recovery and reduces lesion size in a rat model of spinal cord injury. *Brain Res.* 2019 Dec;1724:146424.
6. Edlund, U AAC. Degradable Polymer Microspheres for Controlled Drug Delivery. In: Degradable aliphatic polyesters. Berlin ; New York: Springer; 2002. p. 67–112. (Advances in polymer science).
7. Chakraborty A, Ciciriello AJ, Dumont CM, Pearson RM. Nanoparticle-based delivery to treat spinal cord injury - a mini-review. *AAPS PharmSciTech.* 2021 Mar 12;22(3):101.
8. Petros RA, DeSimone JM. Strategies in the design of nanoparticles for therapeutic applications. *Nat Rev Drug Discov.* 2010 Aug;9(8):615–27.
9. El-Say KM, El-Sawy HS. Polymeric nanoparticles: Promising platform for drug delivery. *Int J Pharm.* 2017 Aug;528(1–2):675–91.
10. Kreuter J. Drug delivery to the central nervous system by polymeric nanoparticles: What do we know? *Adv Drug Deliv Rev.* 2014 May;71:2–14.
11. Fredenberg S, Wahlgren M, Reslow M, Axelsson A. The mechanisms of drug release in poly(lactic-co-glycolic acid)-based drug delivery systems—A review. *Int J Pharm.* 2011 Aug;415(1–2):34–52.
12. Kim Y tae, Caldwell JM, Bellamkonda RV. Nanoparticle-mediated local delivery of methylprednisolone after spinal cord injury. *Biomaterials.* 2009 May;30(13):2582–90.
13. Ren H, Han M, Zhou J, Zheng ZF, Lu P, Wang JJ, et al. Repair of spinal cord injury by inhibition of astrocyte growth and inflammatory factor synthesis through local delivery of flavopiridol in PLGA nanoparticles. *Biomaterials.* 2014 Aug;35(24):6585–94.
14. Yao S, Liu H, Yu S, Li Y, Wang X, Wang L. Drug-nanoencapsulated PLGA microspheres prepared by emulsion electrospray with controlled release behavior. *Regen Biomater.* 2016 Oct;3(5):309–17.
15. Karimi Zarchi AA, Abbasi S, Faramarzi MA, Gilani K, Ghazi-Khansari M, Amani A. Development and optimization of N-Acetylcysteine-loaded poly (lactic-co-glycolic acid)

- nanoparticles by electrospray. *Int J Biol Macromol*. 2015 Jan;72:764–70.
16. Bock N, Dargaville TR, Woodruff MA. Electrospraying of polymers with therapeutic molecules: State of the art. *Prog Polym Sci*. 2012 Nov;37(11):1510–51.
 17. Constantini S, Young W. The effects of methylprednisolone and the ganglioside GM1 on acute spinal cord injury in rats. *J Neurosurg*. 1994 Jan;80(1):97–111.
 18. Young W. Chapter 17 Spinal cord contusion models. In: *Progress in Brain Research* [Internet]. Elsevier; 2002 [cited 2022 Jun 8]. p. 231–55. Available from: <https://linkinghub.elsevier.com/retrieve/pii/S0079612302370195>
 19. Nicola F, Marques MR, Odorcyk F, Petenuzzo L, Aristimunha D, Vizuete A, et al. Stem Cells from Human Exfoliated Deciduous Teeth Modulate Early Astrocyte Response after Spinal Cord Contusion. *Mol Neurobiol*. 2019 Jan;56(1):748–60.
 20. Lowry Oliver H, Rosebrough Nira J, Farr AL, Randall Rose J. Protein measurement with the Folin phenol reagent. *J Biol Chem*. 1951 Nov;193(1):265–75.
 21. Wang H, Joseph JA. Quantifying cellular oxidative stress by dichlorofluorescein assay using microplate reader. :5.
 22. Buege JA, Aust SD. [30] Microsomal lipid peroxidation. In: *Methods in Enzymology* [Internet]. Elsevier; 1978 [cited 2022 May 16]. p. 302–10. Available from: <https://linkinghub.elsevier.com/retrieve/pii/S0076687978520326>
 23. Aksenov MY, Markesbery WR. Changes in thiol content and expression of glutathione redox system genes in the hippocampus and cerebellum in Alzheimer's disease. *Neurosci Lett*. 2001 Apr;302(2–3):141–5.
 24. Singh R, Lillard JW. Nanoparticle-based targeted drug delivery. *Exp Mol Pathol*. 2009 Jun;86(3):215–23.
 25. Park J, Ye M, Park K. Biodegradable Polymers for Microencapsulation of Drugs. *Molecules*. 2005 Jan 31;10(1):146–61.
 26. dos Santos MG, Prestes JP, Pranke P. Nanopolymers: Powerful Tools in Neuroprotection and Neuroregeneration. *Curr Nanosci*. 2022 Nov;18(6):668–74.
 27. Wang YR, Mao XF, Wu HY, Wang YX. Liposome-encapsulated clodronate specifically depletes spinal microglia and reduces initial neuropathic pain. *Biochem Biophys Res Commun*. 2018 May;499(3):499–505.
 28. Joshi HP, Jo HJ, Kim YH, An SB, Park CK, Han I. Stem Cell Therapy for Modulating Neuroinflammation in Neuropathic Pain. *Int J Mol Sci*. 2021 May 3;22(9):4853.
 29. Mothilal M, Krishna MC, Teja SPS, Manimaran V, Damodharan N. Formulation and evaluation of naproxen-eudragit® RS 100 nanosuspension using 32 factorial design. 6(7):8.
 30. Danaei M, Dehghankhold M, Ataei S, Hasanzadeh Davarani F, Javanmard R, Dokhani A, et al. Impact of Particle Size and Polydispersity Index on the Clinical Applications of Lipidic Nanocarrier Systems. *Pharmaceutics*. 2018 May 18;10(2):57.
 31. Wang J, Wang BM, Schwendeman SP. Characterization of the initial burst release of a model peptide from poly(d,l-lactide-co-glycolide) microspheres. *J Controlled Release*. 2002 Aug;82(2–3):289–307.
 32. Pineau I, Lacroix S. Proinflammatory cytokine synthesis in the injured mouse spinal cord: Multiphasic expression pattern and identification of the cell types involved. *J Comp Neurol*. 2007 Jan 10;500(2):267–85.
 33. Ezoulin M. Antioxidative properties of galantamine on neuronal damage induced by hydrogen peroxide in SK–N–SH cells. *NeuroToxicology*. 2008 Mar;29(2):270–7.
 34. James ND, Bartus K, Grist J, Bennett DLH, McMahon SB, Bradbury EJ. Conduction Failure following Spinal Cord Injury: Functional and Anatomical Changes from Acute to Chronic Stages. *J Neurosci*. 2011 Dec 14;31(50):18543–55.
 35. Ahuja CS, Wilson JR, Nori S, Kotter MRN, Druschel C, Curt A, et al. Traumatic spinal cord injury. *Nat Rev Dis Primer*. 2017 Dec 21;3(1):17018.
 36. Zrzavy T, Schwaiger C, Wimmer I, Berger T, Bauer J, Butovsky O, et al. Acute and

- non-resolving inflammation associate with oxidative injury after human spinal cord injury. *Brain*. 2021 Feb 12;144(1):144–61.
37. Saito T, Hisahara S, Iwahara N, Emoto MC, Yokokawa K, Suzuki H, et al. Early administration of galantamine from preplaque phase suppresses oxidative stress and improves cognitive behavior in APP^{swe}/PS1^{dE9} mouse model of Alzheimer's disease. *Free Radic Biol Med*. 2019 Dec;145:20–32.
38. Odorczyk FK, Nicola F, Duran-Carabali LE, Figueiró F, Kolling J, Vizúete A, et al. Galantamine administration reduces reactive astrogliosis and upregulates the anti-oxidant enzyme catalase in rats submitted to neonatal hypoxia ischemia. *Int J Dev Neurosci*. 2017 Nov;62(1):15–24.
39. Beijsterveldt L, Geerts R, Verhaeghe T, Willems B, Bode W, Lavrijsen K, et al. Pharmacokinetics and Tissue Distribution of Galantamine and Galantamine-related Radioactivity after Single Intravenous and Oral Administration in the Rat. *Arzneimittelforschung*. 2011 Dec 25;54(02):85–94.
40. Liu Y, Zhang Y, Zheng X, Fang T, Yang X, Luo X, et al. Galantamine improves cognition, hippocampal inflammation, and synaptic plasticity impairments induced by lipopolysaccharide in mice. *J Neuroinflammation*. 2018 Dec;15(1):112.
41. Furukawa S, Yang L, Sameshima H. Galantamine, an acetylcholinesterase inhibitor, reduces brain damage induced by hypoxia-ischemia in newborn rats. *Int J Dev Neurosci*. 2014 Oct;37(1):52–7.
42. Su Y, Zhang B, Sun R, Liu W, Zhu Q, Zhang X, et al. PLGA-based biodegradable microspheres in drug delivery: recent advances in research and application. *Drug Deliv*. 2021 Jan 1;28(1):1397–418.
43. Colegio OR, Chu NQ, Szabo AL, Chu T, Rhebergen AM, Jairam V, et al. Functional polarization of tumour-associated macrophages by tumour-derived lactic acid. *Nature*. 2014 Sep;513(7519):559–63.
44. Ivashkiv LB. The hypoxia–lactate axis tempers inflammation. *Nat Rev Immunol*. 2020 Feb;20(2):85–6.

Artigo 2.

Long-term effects of galantamine particles implantation in a rat model of spinal cord injury

Fernanda Staphenhorst Franca^{1,2}, Laura Sperling^{1,2}, Marcelo Garrido^{1,2}, Luiz Sommer^{1,2}, Cristian Teixeira^{1,2}, João Pedro da Rocha Prestes^{1,2}, Patrick Turck³, Adriane Bello Klein³, Patricia Pranke⁴

¹Hematology and Stem Cell Laboratory, Faculty of Pharmacy, Universidade Federal do Rio Grande do Sul; ²Stem Cell Laboratory, Fundamental Health Sciences Institute, Universidade Federal do Rio Grande do Sul; ³Laboratory of Cardiovascular Physiology and Reactive Oxygen Species, Institute of Basic Health Sciences, Universidade Federal do Rio Grande do Sul;

⁴Instituto de Pesquisa com Células-tronco (IPCT). Porto Alegre, RS, Brazil

Artigo a ser submetido no periódico Neuroscience Letters (Fator de impacto 3.197)

Abstract

Galantamine is an acetylcholinesterase inhibitor and a nicotinic $\alpha 7$ receptor allosteric modulator that has been used for Alzheimer's treatment and is currently being studied for several neurological conditions. Previous studies have shown that intraperitoneal galantamine administration leads to motor improvement in rats after spinal cord injury (SCI), however, the need of repeated dosing and cholinergic side effects of galantamine are the major hurdles for the optimum usage of this drug. Hence, the aim of this study was to assess long term effects of galantamine nanoparticles in a rat model of SCI. The animals were submitted to a contusion SCI and either galantamine, poly (lactic acid-co-glycolic acid) (PLGA) particles or PLGA particles containing galantamine (PG) was administered at the lesion site. The animals' locomotion was evaluated weekly for 6 weeks using the Basso, Beattie and Bresnahan (BBB) locomotor scale. After 6 weeks, the spinal cords were collected and analyzed for oxidative stress parameters, such as reactive oxygen species (ROS) production, lipid peroxidation and non-enzymatic antioxidant defense, as well as for the production of inflammatory cytokines IL-1 and IL-6. Further, morphological analyses were performed by hematoxylin-eosin staining. The animals that received PG were the only group that showed significantly improved motor function in comparison to the injury group. In addition, both PG and galantamine reduced ROS production,

but only PG was able to decrease IL-1 levels. Interestingly, the PLGA group significantly reduced IL-6 levels, showing a possible anti-inflammatory effect of PLGA. Collectively, the data indicate that the use of galantamine nanoparticles leads to important functional, antioxidant and anti-inflammatory effects, being a promising therapeutic approach for SCI.

1. Introduction

Spinal cord injury (SCI) is a debilitating condition, leading to severe consequences to the patients, such as paralysis. After the primary injury, that is most commonly caused by compression, a series of secondary injury events initiate [1]. Collectively, the pathophysiology of SCI can be temporally classified in acute (up to 48 hours), subacute (48 hours to 14 days), intermediate (14 days to 6 months) and chronic (over 6 months) phases [2].

Inflammation takes place within minutes of injury, due to the initial destruction of the microvasculature, leading to an influx of proinflammatory cytokines and inflammatory cells, which remain at the injury site beyond the subacute phase [2]. This inflammatory response is mainly innate, where microglia, astrocytes, neurons and oligodendrocytes secrete proinflammatory cytokines, particularly IL-1, TNF- α and IL-6, recruiting peripheral immune cells [3]. Within hours, neutrophils enter the spinal cord, peaking at 24 hours and decreasing after 3 days in rodents, while monocytes and macrophages enter the spinal cord at 3 to 4 days and persist at the injury site indefinitely [4,5].

These inflammatory cells produce reactive species such as superoxide anion and nitric oxide, and other free radicals are formed due to mitochondrial dysfunction and the disruption of calcium homeostasis. Importantly, the neurons and glial cells are especially prone to oxidative stress due to the high content of polyunsaturated fatty acids and high metabolic activity [4,6]. Hence, oxidative stress, particularly lipid peroxidation, is a hallmark in secondary SCI, leading to important cell death [7].

In the context of inflammation, the cholinergic anti-inflammatory pathway presents as a possible therapeutic target. This pathway was first described in 2000 by Borovikova and colleagues in a study where the authors observed that acetylcholine decreased the release of inflammatory cytokines in a macrophage culture stimulated by lipopolysaccharide (LPS), and that, *in vivo*, vagus nerve stimulation led to decreased systemic TNF levels in rats exposed to lethal doses of LPS [8]. This effect was later discovered to be mediated through the $\alpha 7$ nicotinic acetylcholine receptor ($\alpha 7$ nAChR), which is expressed in the CNS in neurons and glia, in which it is involved in learning and memory processes, and has anti-inflammatory effects in

monocytes, macrophages, microglia and also in astrocytes [9,10]. In microglia, it has been demonstrated that activation of $\alpha 7$ nAChR leads to the transformation of M1 phenotype to M2, shifting from an inflammatory phenotype to an anti-inflammatory one [10].

Hence, considering the neuroprotective effects of $\alpha 7$ nAChR, the use of agonists for this receptor may be a therapeutic strategy for neurological conditions. Galantamine is an $\alpha 7$ nAChR allosteric modulator that also acts as an acetylcholinesterase inhibitor, and it is currently used in mild to moderate Alzheimer's disease patients to treat cognitive impairments. As recently reviewed by Metz and Pavlov, galantamine has been studied in pre-clinical and animal model studies for several neurological conditions, including spinal cord injury, in which intraperitoneal administration led to improved motor functional recovery and decreased lesion size [11,12].

One of the hurdles of systemic drug administration is the decreased bioavailability of the drugs in the target tissue and increased side effects. In the case of galantamine, it has been shown to have gastrointestinal effects and decreased brain bioavailability when administered orally [13,14]. In this context, controlled drug release delivery systems have several advantages, presenting the possibility of increased therapeutic efficiency, decreased drug administration frequency and decreased side effects [15]. One of the possibilities is the use of polymeric nano or microparticles, which can be produced using electrospraying. In a previous study from our group, polymeric galantamine nanoparticles were produced and characterized, and their effects were evaluated *in vitro* and in an *in vivo* model of acute SCI, 3 days after the injury. In that time point, the galantamine particles decreased ROS production, lipid peroxidation and IL-1 levels [16].

In the present work, we evaluated the effects of galantamine nanoparticles treatment 6 weeks after a contusion spinal cord injury in rats. We assessed the animals locomotor recovery after the treatment, as well as oxidative, inflammatory and histological parameters.

2. Methods

2.1. Animal care and spinal cord injury

The experimental protocols were approved by the Institutional Animal Care and Use Committee of the Universidade Federal do Rio Grande do Sul (Porto Alegre, Brazil - CEUA project number 35781). A total of 43 adult male Wistar rats (8-9 weeks old, 250–300 g) raised at the animal facility of the Federal University of Rio Grande do Sul were used in this study. The rats were housed in groups of two to four at a 12 hour light/dark cycle with food and water available *ad libitum*. All surgical procedures were performed under general anesthesia with 75 mg/kg intraperitoneal ketamine mixed with 5 mg/kg xylazine, administering a 50% supplemental

single dose of ketamine whenever necessary. The spinal cord was exposed through laminectomy at T-10, and a 10g rod was dropped from a height of 12.50 cm directly onto the cord using the NYU MASCIS (New York University, Multicenter Animal Spinal Cord Injury Study) impactor [17–19]. After the contusion, the treatments were applied at the lesion site in an intraparenchymal manner in the spinal cord. Afterwards, the muscles and skin were sutured and the animals were kept at 37°C with the aid of a thermal pad. Antibiotics (Baytril, 10 mg/kg) was administered intraperitoneally immediately after surgery and daily for 5 days. The analgesic tramadol was administered subcutaneously after surgery and at 8 and 16 hours post-surgery. The bladders were manually emptied, twice daily, until the recovery of spontaneous micturition

2.2 Treatments

The animals were divided in 5 groups: Sham, that had a laminectomy procedure, but with no injury; spinal cord Injury, that received 10ul of saline at the injury site; Galantamine, that received 10ul of a solution containing 2.5ug of galantamine at the injury site; PLGA, that received 10ul of a solution containing 0.2mg of PLGA particles at the injury site; and PG, that received 10ul of a solution of 0.2 mg of PLGA particles containing 2.5ug of galantamine at the injury site (PG group).

2.3. Locomotor analysis

Motor behavior was evaluated weekly by two blinded observers using the Basso, Beattie and Bresnahan (BBB) locomotor rating scale [20] (n = 6 for the injury group, n = 7 for sham, n = 9 for galantamine treatment, n = 4 for PLGA particles treatment and n = 7 for PG particles group). The sham group did not show any alteration of motor behavior. Animals were free to move in an open-field (1m diameter) and analyzed following criteria such as extent of joint movements, weight support ability and stepping/walking behavior of the hind limbs. Functional scores ranging from 0 (no observable hind limb movement) to 21 (normal locomotion) were assigned for both hind limbs by two observers, independently. The mean value of both hind limbs was calculated. Scoring was performed for a period of 4 min in accordance with the guidelines of the Spinal Cord Injury Project (WM Keck Center for Collaborative Neuroscience, Rutgers State University of NJ, USA)

2.4. Transcardiac perfusion and tissue fixation

Six weeks after the injury, the animals were transcardially perfused with isotonic saline followed by 4% paraformaldehyde in 0.1 M, pH 7.4 phosphate buffer (0.8 mL of perfusion

solution per gram of body weight). The spinal cord was removed, immersed in 25% sucrose for 48 h and processed for hematoxylin and eosin (HE) staining. A 1.5 cm length of the spinal cord centered at the injury site was separated and embedded in tissue-embedding medium (Tissue Tek). Cryostat sections (20 μ m) were cut and mounted onto gelatin-treated slides and stored at -80°C until further processing.

2.5. Spinal cord tissue preparation

The spinal cord tissue was weighed and homogenized using phenyl methyl sulphonyl fluoride (PMSF) 20 mmol/l and 1.15% w/v KCl in a Potter-Elvehjem homogenizer. The suspension was centrifuged at 1000 g for 20 min at $4-5^{\circ}\text{C}$ and the supernatants were collected.

2.6. Oxidative stress analysis

2.6.1. Protein concentration

Total proteins were quantified using the Lowry method [21]. Bovine serum albumin was used as the standard and this was used to express the results.

2.6.2. ROS levels quantification

ROS levels in the spinal cord tissue were measured by quantifying the fluorescence of the oxidation of 2',7'-dichlorofluorescein diacetate (DCFH-DA) (Sigma-Aldrich, USA) by the ROS present in the sample. The samples were incubated with DCFH-DA for 1h. A standard curve with known concentrations of 2',7'-dichlorofluorescein (DCF) was used. The samples were excited at 488 nm; emission was collected with a 525-nm long-pass filter and expressed as nmol/mg protein [22].

2.6.3. Lipid peroxidation analysis

The formation of TBARS during an acid-heating reaction was measured as previously described [23] and it was used as an index of lipid peroxidation. Briefly, the samples were incubated with 0.8 % thiobarbituric acid (TBA) for 1h at 100°C and then centrifuged at 3500 rpm for 10 minutes. The amount of malondialdehyde (MDA), present as thiobarbituric acid reactive substances (TBARS) formed in the supernatant, was measured at 535 nm. The results are expressed as nmol per milligram of protein.

2.6.4. Sulfhydryls

Sulfhydryl content represents a non-enzymatic antioxidant defense, which is inversely correlated with oxidative damage to proteins. For this assay, 0.1 mM of 5,5'-dithiobis-2-nitrobenzoic acid (DTNB) was incubated with the samples for 30 min at room temperature as described by Aksenov and Markesberry [24]. The formation of TNB was measured spectrophotometrically at 412 nm and the results were expressed in nmol/mg protein.

2.7. Inflammatory cytokines evaluation

The levels of pro-inflammatory cytokines IL-1 β and IL-6 in the spinal cord tissue were measured using commercial Enzyme-linked immunosorbent assay (ELISA) kits (Boster) according to the manufacturer's instructions.

2.8. Hematoxylin and eosin staining

The longitudinal and transverse cryostat sections were stained with hematoxylin and eosin following standard procedures and photographed using a Zeiss Imager M2 equipped with an AxioCam MRC.

2.9 Statistical analysis

Statistical analysis was performed using Prism9. Two-way analysis of variance (ANOVA) with Tuckey's multiple comparisons test was used to assess the significance of the treatments over the different time points. For comparison of ROS production, lipid peroxidation levels, antioxidant non-enzymatic defense, IL-1 β and IL-6 levels, one-way ANOVA with Tuckey's multiple comparisons was performed. Data are shown as mean \pm standard deviation. $p < 0.05$ was considered statistically significant. All the experiments were realized in triplicate.

3. Results

3.1. Motor recovery

Galantamine, PLGA and PG particles were administered at the lesion site after the injury. The animals' locomotion was analyzed weekly for six weeks. All animals showed spontaneous recovery, but after 42 days only the animals treated with PG presented a significant improvement in motor function, with a mean score of 11.5, compared to the control group score of 7.25 ($p < 0.05$, two-way ANOVA, Tuckey's multiple comparisons test) (Figure 1).

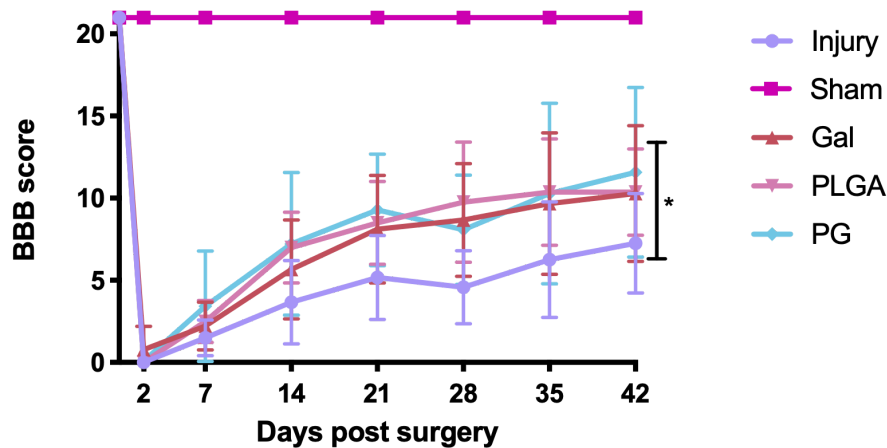


Figure 1. BBB rating scale ranges from a minimum of 0 (no observable hind limb movements) to a maximum of 21 (normal walking). An improvement of hind limb motor function in the PG treated group in comparison with the control group was observed. Injury - animals with spinal cord injury (n = 6), Sham - animals that went through laminectomy (n = 5); PLGA - animals with SCI treated with PLGA particles (n = 4); Gal - animals with SCI treated with galantamine (n = 9); PG - animals with SCI treated with PLGA particles containing galantamine (n = 7). Values represent mean \pm SEM. * $p < 0.05$, two-way ANOVA with Tuckey's multiple comparisons test.

3.2. Oxidative stress after spinal cord injury

Six weeks after the injury, the animals were euthanized and the spinal cords were collected for analysis. Both PG and galantamine were able to decrease ROS production in comparison to the injury group (Figure 2A), and none of the treatments showed differences in lipid peroxidation levels. Furthermore, galantamine was the only group that led to an increase in antioxidant defense levels compared to the injury group (Figure 2C).

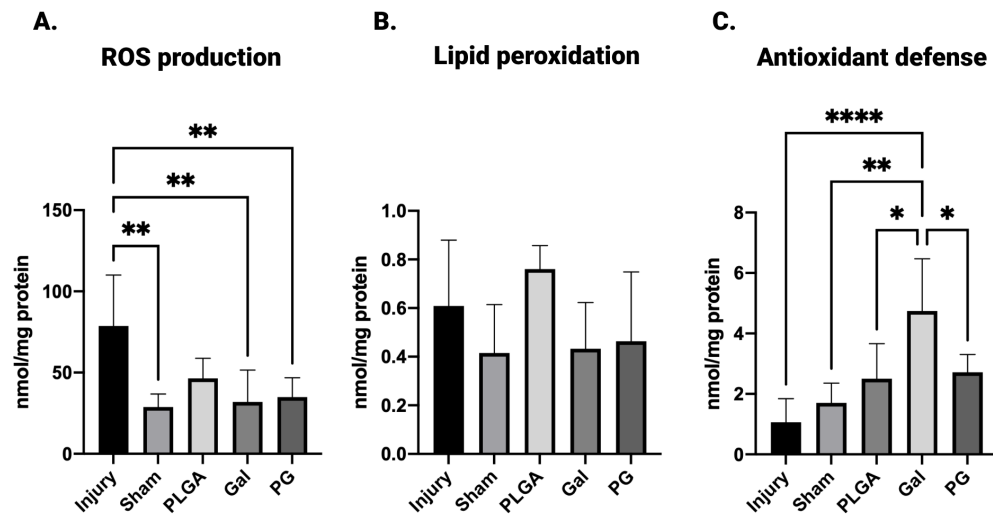


Figure 2. Oxidative stress analysis. (A) DCF analysis showing a decrease in ROS production for the groups treated with galantamine and PG, as well as the sham group, compared to the injury group. (B) TBARS analysis showed no significant differences in lipid peroxidation levels for any of the treatment groups. (C) Sulfhydryls quantification demonstrated an increase in the antioxidant defense levels in the animals treated with galantamine compared to all the other groups. Injury - animals with spinal cord injury ($n = 6$), Sham - animals that went through laminectomy ($n = 5$); PLGA - animals with SCI treated with PLGA particles ($n = 4$); Gal - animals with SCI treated with galantamine ($n = 9$); PG - animals with SCI treated with PLGA particles containing galantamine ($n = 7$). * $p < 0.05$, ** $p < 0.01$, **** $p < 0.0001$. One-way ANOVA with Tuckey's multiple comparison test. Results are expressed as mean \pm standard deviation.

3.3. Inflammation after Spinal cord injury

When analyzing inflammation, PG was the only group that significantly decreased IL-1 β levels compared to the injury group. Interestingly, animals treated with PLGA alone were the only group that significantly decreased IL-6 levels, and presented the smallest IL-6 levels of all groups, including sham (Figure 3).

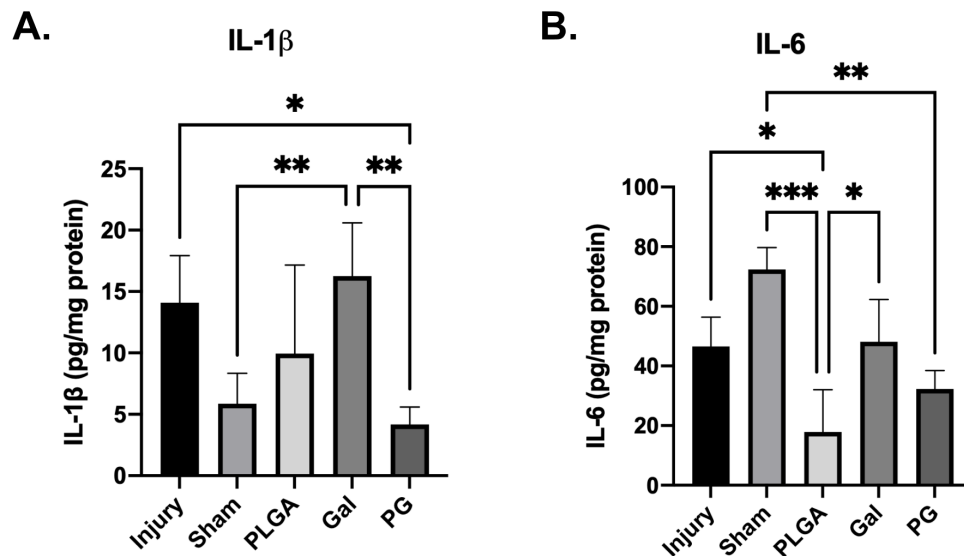


Figure 3. Inflammatory cytokines levels. (A) IL-1 β levels in animals treated with PG are significantly reduced when compared to the injury group. (B) IL-6 levels were significantly decreased in animals treated with PLGA in comparison to the injury group. Injury - animals with spinal cord injury (n = 6), Sham - animals that went through laminectomy (n = 5); PLGA - animals with SCI treated with PLGA particles (n = 4); Gal - animals with SCI treated with galantamine (n = 9); PG - animals with SCI treated with PLGA particles containing galantamine (n = 7). *p < 0.05, **p < 0.01, *** p < 0.001. One-way ANOVA with Tuckey's multiple comparison test. Results are expressed as mean \pm standard deviation.

3.4 Morphological evaluation of the spinal cord

When analyzing the spinal cord morphology, it was observed that all the samples presented a large cystic cavity that was filled with some connective tissue fibers and some polymeric material on the PLGA groups (Figure 4). The rostral side of the spinal cord maintains the architecture of the healthy tissue, while the caudal, post-lesioned side shows some degeneration.

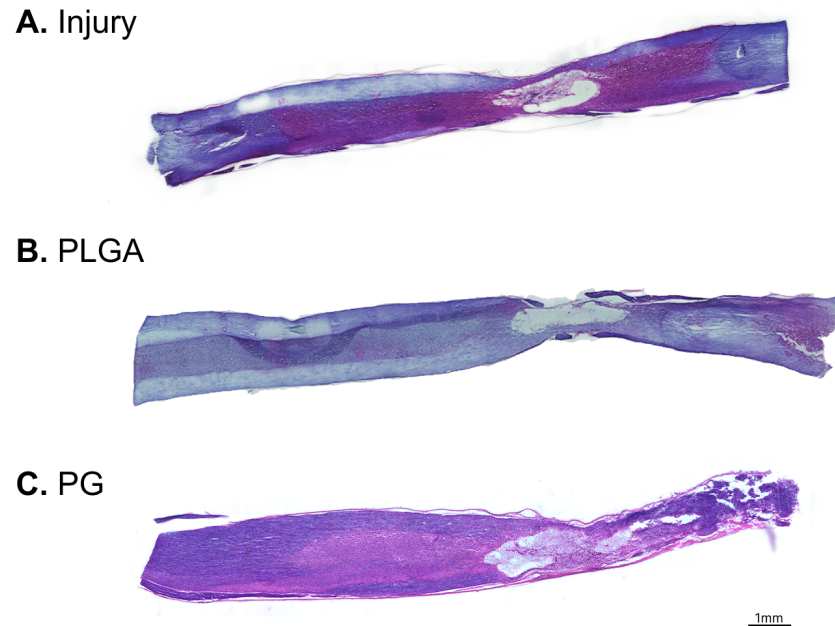


Figure 4. Morphology of the lesioned spinal cord, as shown by representative images from longitudinal 20 μm thick sections of the spinal cord, stained with hematoxylin and eosin. (A) Injury - animals with spinal cord injury, (B) PLGA - animals with SCI treated with PLGA particles and (C) PG - animals with SCI treated with PLGA particles containing galantamine. 10x magnification.

4. Discussion

The CNS has a low regenerative capacity, so traumatic injuries to the CNS lead to debilitating conditions with little recovery chances. Galantamine has been proposed as a therapy for several neural conditions, being able to improve cognitive parameters, inflammation, oxidative stress and increasing neuroprotection [11]. In a previous study from our group, galantamine nanoparticles improved inflammatory and oxidative parameters in acute SCI [16]. In the present work, the long-term effects of galantamine nanoparticles in contusion SCI were analyzed.

Therapeutic effects on the acute and subacute phases of SCI have the potential of containing the spread of the damage, which can lead to improved motor function on more advanced phases. Indeed, the animals treated with PG presented the highest BBB score after 42 days, being the only group statistically different from the injury group. A single administration of galantamine in the tissue parenchyma also showed improved motor function, although not statistically significant. The previous study that characterized PG particles demonstrated that

galantamine is released in a burst profile, where most of the drug is released in the first hour, but galantamine release was observed for up to 35 days [16]. This could explain the beneficial effects of the nanoparticle administration in comparison to a single dose of galantamine after the injury. Another study using galantamine for SCI administered the drug intraperitoneally for 5 days, and it was observed a significant improvement in motor function since day 7, improving continuously up to 42 days [12]. The different administration route and repeated drug administration could explain the differences, since it is hard to estimate the drug concentration and bioavailability at the injury site. .

Galantamine acts both as an acetylcholinesterase inhibitor and as an $\alpha 7$ nAChR allosteric modulator, therefore it acts in the cholinergic antiinflammatory pathway [25]. A recent study demonstrated that vagus nerve stimulation for 14 days led to an improvement in functional recovery after compression SCI, and that this effect was decreased after $\alpha 7$ nAChR blockade [26]. Hence, PG effects on locomotion could be related to the galantamine effects on $\alpha 7$ nAChR.

Galantamine is also described as an antioxidant. The enol group in its molecule acts as a ROS scavenger, and its role protecting against oxidative stress has been observed in neuronal culture exposed to amyloid-beta peptide [27] and in SK-N-SH cells exposed by hydrogen peroxide [28]. *In vivo*, PG particles decreased ROS and lipid peroxidation 3 days after SCI, and the latter was also observed with galantamine [16]. In the present study, both PG and galantamine decreased ROS after 42 days, but neither affected lipid peroxidation levels. Further, galantamine increased the antioxidant defense, as demonstrated by increase in sulfhydryl levels. The decrease of ROS production after 42 days indicates the long-term effect of the treatments, even with a single dose administration of galantamine. The pathophysiology of SCI is complex and involves multiple mechanisms, so even though ROS production was not affected by galantamine after 3 days, the effects of galantamine administration in $\alpha 7$ nAChR can lead to long-term effects, leading to significant results after 42 days.

PG treatment also led to decreased levels of IL-1 β , an important inflammatory cytokine. Inflammation is an important event in SCI, and it orchestrates most of the pathological response to the injury. IL-1 β is released by resident and infiltrating inflammatory cells after the injury and it can enhance vascular permeability, recruiting additional inflammatory cells and leading to neuronal and glial death [4]. Vagus nerve stimulation also decreased IL-1 β and IL-6 levels due to $\alpha 7$ nAChR activation [26]. Here, galantamine alone did not alter cytokine levels, probably due to being administered in a single dose. Interestingly, PLGA particles was the only treatment able to reduce IL-6 levels. This effect was also observed in the previous work analyzing 3 days after the injury. One possible explanation for this result is the fact that PLGA is degraded to glycolic and

lactic acid, and studies have demonstrated an important role of lactate in shifting macrophages phenotypes from M1 to M2 [29]. Morphologically, not many differences were observed between the treatment groups, but we could observe the presence of the material in the PLGA and PG groups.

Conclusion

The present study demonstrated that galantamine nanoparticles improved motor function in rats 42 days after contusion SCI. This treatment also decreased ROS production and IL-1 β , having important effects in oxidative stress and inflammation, two hallmarks of SCI.

References

- [1] R.J. Dumont, D.O. Okonkwo, S. Verma, R.J. Hurlbert, P.T. Boulos, D.B. Ellegala, A.S. Dumont, Acute Spinal Cord Injury, Part I: Pathophysiologic Mechanisms:, Clin. Neuropharmacol. 24 (2001) 254–264. <https://doi.org/10.1097/00002826-200109000-00002>.
- [2] C.S. Ahuja, J.R. Wilson, S. Nori, M.R.N. Kotter, C. Druschel, A. Curt, M.G. Fehlings, Traumatic spinal cord injury, Nat. Rev. Dis. Primer. 3 (2017) 17018. <https://doi.org/10.1038/nrdp.2017.18>.
- [3] I. Pineau, S. Lacroix, Proinflammatory cytokine synthesis in the injured mouse spinal cord: Multiphasic expression pattern and identification of the cell types involved, J. Comp. Neurol. 500 (2007) 267–285. <https://doi.org/10.1002/cne.21149>.
- [4] D.J. Donnelly, P.G. Popovich, Inflammation and its role in neuroprotection, axonal regeneration and functional recovery after spinal cord injury, Exp. Neurol. 209 (2008) 378–388. <https://doi.org/10.1016/j.expneurol.2007.06.009>.
- [5] J.C. Gensel, B. Zhang, Macrophage activation and its role in repair and pathology after spinal cord injury, Brain Res. 1619 (2015) 1–11. <https://doi.org/10.1016/j.brainres.2014.12.045>.
- [6] Z. Jia, H. Zhu, J. Li, X. Wang, H. Misra, Y. Li, Oxidative stress in spinal cord injury and antioxidant-based intervention, Spinal Cord. 50 (2012) 264–274. <https://doi.org/10.1038/sc.2011.111>.
- [7] E.D. Hall, J.M. Braugher, J.M. McCall, Antioxidant effects in brain and spinal cord injury, J. Neurotrauma. 9 Suppl 1 (1992) S165-172.
- [8] L.V. Borovikova, S. Ivanova, M. Zhang, H. Yang, G.I. Botchkina, L.R. Watkins, H. Wang, N. Abumrad, J.W. Eaton, K.J. Tracey, Vagus nerve stimulation attenuates the systemic inflammatory response to endotoxin, 405 (2000) 5.
- [9] H. Patel, J. McIntire, S. Ryan, A. Dunah, R. Loring, Anti-inflammatory effects of astroglial $\alpha 7$ nicotinic acetylcholine receptors are mediated by inhibition of the NF- κ B pathway and activation of the Nrf2 pathway, J. Neuroinflammation. 14 (2017) 192. <https://doi.org/10.1186/s12974-017-0967-6>.
- [10] Q. Zhang, Y. Lu, H. Bian, L. Guo, H. Zhu, Activation of the $\alpha 7$ nicotinic receptor promotes lipopolysaccharide-induced conversion of M1 microglia to M2, Am. J. Transl. Res. 9 (2017) 971–985.
- [11] C.N. Metz, V.A. Pavlov, Treating disorders across the lifespan by modulating cholinergic signaling with galantamine, J. Neurochem. 158 (2021) 1359–1380. <https://doi.org/10.1111/jnc.15243>.

- [12] L.E. Sperling, K. Pires Reis, F. Nicola, C. Euzebio Teixeira, G. Gulielmin Didó, M. Garrido dos Santos, E. Konrath, C.A. Netto, P. Pranke, Galantamine improves functional recovery and reduces lesion size in a rat model of spinal cord injury, *Brain Res.* 1724 (2019) 146424. <https://doi.org/10.1016/j.brainres.2019.146424>.
- [13] G. Marucci, M. Buccioni, D.D. Ben, C. Lambertucci, R. Volpini, F. Amenta, Efficacy of acetylcholinesterase inhibitors in Alzheimer's disease, *Neuropharmacology.* 190 (2021) 108352. <https://doi.org/10.1016/j.neuropharm.2020.108352>.
- [14] Sunena, S.K. Singh, D.N. Mishra, Nose to Brain Delivery of Galantamine Loaded Nanoparticles: In-vivo Pharmacodynamic and Biochemical Study in Mice, *Curr. Drug Deliv.* 16 (2019) 51–58. <https://doi.org/10.2174/1567201815666181004094707>.
- [15] N. Kamaly, B. Yameen, J. Wu, O.C. Farokhzad, Degradable Controlled-Release Polymers and Polymeric Nanoparticles: Mechanisms of Controlling Drug Release, *Chem. Rev.* 116 (2016) 2602–2663. <https://doi.org/10.1021/acs.chemrev.5b00346>.
- [16] F. Stapenhorst, L.E. Sperling, M. Garrido dos Santos, L.C. Sommer, C. Teixeira, G. Gulielmin Didó, J.P. Prestes, T. Oliveira, P. Turck, A. Belló-Klein, P. Pranke, Galantamine-PLGA nanoparticles decrease oxidative stress and inflammation in a model of acute spinal cord injury, *Biomed. Mater. (A ser aceito)*.
- [17] S. Constantini, W. Young, The effects of methylprednisolone and the ganglioside GM1 on acute spinal cord injury in rats, *J. Neurosurg.* 80 (1994) 97–111. <https://doi.org/10.3171/jns.1994.80.1.0097>.
- [18] F. Nicola, M.R. Marques, F. Odorczyk, L. Petenuzzo, D. Aristimunha, A. Vizuetete, E.F. Sanches, D.P. Pereira, N. Maurmann, C.-A. Gonçalves, P. Pranke, C.A. Netto, Stem Cells from Human Exfoliated Deciduous Teeth Modulate Early Astrocyte Response after Spinal Cord Contusion, *Mol. Neurobiol.* 56 (2019) 748–760. <https://doi.org/10.1007/s12035-018-1127-4>.
- [19] W. Young, Chapter 17 Spinal cord contusion models, in: *Prog. Brain Res.*, Elsevier, 2002: pp. 231–255. [https://doi.org/10.1016/S0079-6123\(02\)37019-5](https://doi.org/10.1016/S0079-6123(02)37019-5).
- [20] D.M. Basso, M.S. Beattie, J.C. Bresnahan, A Sensitive and Reliable Locomotor Rating Scale for Open Field Testing in Rats, *J. Neurotrauma.* 12 (1995) 1–21. <https://doi.org/10.1089/neu.1995.12.1>.
- [21] Oliver H. Lowry, Nira J. Rosebrough, A.L. Farr, Rose J. Randall, Protein measurement with the Folin phenol reagent, *J. Biol. Chem.* 193 (1951) 265–275. [https://doi.org/10.1016/S0021-9258\(19\)52451-6](https://doi.org/10.1016/S0021-9258(19)52451-6).
- [22] H. Wang, J.A. Joseph, Quantifying cellular oxidative stress by dichlorofluorescein assay using microplate reader¹¹Mention of a trade name, proprietary product, or specific equipment does not constitute a guarantee by the United States Department of Agriculture and does not imply its approval to the exclusion of other products that may be suitable., *Free Radic. Biol. Med.* 27 (1999) 612–616. [https://doi.org/10.1016/S0891-5849\(99\)00107-0](https://doi.org/10.1016/S0891-5849(99)00107-0).
- [23] J.A. Buege, S.D. Aust, Microsomal lipid peroxidation, in: *Methods Enzymol.*, Elsevier, 1978: pp. 302–310. [https://doi.org/10.1016/S0076-6879\(78\)52032-6](https://doi.org/10.1016/S0076-6879(78)52032-6).
- [24] M.Y. Aksenov, W.R. Markesbery, Changes in thiol content and expression of glutathione redox system genes in the hippocampus and cerebellum in Alzheimer's disease, *Neurosci. Lett.* 302 (2001) 141–145. [https://doi.org/10.1016/S0304-3940\(01\)01636-6](https://doi.org/10.1016/S0304-3940(01)01636-6).
- [25] M. Villarroya, A.G. García, J. Marco-Contelles, M.G. López, An update on the pharmacology of galantamine, *Expert Opin. Investig. Drugs.* 16 (2007) 1987–1998. <https://doi.org/10.1517/13543784.16.12.1987>.
- [26] H. Chen, Z. Feng, L. Min, W. Deng, M. Tan, J. Hong, Q. Gong, D. Zhang, H. Liu, J. Hou, Vagus Nerve Stimulation Reduces Neuroinflammation Through Microglia Polarization Regulation to Improve Functional Recovery After Spinal Cord Injury, *Front. Neurosci.* 16 (2022) 813472. <https://doi.org/10.3389/fnins.2022.813472>.

- [27] J.B. Melo, C. Sousa, P. Garção, C.R. Oliveira, P. Agostinho, Galantamine protects against oxidative stress induced by amyloid-beta peptide in cortical neurons, *Eur. J. Neurosci.* 29 (2009) 455–464. <https://doi.org/10.1111/j.1460-9568.2009.06612.x>.
- [28] M. Ezoulin, Antioxidative properties of galantamine on neuronal damage induced by hydrogen peroxide in SK–N–SH cells, *NeuroToxicology.* 29 (2008) 270–277. <https://doi.org/10.1016/j.neuro.2007.11.004>.
- [29] O.R. Colegio, N.-Q. Chu, A.L. Szabo, T. Chu, A.M. Rhebergen, V. Jairam, N. Cyrus, C.E. Brokowski, S.C. Eisenbarth, G.M. Phillips, G.W. Cline, A.J. Phillips, R. Medzhitov, Functional polarization of tumour-associated macrophages by tumour-derived lactic acid, *Nature.* 513 (2014) 559–563. <https://doi.org/10.1038/nature13490>.

6. DISCUSSÃO

O presente trabalho teve como objetivo avaliar os efeitos a curto e longo prazo do tratamento com nanopartículas de galantamina em um modelo animal de lesão da medula espinal. A LME é uma síndrome neurológica que acarreta em graves sintomas e grandes impactos na vida dos pacientes acometidos, podendo levar à paraplegia. Apesar disso, ainda não existem tratamentos eficazes disponíveis. Portanto, faz-se necessária a busca por novos tratamentos que sejam mais eficazes para o tratamento da LME.

Neste estudo, foram produzidas nanopartículas poliméricas contendo galantamina para o uso no tratamento da LME. No primeiro artigo, foi realizada a padronização da produção das partículas e avaliação dos efeitos *in vitro* em um modelo neuronal, bem como avaliação dos efeitos a curto prazo, na fase aguda da LME. No segundo artigo, as partículas, já padronizadas, foram aplicadas na LME e os efeitos na fase crônica da lesão foram avaliados.

6.1. CARACTERIZAÇÃO DAS NANOPARTÍCULAS

A galantamina é um inibidor da acetilcolinesterase e um modulador alostérico do nAChR $\alpha 7$, tendo evidências de atuar como anti-inflamatório, antioxidante e neuroprotetor. Devido a essas propriedades, a galantamina já foi utilizada em estudos de diversas síndromes neurológicas (METZ; PAVLOV, 2021). Um trabalho prévio do presente grupo de pesquisa foi o primeiro estudo reportado a utilizar a galantamina na LME, através da administração intraperitoneal e observou-se que os animais tratados com esse fármaco apresentaram melhora funcional e redução do tamanho da lesão (SPERLING et al., 2019). Entretanto, a administração sistêmica de fármacos apresenta desvantagens como maiores efeitos colaterais, menor biodisponibilidade da droga no local alvo e a necessidade de repetição da administração. Assim, o uso de nanopartículas poliméricas como carreadores de drogas surge como uma alternativa devido à capacidade de possuir uma liberação controlada do fármaco e a possibilidade da administração direta no tecido alvo (PRAJAPATI; JANI; KAPADIA, 2015).

O polímero escolhido para a produção das nanopartículas poliméricas foi o PLGA, devido a sua biodegradabilidade e biocompatibilidade. Esse polímero é degradado em ácido lático e ácido glicólico, que são metabolizados pelas células através do ciclo de Krebs em água e CO_2 eliminado pela respiração (PARK; YE; PARK, 2005). Foi utilizada a técnica de *electrospraying*, que apresenta vantagens de ter seus parâmetros regulados para a obtenção de características de interesse. No presente trabalho, a adição de galantamina levou a alterações nas características das partículas em comparação com partículas produzidas apenas de PLGA,

como uma morfologia mais irregular e diminuição do diâmetro e do potencial zeta. Essas alterações podem ser explicadas pelo fato de que a galantamina foi diluída em água antes de ser adicionada na solução polimérica. Um estudo de Yao e colaboradores demonstrou que o aumento da razão do volume aquoso em relação à fase orgânica leva a alterações eletrostáticas, as quais resultam em partículas menores e com morfologia menos homogênea (YAO et al., 2016). Entretanto, os parâmetros obtidos demonstram que as partículas são adequadas para administração local.

Ao analisar a liberação de galantamina, observou-se um perfil em *burst*, em que a maior parte do fármaco é liberado nas primeiras horas. A presença desse perfil é geralmente atribuída a distribuição da droga na superfície da partícula (FREDENBERG et al., 2011). Esse pode ser o caso das partículas deste trabalho, tendo em vista que Yao e colaboradores também observaram que o aumento da fase aquosa na emulsão polimérica levou a uma liberação mais rápida e distribuição do fármaco na superfície das partículas (YAO et al., 2016). Ainda, neste trabalho, foi possível detectar galantamina em amostras analisadas por até 35 dias.

6.2. EFEITOS IN VITRO

Considerando os efeitos antioxidantes e neuroprotetores já estabelecidos da galantamina, o presente estudo analisou o potencial dos tratamentos na proteção à perda de viabilidade e à produção de espécies reativas de oxigênio em um modelo neuronal *in vitro* após a exposição ao peróxido de hidrogênio. A linhagem de células PC12 é uma linhagem derivada de um feocromocitoma da adrenal de ratos, tendo, portanto, origem embrionária da crista neural (GREENE; TISCHLER, 1976). Essa linhagem já foi amplamente estabelecida como um modelo neuronal (WESTERINK; EWING, 2007). Nas concentrações analisadas, apenas a galantamina livre foi capaz de prevenir a perda de viabilidade das células PC12 após a exposição ao peróxido. Esse resultado pode ser explicado pela menor concentração de galantamina nas nanopartículas, devido à baixa taxa de encapsulamento. Quando analisamos a produção de EROs, os tratamentos não foram capazes de diminuir a produção dessas moléculas no tempo analisado, de 24h. Um estudo de Ezoulin e colaboradores avaliou a produção de EROS de células SK-N-SH após exposição a 500uM de peróxido de hidrogênio juntamente com concentrações de 0,1 a 100uM de galantamina por 2h. Nesse estudo, houve redução da produção de EROs em todas as concentrações avaliadas (EZOULIN, 2008). No presente trabalho, foi utilizada uma concentração menor de peróxido de hidrogênio (200 uM) e uma concentração de galantamina de 5ug/ml (17,4 uM), durante 24h. As diferenças dos resultados podem ser

devido ao maior tempo de exposição ao peróxido, em que os tratamentos não foram capazes de diminuir significativamente a produção de EROs.

6.3. EFEITOS IN VIVO

6.3.1. Recuperação funcional

O potencial terapêutico das partículas produzidas para o tratamento da LME foi avaliado em um modelo animal de lesão medular por contusão. A atividade locomotora dos animais foi avaliada semanalmente após o tratamento, durante 6 semanas, utilizando a escala BBB (BASSO; BEATTIE; BRESNAHAN, 1995). No segundo dia após a lesão, todos os animais lesionados apresentaram score 0, com perda total da movimentação das patas traseiras, confirmando que a contusão foi bem sucedida. A maioria dos casos de LME em humanos não resulta na transecção completa da medula, tendo uma parte de axônios não lesionados e, assim, há um período de recuperação funcional espontânea devido a mecanismos de plasticidade (EDGERTON et al., 2001; FAWCETT et al., 2007). Após 42 dias, o único grupo de tratamento que demonstrou uma melhora significativa da função motora foi o grupo tratado com PG. Em estudo prévio do grupo, a administração intraperitoneal de galantamina durante 5 dias após a LME levou à melhora significativa da função motora (SPERLING et al., 2019). No presente trabalho, uma única administração de galantamina diretamente no local da lesão não levou a melhoras significativas após 42 dias. Assim, os resultados sugerem que é necessária a presença da galantamina durante as fases iniciais da lesão, que pode ser obtida na administração utilizando nanopartículas.

6.3.2. Estresse oxidativo

Nas avaliações relativas ao estado redox das medulas, 3 dias após a lesão, apenas o grupo PG apresentou diminuição dos níveis de EROs, ao passo que 42 dias após a lesão, tanto o grupo PG como o grupo galantamina apresentaram menores níveis de EROs em relação ao grupo lesão. Essa diminuição da produção de EROs foi acompanhada da diminuição do nível de peroxidação lipídica após 3 dias, tanto nos animais que receberam galantamina como nos que receberam PG. Esse efeito, entretanto, não foi observado em nenhum grupo experimental após 42 dias. Ainda, um aumento da defesa antioxidante não enzimática foi observado apenas no grupo galantamina 42 dias após a lesão. Coletivamente, esses resultados indicam uma importante atividade antioxidante da galantamina na LME, em que o grupo PG teve um importante papel na fase subaguda da lesão que se manteve na fase crônica. Apesar da

aplicação da galantamina não ter apresentado melhoras locomotoras, este tratamento levou a uma diminuição do estresse oxidativo a longo prazo. O papel antioxidante da galantamina já foi amplamente descrito e seus benefícios foram observados em diversas patologias neurológicas. Em um modelo de camundongo de doença de Alzheimer, a administração de galantamina antes da fase de acúmulo de placas de beta amiloide levou a diminuição do estresse oxidativo, com consequentes melhoras cognitivas (SAITO et al., 2019). Já em um modelo de hipóxia-isquemia neonatal, o tratamento com galantamina anteriormente à exposição à hipóxia levou à superexpressão da enzima antioxidante catalase e aumentou a sobrevivência neuronal (ODORCYK et al., 2017). Entretanto, de acordo com a revisão bibliográfica, este foi o primeiro estudo que avaliou o papel antioxidante da galantamina na LME.

6.3.3. Inflamação

Ao avaliar os parâmetros inflamatórios, os níveis das citocinas inflamatórias IL-1 β e IL-6 foram mensurados. Em ambos os tempos analisados, o grupo de animais tratados com PG foi o único grupo que apresentou diminuição significativa dos níveis de IL-1 β , ao passo que os animais tratados com PLGA foram os únicos que apresentaram níveis diminuídos de IL-6, em comparação com o grupo lesão. A atividade anti-inflamatória da galantamina já foi descrita em outros modelos de doenças neurais. Em camundongos tratados com LPS, o pré-tratamento com galantamina diminuiu os níveis das citocinas inflamatórias IL-1 β , IL-6 e TNF- α e diminuiu a expressão de marcadores microgliciais no hipocampo (LIU et al., 2018b). Além disso, em um modelo de camundongos de disfunção cognitiva pós-operatória, a administração intraperitoneal de galantamina diminuiu os níveis de citocinas inflamatórias e o acúmulo de microglia (WANG et al., 2019a).

A diminuição dos níveis de IL-6 nos grupos tratados com PLGA pode ter ocorrido devido à degradação do PLGA em ácido lático e ácido glicólico. Recentemente, o lactato tem sido descrito como um agente anti-inflamatório e foi observado que altas concentrações do mesmo levam à polarização de macrófagos associados a tumores para um fenótipo M2, que possui características anti-inflamatórias (COLEGIO et al., 2014). Ainda, o ácido lático inibe a migração de células T CD8+, enquanto o lactato inibe a migração de células T CD4+, demonstrando o papel dessa molécula na modulação da resposta inflamatória (HAAS et al., 2015). Entretanto, para confirmar a hipótese de que este seria o motivo da diminuição dos níveis de IL-6 nos animais tratados com PLGA, mais estudos seriam necessários.

7. CONCLUSÕES

- Foi possível produzir nanopartículas contendo galantamina pela técnica de eletropulverização.
- As nanopartículas apresentaram características físicas adequadas para a aplicação na LME.
- A galantamina foi liberada das nanopartículas em um perfil de *burst* na primeira hora do experimento, sendo detectada por até 35 dias.
- As nanopartículas não foram capazes de prevenir a perda de viabilidade celular nem a produção de espécies reativas de oxigênio em células expostas ao peróxido de hidrogênio. Entretanto, a galantamina preveniu a perda de viabilidade nestas células.
- O tratamento com PG levou a melhora locomotora dos animais 42 dias após a lesão.
- Os animais tratados com PG apresentaram diminuição de marcadores de estresse oxidativo e de inflamação 3 e 42 dias após a lesão.
- Os animais tratados com galantamina apresentaram diminuição de marcadores de estresse oxidativo 3 e 42 dias após a lesão.
- O tratamento com PLGA levou a diminuição dos níveis de IL-6 3 e 42 dias após a lesão.

O presente trabalho explorou uma nova estratégia de tratamento para a LME, que seria a utilização de nanopartículas para a liberação local de galantamina. Além de ter sido uma estratégia inovadora na LME, este foi o primeiro estudo que explorou os efeitos anti-inflamatórios e antioxidantes da galantamina na LME, no qual foi comparado os efeitos na fase sub-aguda e crônica da lesão. No entanto, mais estudos são necessários para avaliar se diferentes concentrações de galantamina adicionada na formulação das nanopartículas poderiam produzir diferentes resultados. Ainda, poderia-se avaliar se alterando a formulação das nanopartículas, utilizando-se polímeros de degradação mais lenta, seria possível melhorar a cinética de liberação da galantamina para que o fármaco seja liberado mais lentamente ao longo do tempo. Os resultados aqui obtidos demonstram que a galantamina apresenta-se como uma estratégia promissora para o tratamento da LME, e explorar novas formas de liberação de fármacos pode ser um caminho para tratamentos mais eficazes da LME.

8. PERSPECTIVAS

Como perspectivas, pretende-se aumentar a eficiência de encapsulamento e o período de liberação de galantamina das nanopartículas, bem como testar diferentes concentrações de

galantamina. Além disso, analisar a expressão de marcadores neuronais e gliais após o tratamento, além de medir o tamanho da lesão. Por fim, pretende-se analisar o papel do lactato na inflamação e na melhora locomotora após a LME, com o objetivo de desenvolver uma estratégia nanotecnológica eficaz no tratamento da lesão de medula espinal.

9. REFERÊNCIAS

- AARSLAND, D.; HUTCHINSON, M.; LARSEN, J. P. Cognitive, psychiatric and motor response to galantamine in Parkinson's disease with dementia. **International Journal of Geriatric Psychiatry**, v. 18, n. 10, p. 937–941, 2003.
- AHUJA, C. S. et al. Traumatic Spinal Cord Injury—Repair and Regeneration. **Neurosurgery**, v. 80, n. 3S, p. S9–S22, mar. 2017a.
- AHUJA, C. S. et al. Traumatic spinal cord injury. **Nature Reviews Disease Primers**, v. 3, n. 1, p. 17018, 21 dez. 2017b.
- ANJUM, A. et al. Spinal Cord Injury: Pathophysiology, Multimolecular Interactions, and Underlying Recovery Mechanisms. **International Journal of Molecular Sciences**, v. 21, n. 20, p. 7533, 13 out. 2020.
- BALDWIN, S. A. et al. The presence of 4-hydroxynonenal/protein complex as an indicator of oxidative stress after experimental spinal cord contusion in a rat model. **Journal of Neurosurgery**, v. 88, n. 5, p. 874–883, maio 1998.
- BASSO, D. M.; BEATTIE, M. S.; BRESNAHAN, J. C. A Sensitive and Reliable Locomotor Rating Scale for Open Field Testing in Rats. **Journal of Neurotrauma**, v. 12, n. 1, p. 1–21, fev. 1995.
- BOCK, N.; DARGAVILLE, T. R.; WOODRUFF, M. A. Electrospraying of polymers with therapeutic molecules: State of the art. **Progress in Polymer Science**, v. 37, n. 11, p. 1510–1551, nov. 2012.
- BOROVIKOVA, L. V. et al. Vagus nerve stimulation attenuates the systemic inflammatory response to endotoxin. v. 405, p. 5, 2000.
- BROCKIE, S.; HONG, J.; FEHLINGS, M. G. The Role of Microglia in Modulating Neuroinflammation after Spinal Cord Injury. **International Journal of Molecular Sciences**, v. 22, n. 18, p. 9706, 8 set. 2021.
- BRODAL, P. **The central nervous system: structure and function**. 4th ed ed. New York: Oxford University Press, 2010.
- BUCHANAN, R. W. et al. Galantamine for the Treatment of Cognitive Impairments in People With Schizophrenia. **American Journal of Psychiatry**, v. 165, n. 1, p. 82–89, jan. 2008.
- CHAMBERS, D.; HUANG, C.; MATTHEWS, G. **Basic Physiology for Anaesthetists**. 1. ed. [s.l.] Cambridge University Press, 2014.
- CHANDAR, K.; FREEMAN, B. K. Spinal Cord Anatomy. Em: **Encyclopedia of the Neurological Sciences**. [s.l.] Elsevier, 2014. p. 254–263.

- CHOUËIRY, J. et al. Combining CDP-choline and galantamine, an optimized $\alpha 7$ nicotinic strategy, to ameliorate sensory gating to speech stimuli in schizophrenia. **International Journal of Psychophysiology**, The Neurophysiology of Schizophrenia: A Critical Update. v. 145, p. 70–82, 1 nov. 2019.
- COLEGIO, O. R. et al. Functional polarization of tumour-associated macrophages by tumour-derived lactic acid. **Nature**, v. 513, n. 7519, p. 559–563, set. 2014.
- COLOMBO, E.; FARINA, C. Astrocytes: Key Regulators of Neuroinflammation. **Trends in Immunology**, v. 37, n. 9, p. 608–620, set. 2016.
- CONLEY, R. R. et al. The effects of galantamine on psychopathology in chronic stable schizophrenia. **Clinical neuropharmacology**, v. 32, n. 2, p. 69–74, 1 mar. 2009.
- DONNELLY, D. J.; POPOVICH, P. G. Inflammation and its role in neuroprotection, axonal regeneration and functional recovery after spinal cord injury. **Experimental Neurology**, v. 209, n. 2, p. 378–388, fev. 2008.
- EDGERTON, V. R. et al. Retraining the injured spinal cord. **The Journal of Physiology**, v. 533, n. Pt 1, p. 15–22, 15 maio 2001.
- EDLUND, U, A., A. C. Degradable Polymer Microspheres for Controlled Drug Delivery. Em: **Degradable aliphatic polyesters**. Advances in polymer science. Berlin ; New York: Springer, 2002. p. 67–112.
- EL-SAY, K. M.; EL-SAWY, H. S. Polymeric nanoparticles: Promising platform for drug delivery. **International Journal of Pharmaceutics**, v. 528, n. 1–2, p. 675–691, ago. 2017.
- ESCARTIN, C. et al. Reactive astrocyte nomenclature, definitions, and future directions. **Nature Neuroscience**, v. 24, n. 3, p. 312–325, mar. 2021.
- EZOULIN, M. Antioxidative properties of galantamine on neuronal damage induced by hydrogen peroxide in SK–N–SH cells. **NeuroToxicology**, v. 29, n. 2, p. 270–277, mar. 2008.
- FATIMA, G. et al. Oxidative stress and antioxidative parameters in patients with spinal cord injury: implications in the pathogenesis of disease. **Spinal Cord**, v. 53, n. 1, p. 3–6, jan. 2015.
- FAULKNER, J. R. Reactive Astrocytes Protect Tissue and Preserve Function after Spinal Cord Injury. **Journal of Neuroscience**, v. 24, n. 9, p. 2143–2155, 3 mar. 2004.
- FAWCETT, J. W. et al. Guidelines for the conduct of clinical trials for spinal cord injury as developed by the ICCP panel: spontaneous recovery after spinal cord injury and statistical power needed for therapeutic clinical trials. **Spinal Cord**, v. 45, n. 3, p. 190–205, mar. 2007.
- FREDENBERG, S. et al. The mechanisms of drug release in poly(lactic-co-glycolic acid)-based drug delivery systems—A review. **International Journal of Pharmaceutics**, v. 415, n. 1–2, p. 34–52, ago. 2011.
- GENSEL, J. C.; ZHANG, B. Macrophage activation and its role in repair and pathology after spinal cord injury. **Brain Research**, v. 1619, p. 1–11, set. 2015.
- GHALEIHA, A. et al. Galantamine efficacy and tolerability as an augmentative therapy in autistic children: A randomized, double-blind, placebo-controlled trial. **Journal of Psychopharmacology**, v. 28, n. 7, p. 677–685, 1 jul. 2014.

- GINHOUX, F. et al. Fate Mapping Analysis Reveals That Adult Microglia Derive from Primitive Macrophages. **Science**, v. 330, n. 6005, p. 841–845, 5 nov. 2010.
- GREENE, L. A.; TISCHLER, A. S. Establishment of a noradrenergic clonal line of rat adrenal pheochromocytoma cells which respond to nerve growth factor. **Proceedings of the National Academy of Sciences of the United States of America**, v. 73, n. 7, p. 2424–2428, jul. 1976.
- GUEST, J. et al. Pathophysiology, Classification and Comorbidities after Traumatic Spinal Cord Injury. **Journal of Personalized Medicine**, v. 12, n. 7, p. 1126, 11 jul. 2022.
- HAAS, R. et al. Lactate Regulates Metabolic and Pro-inflammatory Circuits in Control of T Cell Migration and Effector Functions. **PLOS Biology**, v. 13, n. 7, p. e1002202, 16 jul. 2015.
- HALL, E. D. Antioxidant Therapies for Acute Spinal Cord Injury. **Neurotherapeutics**, v. 8, n. 2, p. 152–167, abr. 2011.
- HAN, Z. et al. Alpha-7 nicotinic acetylcholine receptor agonist treatment reduces neuroinflammation, oxidative stress, and brain injury in mice with ischemic stroke and bone fracture. **Journal of Neurochemistry**, v. 131, n. 4, p. 498–508, nov. 2014.
- JI, H. et al. Central cholinergic activation of a vagus nerve-to-spleen circuit alleviates experimental colitis. **Mucosal Immunology**, v. 7, n. 2, p. 335–347, mar. 2014.
- JIA, Z. et al. Oxidative stress in spinal cord injury and antioxidant-based intervention. **Spinal Cord**, v. 50, n. 4, p. 264–274, abr. 2012.
- JONES, T.; MCDANIEL, E.; POPOVICH, P. Inflammatory-Mediated Injury and Repair in the Traumatically Injured Spinal Cord. **Current Pharmaceutical Design**, v. 11, n. 10, p. 1223–1236, 1 abr. 2005.
- KAUFER, D. I. et al. Reduction of Caregiver Burden in Alzheimer's Disease by Treatment with Galantamine. **CNS Spectrums**, v. 10, n. 6, p. 481–488, jun. 2005.
- KIM, Y.; CALDWELL, J.-M.; BELLAMKONDA, R. V. Nanoparticle-mediated local delivery of methylprednisolone after spinal cord injury. **Biomaterials**, v. 30, n. 13, p. 2582–2590, maio 2009.
- KOOLA, M. M. et al. Meta-analysis of randomized controlled trials of galantamine in schizophrenia: significant cognitive enhancement. **Psychiatry Research**, v. 291, p. 113285, 1 set. 2020.
- KRONSCHLÄGER, M. T. et al. Lamina-specific properties of spinal astrocytes. **Glia**, v. 69, n. 7, p. 1749–1766, jul. 2021.
- LIN, Y.-T. et al. Association between acetylcholinesterase inhibitors and risk of stroke in patients with dementia. **Scientific Reports**, v. 6, n. 1, p. 29266, 5 jul. 2016.
- LIU, S.-Y. et al. The effect of LRRK2 mutations on the cholinergic system in manifest and premanifest stages of Parkinson's disease: a cross-sectional PET study. **The Lancet Neurology**, v. 17, n. 4, p. 309–316, 1 abr. 2018a.
- LIU, Y. et al. Galantamine improves cognition, hippocampal inflammation, and synaptic plasticity impairments induced by lipopolysaccharide in mice. **Journal of Neuroinflammation**, v. 15, n. 1, p. 112, dez. 2018b.

- MACDONALD, A. et al. Single Cell Transcriptomics of Ependymal Cells Across Age, Region and Species Reveals Cilia-Related and Metal Ion Regulatory Roles as Major Conserved Ependymal Cell Functions. **Frontiers in Cellular Neuroscience**, v. 15, p. 703951, 15 jul. 2021.
- MACKS, C. et al. Rolipram-Loaded Polymeric Micelle Nanoparticle Reduces Secondary Injury after Rat Compression Spinal Cord Injury. **Journal of Neurotrauma**, v. 35, n. 3, p. 582–592, fev. 2018.
- MELO, J. B. et al. Galantamine protects against oxidative stress induced by amyloid-beta peptide in cortical neurons. **European Journal of Neuroscience**, v. 29, n. 3, p. 455–464, fev. 2009.
- METZ, C. N.; PAVLOV, V. A. Treating disorders across the lifespan by modulating cholinergic signaling with galantamine. **Journal of Neurochemistry**, v. 158, n. 6, p. 1359–1380, set. 2021.
- MINISTÉRIO DA SAÚDE. Diretrizes de Atenção à Pessoa com Lesão Medular. p. 70, 2013.
- MORENO-MANZANO, V. Ependymal cells in the spinal cord as neuronal progenitors. **Current Opinion in Pharmacology**, v. 50, p. 82–87, fev. 2020.
- NÓGRÁDI, A. **Transplantation of neural tissue into the spinal cord**. 2nd ed ed. Georgetown, Tex: Landes Bioscience : Eureka.com, 2006.
- ODORCYK, F. K. et al. Galantamine administration reduces reactive astrogliosis and upregulates the anti-oxidant enzyme catalase in rats submitted to neonatal hypoxia ischemia. **International Journal of Developmental Neuroscience**, v. 62, n. 1, p. 15–24, nov. 2017.
- PARK, J.; YE, M.; PARK, K. Biodegradable Polymers for Microencapsulation of Drugs. **Molecules**, v. 10, n. 1, p. 146–161, 31 jan. 2005.
- PARK, K. Nanotechnology: What it can do for drug delivery. **Journal of controlled release : official journal of the Controlled Release Society**, v. 120, n. 1–2, p. 1–3, 16 jul. 2007.
- PATEL, H. et al. Anti-inflammatory effects of astroglial $\alpha 7$ nicotinic acetylcholine receptors are mediated by inhibition of the NF- κ B pathway and activation of the Nrf2 pathway. **Journal of Neuroinflammation**, v. 14, n. 1, p. 192, dez. 2017.
- PAVLOV, V. A. et al. Brain acetylcholinesterase activity controls systemic cytokine levels through the cholinergic anti-inflammatory pathway. **Brain, Behavior, and Immunity**, v. 23, n. 1, p. 41–45, jan. 2009.
- PETRIKIS, P. et al. Treatment of Huntington's disease with galantamine. **International Clinical Psychopharmacology**, v. 19, n. 1, p. 49–50, jan. 2004.
- PHAM, G. S.; WANG, L. A.; MATHIS, K. W. Pharmacological potentiation of the efferent vagus nerve attenuates blood pressure and renal injury in a murine model of systemic lupus erythematosus. **American Journal of Physiology-Regulatory, Integrative and Comparative Physiology**, v. 315, n. 6, p. R1261–R1271, 1 dez. 2018.
- PRAJAPATI, V. D.; JANI, G. K.; KAPADIA, J. R. Current knowledge on biodegradable microspheres in drug delivery. **Expert Opinion on Drug Delivery**, v. 12, n. 8, p. 1283–1299, 3 ago. 2015.
- REIS, K. P. et al. Application of PLGA/FGF-2 coaxial microfibers in spinal cord tissue

engineering: an *in vitro* and *in vivo* investigation. **Regenerative Medicine**, v. 13, n. 7, p. 785–801, out. 2018.

REVELLI, U.; GRASO, E. Nivaline (*Galanthus nivalis*) therapy in polimyelitis. **Minerva Medica**, v. 53, p. 881–884, 24 mar. 1962.

REXED, B. The cytoarchitectonic organization of the spinal cord in the cat. **Journal of Comparative Neurology**, v. 96, n. 3, p. 415–495, 1952.

SAITO, T. et al. Early administration of galantamine from preplaque phase suppresses oxidative stress and improves cognitive behavior in APP^{swe}/PS1^{dE9} mouse model of Alzheimer's disease. **Free Radical Biology and Medicine**, v. 145, p. 20–32, dez. 2019.

SCHUBERT, M. H.; YOUNG, K. A.; HICKS, P. B. Galantamine Improves Cognition in Schizophrenic Patients Stabilized on Risperidone. **Biological Psychiatry**, v. 60, n. 6, p. 530–533, 15 set. 2006.

SPERLING, L. E. et al. Galantamine improves functional recovery and reduces lesion size in a rat model of spinal cord injury. **Brain Research**, v. 1724, p. 146424, dez. 2019.

SPRINGER, J. E. et al. 4-Hydroxynonenal, a Lipid Peroxidation Product, Rapidly Accumulates Following Traumatic Spinal Cord Injury and Inhibits Glutamate Uptake. **Journal of Neurochemistry**, v. 68, n. 6, p. 2469–2476, 18 nov. 2002.

SU, Y. et al. PLGA-based biodegradable microspheres in drug delivery: recent advances in research and application. **Drug Delivery**, v. 28, n. 1, p. 1397–1418, 1 jan. 2021.

SUGANO, N. et al. Nicotine Inhibits the Production of Inflammatory Mediators in U937 Cells through Modulation of Nuclear Factor- κ B Activation. **Biochemical and Biophysical Research Communications**, v. 252, n. 1, p. 25–28, nov. 1998.

SUN, D.; JAKOBS, T. C. Structural Remodeling of Astrocytes in the Injured CNS. **The Neuroscientist**, v. 18, n. 6, p. 567–588, dez. 2012.

TAN, E. C. K. et al. Acetylcholinesterase inhibitors and risk of stroke and death in people with dementia. **Alzheimer's & Dementia**, v. 14, n. 7, p. 944–951, 2018.

TAOKA, Y. et al. Superoxide radicals play important roles in the pathogenesis of spinal cord injury. **Paraplegia**, v. 33, n. 8, p. 450–453, ago. 1995.

TARIOT, P. N. et al. A 5-month, randomized, placebo-controlled trial of galantamine in AD. **Neurology**, v. 54, n. 12, p. 2269–2276, 27 jun. 2000.

TENOVUO, O. Central acetylcholinesterase inhibitors in the treatment of chronic traumatic brain injury—clinical experience in 111 patients. **Progress in Neuro-Psychopharmacology and Biological Psychiatry**, v. 29, n. 1, p. 61–67, 1 jan. 2005.

TSVETKOVA, D. et al. Antioxidant Activity of Galantamine and Some of its Derivatives. **Current Medicinal Chemistry**, v. 20, n. 36, p. 4595–4608, 31 nov. 2013.

VILLARROYA, M. et al. An update on the pharmacology of galantamine. **Expert Opinion on Investigational Drugs**, v. 16, n. 12, p. 1987–1998, dez. 2007.

WANG, H. et al. Nicotinic acetylcholine receptor $\alpha 7$ subunit is an essential regulator of

inflammation. v. 421, p. 5, 2003.

WANG, T. et al. Galantamine reversed early postoperative cognitive deficit via alleviating inflammation and enhancing synaptic transmission in mouse hippocampus. **European Journal of Pharmacology**, v. 846, p. 63–72, mar. 2019a.

WANG, X.-J. et al. Combinational protective therapy for spinal cord injury medicated by sialic acid-driven and polyethylene glycol based micelles. **Biomaterials**, v. 217, p. 119326, out. 2019b.

WESTERINK, R. H. S.; EWING, A. G. The PC12 cell as model for neurosecretion: PC12 cells as model for neurosecretion. **Acta Physiologica**, v. 192, n. 2, p. 273–285, 15 nov. 2007.

WILKINSON, D.; MURRAY, J.; GROUP, THE G. R. Galantamine: a randomized, double-blind, dose comparison in patients with Alzheimer's disease. **International Journal of Geriatric Psychiatry**, v. 16, n. 9, p. 852–857, 2001.

WU, W. et al. Neuroprotective ferulic acid (FA)–glycol chitosan (GC) nanoparticles for functional restoration of traumatically injured spinal cord. **Biomaterials**, v. 35, n. 7, p. 2355–2364, fev. 2014.

YAO, S. et al. Drug-nanoencapsulated PLGA microspheres prepared by emulsion electrospray with controlled release behavior. **Regenerative Biomaterials**, v. 3, n. 5, p. 309–317, out. 2016.

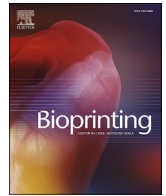
YUAN, Y.-M.; HE, C. The glial scar in spinal cord injury and repair. **Neuroscience Bulletin**, v. 29, n. 4, p. 421–435, ago. 2013.

ZHANG, L. et al. The origin and repopulation of microglia. **Developmental Neurobiology**, v. 82, n. 1, p. 112–124, jan. 2022.

ZHANG, Q. et al. Activation of the $\alpha 7$ nicotinic receptor promotes lipopolysaccharide-induced conversion of M1 microglia to M2. **American Journal of Translational Research**, v. 9, n. 3, p. 971–985, 15 mar. 2017.

ANEXO I - Artigo de revisão

Artigo de revisão publicado na revista Bioprinting.



Bioprinting: A promising approach for tissue regeneration

Fernanda Stapenhorst^{a,b,c}, Marcelo Garrido dos Santos^{a,b,c,d}, João Pedro Prestes^{a,b,c},
Bruno José Alcantara^{a,b,c}, Maurício Felisberto Borges^{a,b,c}, Patricia Pranke^{a,b,c,*}

^a Hematology and Stem Cell Laboratory, Faculty of Pharmacy, Universidade Federal do Rio Grande do Sul, Brazil

^b Stem Cell Laboratory, Fundamental Health Science Institute, Universidade Federal do Rio Grande do Sul, Brazil

^c Instituto de Pesquisa com Células-tronco (IPCT), Porto Alegre, RS, Brazil

^d Federal University of Health Sciences of Porto Alegre, Brazil

ARTICLE INFO

Keywords:

Bioprinting
Regenerative medicine
Tissue engineering
Bioink

ABSTRACT

Bioprinting of organs and tissues is an emerging technique in the field of tissue engineering, presenting as a promising approach in regenerative medicine. Several tissues have been studied in the light of bioprinting, from the poorly regenerative neural tissue to the highly proliferative skin tissue. The very different characteristics of these tissues must be taken into account when trying to bioprint a laboratory made substitute, including mechanical and biological key features for proper tissue regeneration. Furthermore, the different bioprinting techniques currently available, as well as the search for the optimal bioink for each tissue, led to a broad spectrum of studies in this field. Hence, the aim of this review is to describe what has been tested from the beginning of this new approach to current days in terms of bioinks and printing techniques in a wide range of tissues, shedding a light to new studies that might attempt a regenerative approach using bioprinting.

1. Introduction

Tissue engineering is a recent research field first introduced in a study published by Vacanti and Langer in 1991 [1]. Their aim was to generate an individual therapy for each patient, promoting regeneration, remodeling and growth of the damaged tissue [2]. This technology produces biomaterials suitable for drug screening and for the development of bio-scaffolds that mimic biological tissue for *in vitro* studies as well as *in vivo* transplantation [3].

The production of these scaffolds is a complex procedure that comprises the combination of cells adequate for the construct purpose, bioactive molecules, such as growth factors, and a scaffold that is able to maintain cell viability, proliferation and similarity to the extracellular environment of the target tissue [4]. Concerning the scaffold production process, numerous polymers, both synthetic and natural, as well as hydrogels, ceramics, metals and composites with polymers can be used due to their biocompatibility [5]. These biomaterials are a possible option to create 2D and 3D structures that allow for cell interaction and proliferation. A conventional 2D cell culture in culture dishes or even in scaffolds stimulates rapid proliferation but this growth stops when cells reach confluence. To diminish the lack of space and the deficient nutrient supply, 3D cell cultures have been developed [6].

The 3D structures used for cell culture can be produced using a regular 3D printer or a 3D bioprinter. 3D bioprinting consists of the production of three-dimensional constructs using a bioink, with a high reproducibility and control over the architecture of the material. A bioink is the mixture of hydrogels or polymers, capable of maintaining a 3D structure and allowing for cell adhesion and proliferation with cells, usually stem cells. Drugs and other bioactive molecules can be incorporated into the bioink to enhance, for example, differentiation and other cellular processes [7]. The main types of biomaterials found in this review are summarized in Fig. 1.

There are different types of technology for 3D bioprinting and the three major types of bioprinting are inkjet, microextrusion and laser-assisted bioprinting [8] (Fig. 2). Inkjet bioprinting is based on a thermal or acoustic delivery of bioink or cells. Inkjet bioprinters can be modified to print biomaterials other than bioinks. Extrusion bioprinting constructs are produced by dispensing a controlled amount of bioink through a needle using pneumatic pressure or mechanical pistons, thereby producing a 3D structure. Laser-assisted bioprinters use a high-energy laser to create a high-pressure system that ejects the biomaterial onto the collecting plate [9].

The large number of materials available for 3D bioprinting allows for the production of structures with different physical and biochemical characteristics. These differences are employed in the production of

* Corresponding author. Hematology and Stem Cell Laboratory (UFRGS), Stem Cell Laboratory (UFRGS), IPCT Universidade Federal do Rio Grande do Sul, Brazil.
E-mail address: patriciapranke@ufrgs.br (P. Pranke).

| Abbreviations | |
|---------------|--|
| ACPC | articular cartilage-resident chondroprogenitor cells |
| ADSC | adipose-derived stem cells |
| AECs | amniotic epithelial cells |
| AlgMA | alginate methacrylate |
| ALP | alkaline phosphatase |
| BM-MSC | bone marrow mesenchymal stem cells |
| cECM | cartilage extracellular matrix |
| CMC | carboxymethylchitosan |
| CMCel | carboxymethylcellulose |
| CMCelMA | carboxymethylcellulose methacrylate |
| CNC | cellulose nanocrystal |
| CNF | cellulose nanofibrils |
| CNS | central nervous system |
| CPC | calcium phosphate cement |
| CS-AEMA | chondroitin sulfate 2-aminoethyl methacrylate |
| dECM | decellularized extracellular matrix |
| DC-Gel | dopamine conjugated gelatin |
| DC-GelMA | dopamine conjugated gelatin methacrylated |
| DC-HA | dopamine conjugated hyaluronic acid |
| ECM | extracellular matrix |
| GAG | glycosaminoglycans |
| GelMA | gelatin methacrylate |
| GFAP | glial fibrillary acidic protein |
| HA | hyaluronic acid |
| hAC | human auricular chondrocyte |
| HAMA | hyaluronic acid methacrylated |
| HAP: | hydroxyapatite |
| hepG2 | hepatoma cells |
| hESC-LESC | human embryonic stem cell derived limbal epithelial |
| | stem cells |
| hDF | human dermal fibroblasts |
| hMSC | human mesenchymal stem cells |
| hNSC | human neural stem cells |
| HUVECs | human umbilical vein endothelial cells |
| IPN | interpenetrating polymer network |
| LAP | lithium-acylphosphinate |
| LPN | laponite |
| MMP | matrix metalloproteinase |
| MSC | mesenchymal stem cell |
| NICE | nanoengineered-ionic-covalent-entanglement |
| NCS | neural stem cells |
| nSi | nanosilicates |
| NTE | neural tissue engineering |
| PCL: | poly(ϵ -caprolactone) |
| PDLLA | poly-D,L-lactic acid |
| PEG | polyethylene glycol |
| PEGDA | polyethylene glycol diacrylate |
| PEOXA | poly (2-ethyl-2-oxazoline) |
| PF127 | pluronic F-127 |
| PF127-SH | pluronic F-127 synthetic thiolated |
| PLA | polylactic acid |
| PLGA | poly(lactic-co-glycolic acid) |
| PU | polyurethane |
| PVA | polyvinyl alcohol |
| RGD | acrylated Arg-Gly-Asp |
| SCI | spinal cord injury |
| TBI | traumatic brain injury |
| TCP | β -tricalcium phosphate |
| WJMSCs | Wharton's jelly-derived mesenchymal stem cells |
| VML: | volumetric muscle loss |

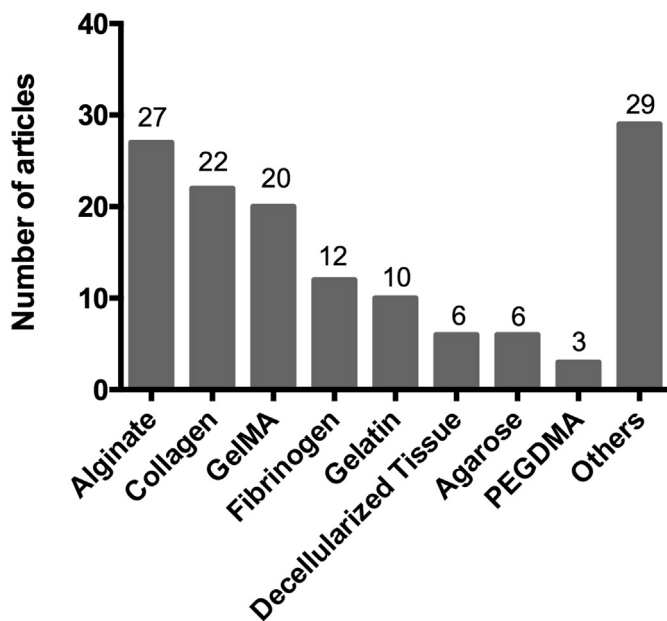


Fig. 1. Materials used as bioink components in the original articles herein reviewed. Alginate and collagen are the most commonly used materials in bioprinting.

constructs to regenerate different tissue types. In this review, we have focused on the bioprinting of the main tissue types: Nervous, skin, cartilage, vascular, bone and muscle. When searching for the term

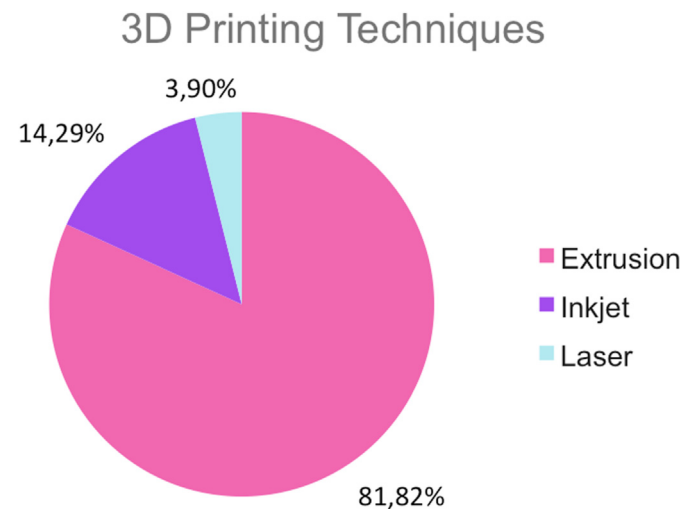


Fig. 2. Percentage of printing techniques used on the papers reviewed in this study.

“bioprinting” in PubMed, 1851 articles come up, of which 547 are reviews. We analyzed the percentage of original articles from the previously mentioned tissue types, and the results are presented in Fig. 3. Vascular and bone tissue represent the majority of tissue types studied in the field of bioprinting.

The aim in this review is to summarize the latest tendencies in bioprinting studies for the main tissue types within the scope of regenerative medicine. Here, the focus is on the bioprinting techniques employed, the

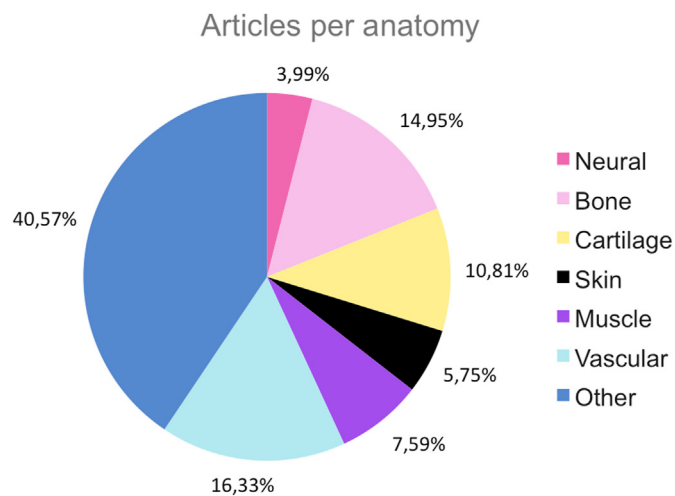


Fig. 3. Percentage of articles per tissue on PubMed when combining the terms with “bioprinting”.

printing parameters, the bioink composition and the main results obtained. Considering the vastness of this still new field in regenerative medicine, the aim here is to shed light on the main methods employed for regenerating multiple tissue types.

2. Bioprinting for different tissues

2.1. Nervous system

Neural tissue comprises a highly complex system which makes the regeneration process difficult due to its poor capability of self-healing. Injuries in the central nervous system, such as traumatic brain injury (TBI) and spinal cord injury (SCI) lead to life-long disabilities, and to this date there is no effective treatment for these disorders [10]. Furthermore, following a neural injury, the formation of scar tissue inhibits the regeneration process. The regeneration of the peripheral nervous system also represents a challenge, even though it has a greater regeneration capacity than the central nervous system (CNS) [11]. Considering the problems mentioned above, neural tissue engineering (NTE) has been proposed as a strategy for nervous system regeneration. In this context, bioprinting has been used with a variety of materials for the bioinks and with different cells, yielding different results.

Gu and colleagues employed microextrusion bioprinting to produce a 3D neural mini-tissue construct using a bioink composed of polysaccharides alginate, carboxymethylchitosan (CMC), agarose and human neural stem cells (hNSC). The bioink presented a compression modulus of around 7.5 kPa. The concentration of CMC had a direct influence on the porosity of the bioink and on cell viability, where higher concentrations of CMC led to higher porosity on its surface and higher cell viability. The cells on the 3D constructs presented higher expression of differentiation markers compared with 2D differentiation [12].

In another work, the authors produced a 3D biomimetic neural tissue using natural and synthetic polymers through microextrusion bioprinting. The bioink was composed of synthetic thiolated Pluronic F-127 (PF127-SH) and natural occurring hyaluronic acid and gelatin. In order to improve hydrogel adhesion, flexibility and reactive properties, gelatin and hyaluronic acid were conjugated with dopamine (DC-Gel and DC-HA, respectively). DC-Gel was further methacrylated to form DC-GelMA. Hence, the bioinks were produced with different concentrations of PF127-SH, DC-HA or DC-GelMA. To access the cell viability, S16Y cell line (Schawn cells from rats' sciatic nerve) was added to the bioink. The inks were then cured using two different methods: photocuring crosslinking and chelation crosslinking. The authors found that

increase of the PF127-SH increased the bioink elastic modulus, and bioinks that were cured by chelating were softer than photocured bioinks. In addition, there was a direct correlation between PF127 concentration and yield stress and viscosity. When analyzing cell viability after printing, it was found that the photocured constructs exhibited higher viability than the chelated constructs on day 1, but there were no differences in viability on day 3. After one week, all the bioinks presented increased viability [13].

A thermo-responsive polyurethane (PU) gel was synthesized and human fibroblasts were reprogrammed with a FoxD3 plasmid during the extrusion process in a bioprinter in order to create a neural-tissue-like construct. Two bioinks were tested, PU1500 and PU2000, according to the molecular weight of the Poly-D,L-lactic acid (PDLLA). Human fibroblasts transfected with FoxD3 plasmid were incorporated. Initially, the influence of the bioinks rheological properties on cell reprogramming was evaluated. It was found that due to its higher viscosity, PU1500 presented a better reprogramming effect than PU2000. Following this, the authors printed the bioink. The average shear stress was of around 190 Pa. Gene expression was evaluated and it was found that both neural crest and stemness markers were increased in the experimental groups compared to the control, demonstrating that the cell reprogramming was successful after extrusion. Neural induction was performed, and gene expression of neural markers 14 days after printing was higher in PU1500 in comparison to the PU2000 bioink, but with no significant difference compared to the non-printed biomaterial. Hence, this study showed the possibility of cell reprogramming and neural differentiation in a 3D bioprinted construct [14].

A hydrogel of PU was also used by another group, where two formulations were tested, PU1 and PU2. PU1 was constituted using poly(ϵ -caprolactone) diol (PCL diol) and poly(L-lactide) diol (PLLA diol) mixed in a 4:1 M ratio. The PU2 was constituted using PCL diol and PDLLA diol in a 4:1 M ratio. To produce the bioink, neural stem cells (NSC) were mixed with the hydrogels. PU1 presented a significantly higher compressive modulus compared to PU2. While PU1 was in a stiffness range that could induce glial differentiation, PU2 was in a stiffness range that could induce neuron differentiation. Indeed, in this work the authors observed that the NSCs that were printed in the PU2 hydrogel presented a high expression of neuron markers, such as nestin and β -tubulin, while the NSCs printed in PU1 expressed higher levels of glial fibrillary acidic protein (GFAP). Moreover, the NSCs mixed in PU hydrogels were injected on zebrafish embryos, and it was shown that without the hydrogels, the NSCs were distributed randomly in the central nervous system of the embryos and presented low cell density. On the other hand, the cells mixed with the hydrogels were more widely distributed and presented higher cell density. Furthermore, adult zebrafish were submitted to a traumatic lesion on the cerebellum and treated with a PU2 3D printed construct. The implanted animals showed a functional recovery in movement and reduced mortality compared to the control [15].

A different approach to induce neural differentiation of NSC in a 3D bioprinted construct was made using a bioink combining GelMA and graphene, considering GelMA's high level of cytocompatibility and graphene's ability to differentiate NSCs into neurons. Initially, hydrogels with different concentrations of GelMA alone were tested for mechanical properties and cytocompatibility using rat pheochromocytoma cells (PC-12). It was observed that the hydrogel stiffness increased when increasing the GelMA concentration, ranging from 27.8 to 162.1 kPa. For cytocompatibility tests, PC12 cells were cultivated on top of GelMA hydrogels, and it was found that GelMA 10% had the highest cell viability. Hence, the bioink was produced combining GelMA 10%, graphene and NSCs cells. This bioink was printed by stereolithography. After 14 days of cultivation, there were no significant differences in cell gene expression between GelMA and Graphene-GelMA. It is of importance to note that there was neurite elongation and higher expression of β -tubulin III in comparison to GFAP, indicating possible neural differentiation [16].

2.2. Skin

Skin is not only the largest organ of the human body but it is also its biggest barrier against external environment aggression that could jeopardize its homeostasis. Its highly complex stratified structure with various cell types (Keratinocytes, Melanocytes, Langerhans cells, Merkel cells, among others) has always been the focus of tissue engineering. Major burns and skin loss due to trauma or tumor resection are still a major challenge because split-thickness skin grafting (current gold standard treatment) is limited to the donor site and commercially available options fail to prevent scar formation and to offer an efficient and affordable treatment.

Developing a skin substitute that could efficiently replace damaged areas has become one of the most challenging areas in tissue engineering, and bioprinting has become a major tool in order to fulfill some of the several specifications from the biological and technical point of view, being the following: achieve a high resolution similar to the heterogeneity of natural tissue, print any desired cell density and variable viscosities of cell suspensions, control cell patterning and not negatively affect cell behaviour by the printing procedure [17].

In 2012, Skardal *et al* developed an extrusion bioprinting device used for treating full-thickness skin wounds in nu/nu mice. The researchers used amniotic fluid-derived stem cells and bone marrow-derived mesenchymal stem cells (BM-MSCs) suspended in a fibrin-collagen gel and achieved a faster closure and re-epithelialization of wounds when compared to the use of fibrin-collagen gel alone [18].

Another approach was developed by combining collagen and fibrinogen in a bioink composition using a portable 3D inkjet bioprinter that was able to scan full thickness wounds and print over them directly. Human fibroblasts and keratinocytes were mixed in hydrogel prior to printing and the results showed a significant increase in wound regeneration speed, reducing up to two days wound closure in the mice test group [19].

Kristy Derr and colleagues included gelatin and elastin with a fibrinogen and collagen mixture in conjunction with human dermal fibroblasts (hDFs) and normal human epithelial keratinocytes to produce a three-dimensional bioprinted skin equivalent. Built in an extrusion based 3D printer, the construct demonstrated multiple morphology and physiological characteristics important for the skin tissue, such as barrier function, great cell viability and good printability [20].

In another study, the authors also used fibrinogen, but instead of collagen, it was mixed with alginate and gelatin. Preliminary results were obtained by using mouse fibroblasts; normal human fibroblasts and normal primary human epidermal keratinocytes were then used to generate the fully organized and functional bioprinted skin. Histological characterization and immunohistological analysis of the bioprinted skin demonstrated that the 3D construct was morphologically and biologically representative of the normal human skin. Finally, the printability of large skin objects was demonstrated by the printing of an adult-size ear composed of bio-ink and human fibroblasts [21].

Collagen and fibrinogen were also used in addition to agarose in two bioink formulations, one composed of agarose-collagen and the other composed of agarose-fibrinogen. Human umbilical vein endothelial cells or human dermal fibroblasts were incorporated with the hydrogels because of their expected ability to form capillary-like structures to ensure nutrition supply. Their constructs were tailored using a drop-on-demand printing system. After a 14 day incubation period, substantial capillary network formation was observed in agarose-type I collagen hydrogel blends with concentrations of 0.2% or 0.5% collagen and 0.5% agarose. Neither the addition of collagen nor fibrinogen significantly impaired the printing resolution [22].

Furthermore, a fibrinogen-based bioink was employed in a handheld skin printer that was able to form skin tissue sheets of different homogeneous and architected compositions *in situ*. The authors demonstrated compatibility with dermal and epidermal cells embedded in ionically cross-linkable biomaterials (e.g., alginate), and enzymatically cross-

linkable proteins (e.g., fibrin), as well as their mixtures with collagen type I and hyaluronic acid. Upon rapid crosslinking, biomaterial and skin cell-laden sheets of consistent thickness, width and composition were obtained. Proof-of-principle demonstrations for the *in situ* formation of biomaterial sheets in murine and porcine excisional wound models illustrated the capacity of depositing them onto inclined and compliant wound surfaces that are subject to respiratory motion [23].

A novel strategy for skin injuries to the face was tested with the development of a "BioMask". This was a customized bioengineered skin substitute combined with a wound dressing layer to snugly fit onto facial wounds. To achieve this goal, the BioMask was produced using 3D bioprinting with hydrogels made of HA, glycerol, gelatin and fibrinogen. This bioprinting method could be customized through patient's clinical images, such as computed tomography (CT) data. Based on a face CT image, a wound dressing material and cell-laden hydrogels were precisely dispensed and placed in a layer-by-layer fashion through the control of air pressure and a 3-axis stage. The resulting miniature BioMask consisted of three layers; a porous PU layer, a keratinocyte-laden hydrogel layer and a fibroblast-laden hydrogel layer. To validate this novel concept, the bioprinted BioMask was applied to a skin wound on a prefabricated face-shaped structure in mice. Through this *in vivo* study using the 3D BioMask, skin contraction and histological examination showed the regeneration of skin tissue, consisting of the epidermis and dermis layers on the complex facial wounds [24].

A simpler approach to bioprinting skin substitutes can be made by using only collagen-based bioinks, and this was the strategy used to develop skin models for investigation of skin pigmentation in an *in vitro* 3D physiological model. By applying a two-step bioprinting-based strategy to produce 3D *in vitro* pigmented human skin constructs (using human keratinocytes, melanocytes and dermal fibroblast from 3 different skin donors) it was possible to print 3D pigmented skin constructs with uniform skin pigmentation. The histological analysis indicated the presence of a well-developed epidermal region and uniform distribution of melanin granules in the epidermal region of the constructs. Furthermore, the immunochemical analysis revealed the presence of important biomarkers (col VII, HMB-45, K1 and K6) in constructs [25].

Another study using a collagen-based bioink was conducted by Min D and colleagues, in which a 3D bioprinting technique that was capable of producing a full-thickness skin model containing pigmentation was reported. Multiple layers of a fibroblast-containing collagen hydrogel precursor were printed and crosslinked through neutralization using sodium bicarbonate, constituting the dermal layer. Melanocytes and keratinocytes were sequentially printed on top of the dermal layer to induce skin pigmentation upon subsequent air-liquid interface culture. Moreover, the melanocytes-containing epidermal layer showed freckle-like pigmentations at the dermal-epidermal junction, without the use of external ultraviolet light or chemical stimuli, offering the possibility of producing engineered ephelides in biomimetic skin [26].

Collagen was also used in a laser bioprinting technique to create a multi-layered, fully cellularized skin equivalent with fibroblasts and HaCaT keratinocytes. The cells were suspended in a type 1 collagen solution and printed onto a sheet of Matriderm, used as a stabilization matrix. By creating a skin chamber in the dorsal region of mice, for *in vivo* evaluation, it was possible to achieve no contraction of the wound area during the 11-day experiment, partly compensating limitations of the rodent skin lesion models. Despite not having observed complete differentiation of keratinocytes, both printed and murine fibroblasts populated the Matriderm carrier, indicative of the integration and ingrowth of the skin construct within the wound [27].

A bioink with the same material and cellular composition was used by Cubo and colleagues through the employment of an extrusion bioprinter. The authors printed a human bilayered skin using bioinks containing human plasma as well as human fibroblasts and keratinocytes obtained from skin biopsies in an extrusion open source Printbot. The printed human skin was analyzed both in 3D *in vitro* cultures and *in vivo* upon grafting on immunodeficient athymic mice using histological and

immunohistological methods. The skin was very similar to the human one and yet indistinguishable from bilayered dermo-epidermal equivalents handmade in their laboratories [28].

The same bioink components were employed using a robotic bioprinting platform based on 3D solid freeform fabrication technology with eight independently controlled cell-dispensing channels mounted on a three-axis robotic stage. The liquid materials were dispensed by pneumatic pressure and, through this technique, the number of layers, the cell density and their precise location was effectively controlled in the generation of the skin model. Their studies indicated that printing cells and proteins in nano-to-microliter droplets on planar surfaces similar to inkjet printing had a minimal effect on cell viability and function (approx 95%) [29].

In a study by Kim and colleagues, collagen was used with a PCL mesh that prevented the contraction of collagen during tissue maturation. A hybrid 3D cell-printing system was used with the use of extrusion and inkjet modules at the same time. The collagen and PCL construct loaded with fibroblast was engineered using the extrusion-dispensing module, whereas the inkjet-based dispensing module was used to uniformly distribute human epidermal keratinocytes. Taking these approaches together, a human skin model was engineered with a functional transwell system. This skin model revealed favorable biological characteristics that included a stabilized fibroblast-stretched dermis and stratified epidermis layers after 14 days. It was also observed that a 50 times reduction in cost was achieved and 10 times less medium was used than in a conventional culture [30].

Baltazar and colleagues proposed the confection of a vascularized and perfusable skin graft using a collagen-based bioink. The bioink was made of a mixture of human foreskin dermal fibroblasts, human endothelial cells, human endothelial colony forming cells and human placental pericytes with a solution of type 1 collagen in order to replicate the dermis. A second bioink was developed with human foreskin keratinocytes to form the epidermis. A construct was obtained and then grafted into a wound model mouse. The results showed the construct's ability to replicate a vascularized skin tissue, promoting maturation of foreskin keratinocytes and the assembly of interconnected microvascular networks [31].

Collagen was also used combined with gelatin methacrylamide (GelMA) and tyrosinase in another bioink formulation. Tyrosinase was presumed to have the dual function of being an essential bioactive compound in the skin regeneration process and also to be an enzyme, to facilitate the crosslink of collagen and GelMA. Moreover, enzyme crosslinking together with photocrosslinking was able to enhance the mechanical strength of the bioink. The experimental results showed that not only the bioink was able to form stable 3D living constructs using the 3D bioprinting process but also that the cell culture of three major cell lines (human melanocytes, keratinocytes and dermal fibroblasts) exhibited high cell viabilities (above 90%). Animal tests showed that the doped bioinks for 3D bioprinting could help form an epidermis and dermis, and thus have strong potential as a skin bioink [32].

Non-methacrylated gelatin is suitable for bioink composition due to its biocompatibility. Pengchao Liu and colleagues tested a bioink formed with gelatin and alginate in order to print a double layered construct by using an extrusion based 3D bioprinter. Amniotic epithelial cells (AECs) and Wharton's jelly derived mesenchymal stem cells (WJMSCs) were suspended in the bioink solution before being printed in a bilayer structure with AECs on the top layer and WJMSCs on the bottom. By doing so, the authors were able to produce refined structures with high fidelity [33].

The combination of alginate and gelatin was also employed with the addition of mouse planta dermis to form a bioink with mesenchymal stem cells (MSCs). The mechanical properties of the printed construct were evaluated. The developed constructs were able to promote cell proliferation, migration and differentiation. Although in a 2D culture with an extract of the bioink, the study reported greater expression of migration-related genes and proliferation markers, there was less mesenchymal

stem cell differentiation in the sweat gland cells. This therefore proposes an influence of a 3D structure in the cell differentiation role [34].

In an important study Koch and colleagues used laser-assisted bioprinting to demonstrate the 3D arrangement of vital cells as multicellular grafts analogous to the native archetype using fibroblasts and human immortalized keratinocytes embedded in an hydrogel composed of the following: 50% alginate and 50% EDTA, human blood plasma alternated with a hydrogel composed of 25% alginate and 75% EDTA human blood plasma. By the identification of a new formed basal lamina and by the demonstration of newly formed and fully-functional gap junctions between the keratinocytes, it was possible to show evidence of new tissue formation, a unique result to date [35].

An innovative approach on bioprinting skin substitutes was made by Ahn and colleagues using decellularized extracellular matrix (dECM) as the bioink. The researchers investigated the influence of various factors (e.g. bioink concentration, viscosity and extent of crosslinking) on cell printing and established a new 3D cell printing system equipped with heating modules for the precise stacking of the constructs. Because the pH-adjusted bioink isolated from native tissue was safely gelled at 37 °C, the heating system facilitated the precise stacking of the dECM bioinks by enabling simultaneous gelation during printing. A greater printability was observed compared with that of a non-heating system. The mechanical stacking analyses confirmed these results. By using mouse fibroblasts, it was confirmed that the heating system developed did not elicit negative effects, such as cell death in the printed cells [36].

Dermis dECM was also used as a bioink in a study by Won and collaborators, laden with human dermal fibroblasts. The results showed an increase in expression of skin morphology related genes as well as removal of resident cells and DNA from the porcine dermis and levels of collagen and glycosaminoglycans (GAG's) close to the levels of normal skin. Furthermore, the study reported that the construct went through the gelation process at 37 °C and maintained its shape even after 7 days with survival and proliferation of HDFs [37].

2.3. Vascular

One of the greatest challenges in regenerative medicine comes from the fact that human tissue is a complex system of different cells with different functions which work in synchronicity, and for those cells to stay alive they need to be oxygenated and to receive sufficient nutrients. The distance that human cells can survive far from a blood vessel is in the range of 100µm–200µm [38].

The vascular system provides the oxygen and nutrient distribution throughout the body, and every tissue has an intricate hierarchical network of vessels that deliver and remove blood to them. With that in mind, to develop a fully operational tissue *in vitro*, it is also necessary to vascularize that tissue in order to guarantee a homogenous blood distribution.

Several approaches have been developed to address this problem. Recently, Rana Atala et al. developed a multiaxial extrusion system in which the authors were able to create multilayered hollow constructs, each layer composed of different materials; collagen fibrin and alginate was used, along with different cell types, endothelial cells and fibroblasts [39].

Cui et al. developed a hollow construct with a coaxial system using GelMA functionalized with catechol to promote cell adhesion. To create the cylinder format, the authors used a crosslinking slurry containing PF127, sodium periodate and HUVECs as the internal bioink. With this, after crosslinking, the slurry washed away and what remained was the outer wall composed of GelMA and the human umbilical vein endothelial cells (HUVECs), which attached to the inner surface of the resulting tube during the process [40].

Another approach to create a hollow multilayered structure was reported by Schöneberg et al. In this study, a drop-on-demand bioprinting technique was employed; to achieve this, a slicing algorithm was used to calculate the distribution of the bioink droplets precisely and so were

able to maintain an even distribution of the layers at all heights. Their approach to create a hollow structure was to use gelatin as a sacrificial bioink and, thereby, it was washed away with warm sterile PBS (37 °C) after the printing.

Krishnamoorthy and colleagues created a three-dimensional cellular structure based on a GelMA–alginate interpenetrating polymer network (IPN) hydrogel. IPNs are polymers made of multiple polymer networks entangled. Despite having no chemical bond between each other, these networks cannot be pulled apart. This approach focused on creating a construct composed of GelMA–alginate fibers. This produced a construct with better mechanical properties, faster degradation and larger pore sizes than when the components were used individually [41].

There were also efforts made to determine how external forces can contribute to the process. Zhang et al., showed that biomechanical forces, such as actomyosin-mediated cell traction, play a role in development, alignment and maturation of the vascular network, critically regulating the vascular network assembly in a 3D bioprinted tissue. The results showed a well-developed actin meshwork and also contributed to lumen formation [42].

In another study, Solis and colleagues showed that using a thermal inkjet bioprinting system to print human microvascular endothelial cells can trigger the activation of the VEGF pathway in these cells. The authors confirmed that inkjet bioprinted cells had a significant overexpression of HSP70, IL-1 α , VEGF-A, IL-8, and FGF-1. Thus, the process activates the HSP-NF- κ B pathway to produce VEGF [43].

Another interesting approach was used by Wu and colleagues, called omnidirectional printing. In this method, fugitive bioinks are printed within a photocurable gel reservoir and washed away, creating voids which are later filled with another fluid that will solidify with the gel reservoir to form a mechanically robust, chemically crosslinked matrix. In this method, the nozzle can simultaneously move in three dimensions, allowing for a free form production in opposition to the standard layer-by-layer fabrication. This has the advantage of allowing for a more free form creation [44].

Even though advances have been made in the field, most constructs are still on a minor scale, making the scaling to larger translatable constructs a major challenge, and there is still much to be done to create a fully vascularized transplantable construct.

2.4. Cartilage

Cartilage is an avascular tissue that is composed mainly of collagen type II, GAGs, proteoglycans, water and electrolytes, with the cellular part constituted by chondrocytes [45]. Because of both the lack of vascularity and poor replicative capacity of the chondrocytes, this tissue has a limited self-repair ability. Injuries in the articular cartilage can lead to osteoarthritis, a condition with few treatment options, which include autologous chondrocyte implantation and osteochondral allografting. These treatments cause decrease in strength and resilience of the cartilage compared to healthy cartilage [46]. Thus, new regenerative approaches are necessary, and bioprinting can be a viable option by mimicking the native tissue.

Antich and colleagues tested a hyaluronic-based bioink using alginate for articular cartilage regeneration. The cells used were chondrocytes obtained from osteoarthritic patients. HA-based bioink was printed in a polylactic acid (PLA) 3D construct. Compressive tests showed that incorporation of HA increased the modulus. Furthermore, after 4 weeks in culture, the constructs presented increased compressive modulus. After the bioprinting process, the cells presented more than 85% of cell viability, with no significant differences in comparison to the period prior to printing. The cells remained viable in the constructs for up to 4 weeks, and it was observed that there was a higher viability in constructs with HA in comparison to alginate constructs. The ability to form articular cartilage *in vitro* was demonstrated by the formation of an extracellular matrix and increased gene expression specific to hyaline cartilage [47].

Galarraga and colleagues developed an *in situ* crosslinking technique

using a norbornene-HA bioink. To access the cytocompatibility, MSC from the bone marrow of bovine femora were incorporated in the hydrogel. The printed discs presented high cell viability during a 7 day period, and the cells were evenly distributed across the construct. In order to assess the ability to form neocartilage, the constructs were cultivated for up to 56 days in chondrogenic media. After 3 days of cultivation, the embedded cells showed expression of cartilage markers. On day 56, there was an increase in GAG and collagen content in the construct and increased compressive modulus, although still a long way from that of the native bovine articular cartilage. Furthermore, histological analysis showed homogeneous distribution of GAG and increased staining intensity of GAG and collagen type II over time. It is important to remark that there was more collagen type II than collagen type I, showing a resemblance with hyaline cartilage over fibrocartilage [48].

Another approach using HA as a bioink was tested by Duchi et al. The authors developed a Biopen for *in situ* co-axial 3D bioprinting, creating a core-shell structure. The hydrogel tested was GelMA/methacrylated HA (HAMA) with lithium-acylphosphinate (LAP) as the photoinitiator. The bioink presented a compressive modulus of 380 kPa. After viability tests showing that LAP was toxic to the cells, the authors developed a core/shell approach to bioprinting, where the bioink used for both core and shell was GelMA/HAMA, but the shell fraction contained LAP as well. The shell was hence crosslinked. The core/shell structure presented a compressive modulus of around 195 kPa, representing good mechanical characteristics for cartilage regeneration. Adipose-derived mesenchymal stem cells (ADSC) were embedded in the hydrogel and this bioink was printed in the core fraction. The co-axial construct presented higher cell viability compared to mono-axial printing, indicating that a core/shell structure increases cell survival. This data indicates that, if used for *in situ* repair of the cartilage, this structure could protect the ADSC and allow for its proliferation and differentiation [49].

Hyaluronic acid was also used in a bioink in a study where a biopen was developed, with the aim of making *in situ* bioprinting viable. The bioink was produced combining HAMA, GelMA and ADSC. Rheological analyses demonstrated that the bioink presented a shear thinning behavior. Regarding the performance of the biopen, it was shown that it had a good extrusion stability. Four printing pressure ranges were tested and the printing pressure of 140–165 kPa was needed to form continuous lines. Furthermore, loading the biopen with two bioinks allowed for the formation of a 2D gradient structure, which can be useful in cartilage bioengineering approaches. Cell viability assay indicated a small decrease in cell viability on day 1 after printing, most likely due to the UV exposure. This effect was not observed on day 3, indicating that shear stress during extrusion does not affect cell viability [50].

Another approach featuring the use of polymers in the bioink produced a double network hydrogel, where two different crosslinked polymers, poly(2-ethyl-2-oxazoline) (PEOXA) and alginate, were mixed to form the bioink, with four concentrations of cellulose nanofibrils (CNF) and human auricular chondrocytes (hAC). Rheological analysis demonstrated improved mechanical properties and viscoelasticity of the double network hydrogel when compared to PEOXA and alginate hydrogels alone. The compressive modulus of the double network hydrogel was around 3 to 10 times higher than that of the other formulations. The addition of CNF to the double network hydrogel did not change the compressive modulus but increased viscosity and improved shear thinning and recovery properties. The bioink showed a high cell viability, up to 90% on days 1 and 7 after printing. These values were comparable to the non-printed cells encapsulated in the hydrogel [51].

Collagen has also been explored as a possible material for bioinks, especially considering that it naturally occurs in the cartilage tissue. Bovine chondrocytes and type I collagen were used to produce a bioink with four cell densities. Formulations with higher cell densities had higher viscosity and lower yield stress. Printability tests showed higher resolution and improved printability for formulations with higher cell densities. Viability tests were performed and high viability was demonstrated on day 0, which remained high throughout 14 days in culture.

The bioprinted constructs exhibited high GAG content, and it was noted that there was no GAG content on day 0, demonstrating the ability of the construct's chondrocytes to produce GAG [52].

In order to overcome the low mechanical strength of bioprinted hydrogels, Xu and colleagues developed a new approach, combining inkjet bioprinting with electrospinning. The bioink was prepared combining fibrinogen, collagen type I and chondrocytes. PCL and PF-127 were the electrospun polymers used to enhance the mechanical properties. The bioink was printed on top of the electrospun fibers. The process led to a scaffold with 2 layers of bioink and 3 of PCL/F-127, intercalated. Mechanical tests showed improved properties of the construct when compared to the hydrogel and the electrospun fibers alone, but still lower than that of native human cartilage. Viability assays demonstrated high cell viability on the printed constructs after one week of cultivation. Histological analyses of the constructs cultivated *in vitro* showed that the chondrocytes were producing extracellular matrix after four weeks. The analyses also demonstrated the presence of organized chondrocytes within the matrix, the presence of collagen and the formation of type II collagen. It is of importance to observe that the GAGs were only present in the printed constructs with cells. Histological analyses of the *in vivo* experiments showed the production of a dense and well organized collagen network after 8 weeks. Furthermore, GAG distribution on the construct resembled typical elastic cartilage while the control group showed no presence of GAG or collagen type II. This result indicates that the printed cells are able to maintain their normal phenotype and produce extracellular matrix [53].

In order to mimic the gradient present on the osteochondral interface, Idaszek and colleagues produced a construct made by the microfluidic bioprinting approach, with the aim of forming a transition from hyaline to calcified cartilage. To achieve this, two bioinks were produced. For the hyaline cartilage, a hydrogel made of alginate, GelMA and chondroitin sulfate 2-aminoethyl methacrylate (CS-AEMA) was mixed either with only human mesenchymal stem cells (hMSC) (HC1) or with a mixture of hMSC and hAC at a 3:1 ratio (HC2). The calcified cartilage bioink was produced combining the same bioink with the addition of β -tricalcium phosphate (TCP) microparticles and HAMA, mixed only with hMSC. The cell viability was higher than 90% in HC1 and HC2 and around 88% for the calcified cartilage bioink. Cell viability remained high for all the bioinks throughout the course of 3 weeks. It was observed that the bioink containing the co-culture of hMSC and hAC (HC2) and the bioink containing TCP (CC) presented increased expression of chondrogenic markers. In addition, the bioprinted construct was implanted in a rat model of trochlea damage, and 12 weeks after implantation, no significant differences were found in the cartilage regeneration in comparison to the control [54].

A similar approach made by the same group used GelMA, alginate, TCP and hMSC in a co-axial bioprinting approach. For the bioprinting procedure, bioink and crosslinking calcium solutions were simultaneously extruded in a core/shell fashion with the bioink in the core fraction. Rheological analyses showed that the addition of TCP led to a marked shear thinning behavior. Surprisingly, the addition of TCP caused a decrease in the bioink compression modulus. The bioink was able to maintain high cell viability after printing. The expression of chondrogenic markers was increased in the alginate-GelMA-TCP bioink compared with the bioink with no TCP. Immunocytochemistry analyses confirmed that the addition of TCP can have an influence on cell chondral differentiation [55].

CNF were also tested as a bioink component for cartilage regeneration, due to their microscopical similarity with collagen fibrils. The authors produced and tested 4 formulations for the bioink composed of CNF and alginate; the bioink with optimal rheological measurements was used for bioprinting with chondrocytes. Viability tests showed higher cell viability before embedding the cells in the bioink compared to after embedding and crosslinking. However, no differences were observed in cell viability in the printed constructs compared to the nonprinted group after 1 day of cultivation. There was an increase in cell viability in the

printed constructs after 7 days of cultivation, demonstrating that the cells were able to proliferate [56].

In contrast to the majority of the studies made with common hydrogels like alginate and gelatin, a study from Rathan and colleagues tested a bioink based on cartilage extracellular matrix (cECM). This bioink was generated by mixing alginate and cECM in two different concentrations and adding BM-MSC cells. The bioinks were printed by extrusion. Rheological measurements showed that the incorporation of cECM did not affect the viscosity of the bioink, nor did it affect the printability of the inks. All the bioinks presented excellent shear-thinning and thixotropic behavior. Compressive stiffness was found to be at least an order of magnitude lower than that of native articular cartilage. To address this issue, 3D-printed PCL networks were used to support the bioink deposition. The cell viability in the printed constructs maintained in chondrogenic media for up to 42 days remained high. The 0,4% cECM bioink was the most chondroinductive, presenting the highest expression of collagen type II gene when compared to the other formulations [57].

GelMA was used as a bioink in a study which aimed to evaluate the potential of multipotent articular cartilage-resident chondroprogenitor cell (ACPCs) to synthesize cartilage extracellular matrix. It was observed that cell-free bioink did not change its compressive modulus for the two months analyzed. On the other hand, cell-laden bioinks had a significant increase in compressive modulus after 4 and 8 weeks, which could be explained by the synthesis of the cartilage matrix. However, the compressive modulus did not reach values similar to those of adult articular cartilage. 3D constructs mimicking the zonal structure of the cartilage were produced with three materials. The superficial zone was composed of GelMA and ACPC, the middle/deep zone was made of GelMA and MSCs and a layer of sacrificial ink was added with PF127 to support GelMA during the production process. The bioprinted constructs presented high cell viability through 14 days of experiment. The zonal-like structure allowed for a biomimetic distribution of GAG in the printed material [58].

A different approach was employed using core-shell nanospheres containing transforming growth factor beta 1 (TGF- β 1) for cartilage regeneration. The bioink was produced by mixing GelMA, photoinitiator and four concentrations of polyethylene glycol diacrylate (PEGDA). For the proliferation assay, BM-MSC cells were added to all four PEGDA concentrations hydrogels. The authors used a stereolithography-based 3D bioprinter to perform the bioprinting. There was an increase in the compressive modulus when adding PEGDA in comparison to GelMA alone, and this addition also increased the printing resolution with no concentration dependence. However, on proliferation analysis, the cells presented the lowest proliferation rate on the highest concentration of PEGDA. Chondrogenic differentiation studies showed that the cells encapsulated in the construct containing TGF- β 1 nanospheres presented a higher expression of chondrogenic markers in comparison with the bioink without the spheres after chondrogenic induction. Furthermore, chondrogenic extracellular matrix secretion was observed in both bioinks [59].

2.5. Bone

Bone regeneration is a complex process involving structural and functional bone reconstruction. Common bone substitutes are grafts, such as autografts, allografts and xenografts. Considering the risks involved in the use of this kind of material, novel bone substitutes are being developed, but in order to have successful regeneration, there must be sufficient osseointegration of the material. This process involves a chain of events that are affected by the physical and chemical properties of the bone substitutes [60]. Thus, bioprinting is also an alternative for bone regeneration, and the search of the optimal material that leads to a successful regeneration is its main goal.

A biphasic scaffold was developed by bioprinting using calcium phosphate cement (CPC) and a cell-laden bioink. For this, the bioink was made by mixing alginate and methylcellulose, and for the cell tests, CPC

was added to the hMSC and the bioink was plotted with an alternating layer pattern. Post-plotting treatment allowed for the plotting of a biphasic scaffold. Mechanical testing showed that adding CPC increased the material compressive modulus when compared to alginate/methylcellulose alone. The addition of CPC in the bioink resulted in a decrease in cell viability which was compensated afterwards by cell adherence and proliferation [61].

The use of hydroxyapatite (HAp) in bone tissue engineering is widely incorporated as it is the main inorganic component of natural bone. Bendsten and colleagues used HAp diluted in polyvinyl alcohol (PVA) as well as alginate to formulate a bioink, and tested 7 different formulations. The bioinks were then bioprinted by extrusion and the formulation with the best printability and rheological properties was used for the following tests. This bioink presented a compressive modulus of 10.3 kPa, which decreased over 14 days to 2.4 kPa. Following this, MC3T3 cells were incorporated into the bioink. Viability tests showed that the presence of PVA-HAp increased cell viability after printing and crosslinking [62].

Another approach for 3D bioprinting is the use of growth factors to functionalize bioinks. Byambaa and colleagues used a GelMA-based bioink functionalized with vascular endothelial growth factor (VEGF) to produce vascularized bone tissue. For the vascularized construct, the authors used two different Gelma concentrations, two different cell lines, silicate nanoplatelets and three different VEGF concentrations to print a scaffold composed of four cylinders. The inner rod was produced with 5% GelMA conjugated with VEGF, HUVECs and hMSC. The low GelMA concentration was used to allow for a fast degradation forming a lumen in the core of the structure. Three other layers were printed using GelMA 10% with silicate nanoplatelets to induce osteogenic differentiation, hMSC and decreasing VEGF concentrations of 68.5, 34.2 and 17.1 ng/mL from the outside to the inside of the construct. Compression tests indicate that chemical modifications did not affect the mechanical strength of the hydrogel. The bioactivity of the cells embedded in the 5% GelMA-VEGF to support capillary formation showed that the HUVECs encapsulated in that bioink formed a more capillary-like network compared to the control. The co-culture of the HUVECs and hMSC was able to produce a vascularized bone tissue with high cell viability and proliferation [63].

In another study using GelMA, a bioink was produced combining Gelma, kappa carrageenan and nanosilicates (nSi) to form a nanoengineered-ionic-covalent-entanglement (NICE). To evaluate the printability of the inks, formulations with a variation of the component concentration were tested. The bioink with better printability was used in the other analyses. Rheological analysis indicates that varying concentrations of each component altered the compressive modulus of the bioink, indicating that every component has a role in the mechanical properties of the bioink. To evaluate cell interaction with the bioink, hMSC were added to NICE hydrogel and printed by extrusion. Histological analysis indicates that the encapsulated cells were able to produce a cartilage and osteoid-like extracellular matrix that was mineralized over time. The authors found that gene expression related to osteochondral differentiation was upregulated in those cells even with the lack of osteoinductive factors [64].

GelMA was also studied in an attempt to improve its biofunctionality by creating a nanoclay composite bioink. For that, GelMA was mixed with a laponite (LPN) suspension, followed by the addition of photoinitiators. The addition of LPN interfered with GelMA photocrosslinking, which was observed by the increase in the soluble fraction of the formulations. The nanocomposite at 7.5 wt% of GelMA preserved its mechanical stiffness independent of LPN concentration, whereas 10 wt% showed a lower modulus with 0.5 and 1 wt% of LPN. Furthermore, incorporation of LPN increased the bioink viscosity in a concentration dependent manner but it did not alter the shear-thinning behavior of the bioinks. Overall, the addition of LPN improved the bioink printability. After these initial tests, HBMSCs were incorporated in the composite and the bioink was printed by extrusion. The constructs presented high cell viability and when cultivated in osteogenic media, they were able to support osteogenic differentiation, as evidenced by mineral deposition [65].

GelMA was also used to create a structure with an interconnected microchannel network within it by using PF127 as a sacrificial ink and MSCs as the cellular component. This bioink was printed directly on the collecting plate or on top of the pluronic micropillars. The constructs containing pluronic were brought to 4 °C to sacrifice the pluronic micropillars and create the open channels. The compressive modulus of the bioprinted material with no channels was around 76 kPa and around 69 for the microchannelled construct. Viability assay indicated that the cells were still viable 24 h after bioprinting. An anatomically shaped humeral head was printed for *in vivo* transplantation. Before the implantation the constructs were chondrogenically primed for 4 weeks and collagen type II staining indicated chondrogenesis of the MSC after this period. The constructs were implanted in a femoral defect model in rats. After 4 weeks of implantation, the microchannelled construct was able to create a vascular network within the bone defect. Histological staining showed a higher incorporation of the construct with the microchannels with the host compared to the non-microchannelled construct, increasing vascularization and implant remodeling. However, total bone volume in the defects was higher in the non-microchannelled construct compared to the microchannelled construct [66].

In a different study, GelMA was used to compose a bioink supplemented with agarose and calcium salt of polyphosphate [polyP·Ca²⁺-complex] to enhance proliferation. The bioink was produced by mixing alginate, GelMA, polyP·Ca²⁺-complex dissolved in agarose and sarcoma osteogenic cells. When polyP·Ca²⁺-complex was added to the bioink formulation, the scaffold increased compressive modulus compared to the scaffold with no polyP·Ca²⁺-complex. The presence of cells caused a decrease in the compressive modulus during a 5 day incubation period in both bioinks. The addition of polyP·Ca²⁺-complex also increased cell viability. The use of polyP·Ca²⁺-complex was not able to induce mineralization, and crystallite formation was only observed when an osteogenic cocktail was used [67].

Inkjet bioprinting was used to print constructs with physiological cell density using a collagen, alginate and fibrinogen to induce osteogenic differentiation. For the viability assays, hMSC were added to the hydrogel. Rheological analysis showed a compressive modulus of around 1120 Pa, and Scanning Electron Microscopy (SEM) revealed a highly porous structure. Cell viability assay indicated that both cell densities were able to maintain cell viability in the 14 days of experiment. Furthermore, the two bioinks presented an increase in cell numbers from day 0–14, indicating cell proliferation. The cells embedded in the bioinks changed from a random alignment to an organized morphology and this effect was more accentuated in the higher cell density bioink. The higher cell density also stimulated increased calcium deposition and a more rapid differentiation into active osteoblasts, with an increased expression of osteogenic biomarkers [68].

Inkjet bioprinting was also used to print bioinks based on agarose and collagen type I with MSCs. In that study, different concentrations of agarose and collagen were mixed and compared with pure collagen and pure agarose. For the cell assays, MSCs were embedded in the hydrogels. It was observed that increasing collagen content led to less precise contours of the bioprinted material, and that higher agarose content presented higher viscosity and gelation temperature. All the formulations presented high cell viability, around 98%, after 21 days of cultivation. It was also demonstrated that the cells could spread more easily and had higher branching capacity in the less stiff formulation. After osteogenic induction, the level of mineralization was assessed and there were no differences among the three formulations; the same was observed for alkaline phosphatase activity. However, the expression of osteogenic markers was increased in the less stiff hydrogel, probably due to the increased cell spreading. Hence, the authors suggest that this hydrogel could be suitable for bone tissue engineering [69].

In another study using inkjet bioprinting, the authors produced a bioink combining polyethylene glycol (PEG), acrylated Arg-Gly-Asp (RGD), acrylated matrix metalloproteinase (MMP) and hMSC. The scaffold produced using PEG with MMP and RGD showed a lower

compressive modulus compared to the scaffold with only PEG, but the compressive modulus increased when the constructs were submitted to osteogenic and chondrogenic differentiation for 21 days. From day 7–21, there was a higher increase in the compressive modulus in osteogenic differentiation than in chondrogenic differentiation. The printed cells maintained an excellent level of viability 24 h after printing. The expression of osteogenic genes was drastically increased in the PEG with peptides group, indicating an osteochondral bone formation. Furthermore, the expression of chondrogenic genes was higher in the PEG peptide construct compared to the construct of only PEG. Thus, it can be concluded that the PEG peptide bioink enhances osteogenic and chondrogenic differentiation [70].

PEG was combined with poly(lactic-co-glycolic acid) (PLGA) to produce a bioink with the aim of producing a scaffold with yield stress and compressive modulus in the same range of human bones. The PLGA-PEG microparticles hydrogel was used to produce bioink formulations using three viscosity modifiers: medium viscosity carboxymethyl cellulose (CMC_{el}), high viscosity CMC_{el} and PF127. hMSC were mixed with high viscosity CMC_{el} and then combined with microparticles hydrogel for bioprinting. The pluronic bioinks were not able to maintain their structure during the printing process. The most promising modifiers were 2% and 3% high viscosity CMC_{el} at minimum ratio, with yield stress and compressive modulus in the same range of human cancellous bone. Lysozyme microspheres were added to the bioink in order to enhance osteogenic differentiation. The authors found that cell viability is highly dependent on carrier ratio [71].

In order to evaluate vascularization and osteogenic differentiation, a hybrid construct made of hydrogels and PCL/HAP, laden with stromal vascular fraction cells from adipose tissue, was conditioned in normal oxygen or hypoxic environments. The hydrogel was produced with HAMA, GelMA and HA. The constructs made of hydrogel alone or hybrid of hydrogel and PCL/HAP were bioprinted by extrusion and then kept either in normoxia or hypoxia for up to 21 days. Viability tests showed that at 14 and 21 days of hypoxia, there were increasing numbers of dead cells in the constructs. IHC staining showed that the cells expressed endothelial markers in both normoxia and hypoxia, but only in hypoxia could there be seen the formation of microvessel-like structures. At day 7, the hypoxia groups also showed an upregulation of vascularization genes but this decreased at day 14 to levels comparable or even lower than the normoxia group. The cell-laden hydrogels were then printed in an alternate order with PCL/HAP a view to creating hybrid bone constructs. IHC analyses showed the presence of encapsulated cells between the PCL/HAP scaffolds. Compressive tests indicated compressive modulus of around 50 MPa. The hybrid constructs were conditioned under hypoxia for 7 days in osteogenic and endothelial media, followed by 14 days in normoxia. In both the normoxia and hypoxia, there was alkaline phosphatase (ALP) staining and ALP activity, and it was demonstrated that hypoxia conditioning did not alter osteogenic differentiation. However, hypoxia led to upregulation of the endothelial genes. Surgical implantation of the constructs in mice showed that constructs conditioned in either normoxia or hypoxia led to *in vivo* vascularization, but hypoxia led to increased vessel lumen size and broader distribution [72].

PCL was also used to enhance the mechanical properties of a hydrogel in a hybrid construct made by Song and colleagues. The hydrogel was composed of alginate and TCP laden with 1x10⁶ BEL-7402 human hepatocarcinoma cells per ml of the bioink. Several hydrogels with different concentrations of alginate (2%, 4% and 6% w/v) and different ratios of TCP to alginate (0:4, 1:4, 8:4) were tested. Rheological analyses showed that viscosity was dependent on alginate concentration, with higher concentrations leading to higher shear-thinning behavior and the necessity for higher printing pressure, whereas the addition of TCP did not affect the shear-thinning properties. 4% of the alginate demonstrated a perfect 3d structure, and all formulations presented a compressive modulus similar to that of a cancellous bone. The constructs were then printed in a 3d model of a rabbit bone defect reconstructed by micro-CT images processed by a software. After 4 h of cultivation, cell viability was

assessed, and it was shown that the cells in the hydrogels composed of alginate alone had high cell viability and that the addition of TCP decreased viability significantly [73].

2.6. Muscle

Volumetric muscle loss (VML), defined as extremity muscle injuries that result in more than 20% tissue damage of the affected muscle, are beyond the endogenous ability of self-healing and result in loss of muscle function [74]. Currently, there is no effective regenerative therapy and current gold standard - autologous tissue transfer - is associated with donor site morbidity and functional deficiency [75]. Moreover, autologous tissue for implantation is often unavailable or smaller than the size of the injured site, resulting in insufficient functional regeneration. Therefore, tissue engineering has become an important tool for developing muscle grafts that could efficiently deal with VML and promote *de novo* muscle regeneration and functional recovery.

An innovative approach for reconstituting muscle was developed by Kim and colleagues, using dECM as a bioink constituent. In this study, the authors used the extrusion bioprinting method with fibrillated PVA as a sacrificial material aligned by a controllable wall shear stress within a micro-sized nozzle with the aim of guiding cellular orientation and facilitating *in vitro* myogenic differentiation and maturation. Through this novel method it was possible to create a uniaxially aligned fibrillated printed construct (made of methacrylate decellularized extracellular matrix together with C2C12 myoblasts) that was able to induce myoblast orientation, resulting in accelerated myogenic differentiation when compared to a GelMA-based structure with the same topographical cues and a dECM-based structure without topographical cues [76].

Decellularized extracellular matrix was also used in a study by Choi and colleagues to develop 3D cell printed prevascularized muscle constructs made of cell-laden dECM, human skeletal muscle cells, vascular dECM and HUVECs through coaxial nozzle printing. The biomaterial was able to mimic the hierarchical architecture of vascularized muscles and showed improved *de novo* muscle fiber formation, vascularization and innervation as well as 85% of functional recovery in VML injuries [77].

The same author used dECM to develop functional skeletal muscle constructs composed of multinucleated and aligned muscle fibers. The dECM-based bioink was printed using a 3D PCL support system. The use of dECM was able to preserve major ECM components, such as laminin, collagen and GAGs while the cellular components were removed. dECM bioink-containing cells were printed in the desired spatial pattern with adequate printability and generated various types of 3D muscle constructs with controllable architectures. The dECM bioink forged a sufficient microenvironment simultaneously with the 3D-printed geometrical constraints in the muscle constructs and provided cells with myogenic conditions for exhibiting high viability, proliferation, myotube formation and myogenic differentiation [78].

A PCL base was also used in a study by Kim and colleagues, together with a gelatin hydrogel and human primary muscle progenitor cells. The bioprinted skeletal muscle tissue showed a highly organized multi-layered muscle bundle made of viable, densely packed and aligned myofiber-like structures. The *In vivo* study showed that the bioprinted muscle constructs reached 82% of functional recovery in a rodent model of tibialis anterior muscle defect at 8 weeks post-implantation. In addition, histological and immunohistological examinations indicated that the bioprinted muscle constructs were well integrated with the host vascular and neural networks [76].

The same author published another paper using the same bioprinting strategy but this time with a mix of human primary muscle progenitor cells and hNSCs in the gelatin bioink to investigate the effects of neural cell integration in the bioprinted skeletal muscle construct to accelerate functional muscle regeneration *in vivo*. Neural input in this bioprinted skeletal muscle construct showed the improvement of myofiber formation, long-term survival and neuromuscular junction formation *in vitro*. More importantly, the bioprinted constructs with neural cell integration

facilitated rapid innervation and maturation into organized muscle tissue that restored normal muscle weight and function in a rodent model of muscle defect injury [79].

The additional stiffness brought about by using a PCL base was also explored in a study by Merceron and colleagues, where the authors presented a 3D integrated organ printing system for the processing and deposition of four different components for the production of a single integrated muscle-tendon unit construct. Thermoplastic PU was co-printed with C2C12 cell-laden fibrin-based bioink for elasticity and muscle development on one side, while PCL was co-printed with fibroblast cell-laden hydrogel-based bioink for stiffness and tendon development on the other. The developed construct presented good mechanical characteristics and >80% cell viability at 1 and 7 days after printing as well as initial tissue development and differentiation [80].

Constantini and colleagues tailored a bioink with a photocurable semi-synthetic biopolymer using PEG-Fibrinogen encapsulating C2C12 cells in 3D constructs composed of aligned hydrogel fibers using a coaxial needle extruder in a microfluidic printing head. After 3–5 days of cultivation, the encapsulated myoblasts began migrating and fusing, forming multinucleated myotubes. The obtained myotubes showed a high degree of alignment along the direction of hydrogel fiber deposition, further revealing maturation, sarcomerogenesis and functionality. Following subcutaneous implantation in the back of immunocompromised mice, bioprinted constructs generated organized artificial muscle tissue *in vivo* [81].

Alginate was also used in a complex 3D scaffold combining a myoblast laden bioink, electrospun micro and nano fibers of PCL and a PCL strut. The bioink composition consisted of alginate and polyethylene oxide. Two disposal patterns of PCL micro and nano fibers were tested: a random and an aligned pattern. Live/dead assay was performed on days 1, 3 and 7. RT-PCR was performed to analyze the expression of MyoD, myogenin, MHC and Troponin T. The results showed that the scaffold was capable of generating good cell viability with both the random and the aligned test group. However, the morphology and formation of the myotubes was influenced strongly by the fiber's orientation [82].

GelMA was combined with several materials in order to create a bioink which could produce a scaffold with structural fidelity with skeletal muscle and a long-standing structure. For the bioink, GelMA was diluted to a 1% or 5% concentration and the 5% GelMA was mixed either with 1% PEGDMA (GelMA-PEGDMA), 1% alginate-methacrylate (GelMA-AlgMA) or 1% carboxymethyl cellulose-methacrylate (GelMA-CMCellMA) and with Irgacure 2959 or LAP. C2C12 cells were added to the hydrogel to perform a cell viability assay with cell density of 1×10^6 cells/mL of the bioink. The cell viability analysis showed that it was possible to use both photoinitiators at maximum concentration of 0,1% with cell survival up to 60%. Compressive tests indicate that the presence of LAP increases compressive modulus compared to Irgacure 2959. The formulations containing alginate presented the highest compressive modulus [83].

2.7. Others

Several studies are being made in the effort of reconstructing damaged cornea using 3D bioprinting. Bektas and colleagues used cell laden GelMA hydrogels to bioprint a corneal stromal equivalent using human corneal keratocytes using an extrusion bioprinter. Cell viability tests showed 98% of viable cells 21 days after printing and, after this time, mechanical properties were close to those of native human cornea. Furthermore, the keratocytes were able to synthesize extracellular matrix, shown by the presence of collagen type I and V, as well as proteoglycan decorin on the edges, but not the center, of the constructs [84] (Bektas, 2020). Sorkio and colleagues used laser-assisted bioprinting with human embryonic stem cell derived limbal epithelial stem cells (hESC-LESC) and ADSC to develop three types of corneal structures: the corneal epithelium, the corneal stroma and structures with both epithelium and stroma. For the epithelium, laminin was used as the base for the

bioink, whereas for the stroma, collagen I was used. The cells presented good viability and tissue organization, and the epithelial construct showed expression of corneal progenitor markers. Furthermore, after incubation with porcine corneal organ culture, the stromal constructs attached and the cells migrated from the printed structure [85].

The liver is a central organ in the metabolism of toxic substances, drugs and endogenous substances. Chronic exposure to xenobiotics, inherited conditions and other insults can lead to permanent damage and physiological loss. 3D bioprinting has been exploited as an alternative to produce functional 3D hepatic tissue. Goulart and colleagues used an extrusion bioprinter to bioprint induced pluripotent stem cells (IPS) in two different approaches using alginate mixed with PF-127 as the bioink. The authors compared cell survival and functional parameters of single cell dispersion and spheroid dispersion of IPS-derived hepatocyte-like cells. *In vitro* assays indicated a reduced cell survival in the single cell groups as well as metabolic malfunction, indicating that a spheroid-based bioprinting may be a suitable alternative to produce functional livers [86].

In order to produce a tissue suitable for *in vivo* application, the bioink rheology is a major component. Wu and colleagues produced a bioink combining GelMA, alginate, cellulose nanocrystal (CNC), fibroblasts and hepatoma cells (hepG2), printed with a microextrusion bioprinter. This formulation presented a mechanical stiffness in the same range of the human liver with a good printability and an excellent shear-thinning behaviour. The bioink was used to print a lobule-like complex structure capable of producing albumin, showing the possibility to create a bioprinted biomimetic structure using numerous cell lines and variable extracellular matrix (ECM) [87].

In an attempt to improve cell survival, Mao and colleagues produce a bioink combining liver decellularized matrix and GelMA to bioprint a construct suitable for liver transplantation and able to restore hepatic function. The authors used digital light process-based bioprinting to fabricate a liver-like tissue using human-induced hepatocytes. The dECM presence increases printability, cell survival and albumin and blood urea nitrogen secretion. That indicates that this microtissue may be a suitable alternative for liver transplantation due to its mechanical properties and hepatocyte-like behaviour [88].

"Israel's heart" result of Noor and colleagues received expressive media coverage in 2019 for its impressive technique and rather dramatic construct. The work consisted in isolation of cells and ECM from the omentum to induce adipocyte into iPSCs and to produce an hydrogel then used to print cardiac patches or a whole heart structure. Computerized tomography scan of the patient's heart guided the cardiac patches production, resulting in a fully personalized tissue segment that fit the anatomic and biomechanical characteristics of the native patient's tissue. The famous Israel's heart structure, however, did not use the same methodology and needed a supporting medium (alginate microparticles in xanthan gum-supplemented growth medium) to execute free form extrusion printing. The supporting medium then underwent an enzymatic degradation, extracting the construct which was subsequently cultured in growth medium. An important authors' statement expressed concern about the safety of the IPCs usage in clinic, based on the known problems of this lineage such as inducing tumors and having an unstable genome. Lastly, results demonstrated that this approach creates far less immune response and an environment that promotes self renewal and differentiation of desired cells, as well as promoting physiological processes that assemble and mature the treated tissue [89].

3. Conclusion

Bioprinting is a novel technology that has been showing promising results for regenerative medicine due to its capacity for engineering tissue substitutes with the appropriate and unique characteristics of each tissue type. The choice of each bioink component and its concentration can provide specific biological and mechanical characteristics for the optimal formulation in order to mimic the native tissue. Each tissue

requires specific characteristics to be able to obtain a good substitute. Bone and cartilage substitutes must present adequate rheological characteristics in order to maintain the construct integrity and stiffness and to obtain maximum tissue regeneration, whereas vascular substitutes must be malleable enough to be shaped correctly in order to regenerate vessels. These properties, alongside the cellular components of the bioinks have been explored in several different studies worldwide to achieve a gold standard in regenerative medicine for each tissue type. A collection of studies adventuring into this new field of knowledge to reach the ideal bioink for every tissue type is required for aiding researchers with the same goal.

Funding

This work was supported by MCTIC, FINEP, CNPq, FAPERGS and IPTC.

CRediT authorship contribution statement

Fernanda Staphenhorst: Conceptualization, Investigation, Writing - original draft, Writing - review & editing, Visualization, Supervision. **Marcelo Garrido dos Santos:** Conceptualization, Investigation, Writing - original draft, Writing - review & editing, Visualization. **João Pedro Prestes:** Conceptualization, Investigation, Writing - original draft. **Bruno José Alcantara:** Conceptualization, Investigation, Writing - original draft. **Maurício Felisberto Borges:** Conceptualization, Investigation, Writing - original draft, Visualization. **Patricia Pranke:** Conceptualization, Writing - review & editing, Supervision, Project administration, Funding acquisition.

Declaration of competing interest

The authors declare that they have no known competing financial interests or personal relationships that could have appeared to influence the work reported in this paper.

Appendix A. Supplementary data

Supplementary data to this article can be found online at <https://doi.org/10.1016/j.bprint.2021.e00130>.

References

- [1] C. Vacanti, R. Langer, B. Schloo, et al., Synthetic polymers seeded with chondrocytes provide a template for new cartilage formation, *Plast. Reconstr. Surg.* 88 (1991) 753–759.
- [2] F.E. Smit, P.M. Dohmen, Cardiovascular tissue engineering: where we come from and where are we now? *Med. Sci. Monit. Basic Res.* 21 (2015) 1–3.
- [3] W. Zhu, X. Ma, M. Gou, D. Mei, K. Zhang, S. Chen, 3D printing of functional biomaterials for tissue engineering, *Curr. Opin. Biotechnol.* 40 (2016) 103–112, <https://doi.org/10.1016/j.copbio.2016.03.014>. Available from.
- [4] T. Baudequin, M. Tabrizian, Multilineage constructs for scaffold-based tissue engineering: a review of tissue-specific challenges, *Adv. Healthc. Mater.* 7 (3) (2018) 1–29.
- [5] S. Naahidi, M. Jafari, M. Logan, Y. Wang, Y. Yuan, H. Bae, et al., Biocompatibility of hydrogel-based scaffolds for tissue engineering applications, *Biotechnol. Adv.* 35 (5) (2017) 530–544, <https://doi.org/10.1016/j.biotechadv.2017.05.006>. Available from.
- [6] D. Steffens, D.I. Braghirolli, N. Maurmann, P. Pranke, Update on the main use of biomaterials and techniques associated with tissue engineering, *Drug Discov. Today* [Internet] 23 (8) (2018) 1474–1488, <https://doi.org/10.1016/j.drudis.2018.03.013>. Available from.
- [7] J. Groll, J.A. Burdick, D.W. Cho, B. Derby, M. Gelinsky, S.C. Heilshorn, et al., A definition of bioinks and their distinction from biomaterial inks, *Biofabrication* 11 (1) (2019).
- [8] X. Zhang, Y. Zhang, Tissue engineering applications of three-dimensional bioprinting, *Cell Biochem. Biophys.* 72 (3) (2015) 777–782.
- [9] N. Hong, G.H. Yang, J.H. Lee, G.H. Kim, 3D bioprinting and its in vivo applications, *J. Biomed. Mater. Res. B Appl. Biomater.* 106 (1) (2018) 444–459.
- [10] B. Niemczyk, P. Sajkiewicz, D. Kolbuk, Injectable hydrogels as novel materials for central nervous system regeneration, *J. Neural Eng.* 15 (5) (2018 Oct 1), 051002. Available from, <https://iopscience.iop.org/article/10.1088/1741-2552/aacbab>.
- [11] X. Gu, F. Ding, D.F. Williams, Neural tissue engineering options for peripheral nerve regeneration [Internet], *Biomaterials* 35 (24) (2014) 6143–6156, <https://doi.org/10.1016/j.biomaterials.2014.04.064>. Available from.
- [12] Q. Gu, E. Tomaskovic-Crook, R. Lozano, Y. Chen, R.M. Kapsa, Q. Zhou, et al., Functional 3D neural mini-tissues from printed gel-based bioink and human neural stem cells, *Adv. Healthc. Mater.* 5 (12) (2016) 1429–1438.
- [13] A.P. Haring, E.G. Thompson, Y. Tong, S. Laheri, E. Cesewski, H. Sontheimer, et al., Process- and bio-inspired hydrogels for 3D bioprinting of soft free-standing neural and glial tissues [Internet], *Biofabrication* 11 (2) (2019 Feb 25), 025009. Available from, <https://iopscience.iop.org/article/10.1088/1758-5090/ab02c9>.
- [14] L. Ho, S. Hsu, hui, Cell reprogramming by 3D bioprinting of human fibroblasts in polyurethane hydrogel for fabrication of neural-like constructs [Internet], *Acta Biomater.* 70 (2018) 57–70, <https://doi.org/10.1016/j.actbio.2018.01.044>. Available from.
- [15] F.Y. Hsieh, H.H. Lin, S. Hsu, hui, 3D bioprinting of neural stem cell-laden thermoresponsive biodegradable polyurethane hydrogel and potential in central nervous system repair [Internet], *Biomaterials* 71 (2015) 48–57, <https://doi.org/10.1016/j.biomaterials.2015.08.028>. Available from.
- [16] W. Zhu, B.T. Harris, L.G. Zhang, Gelatin methacrylamide hydrogel with graphene nanoplatelets for neural cell-laden 3D bioprinting, in: *Proc Annu Int Conf IEEE Eng Med Biol Soc EMBS 2016-Octob*, 2016, p. 4185, 8.
- [17] L. Koch, A. Deiwick, S. Schlie, S. Michael, M. Gruene, V. Coger, et al., Skin tissue generation by laser cell printing [Internet], *Biotechnol. Bioeng.* 7 (109) (2012 Jul) 1855 [cited 2020 Apr 18], <http://www.ncbi.nlm.nih.gov/pubmed/22328297>.
- [18] A. Skardal, D. Mack, E. Kapetanovic, A. Atala, J.D. Jackson, J. Yoo, et al., Bioprinted amniotic fluid-derived stem cells accelerate healing of large skin wounds, *Stem Cells Transl. Med.* 1 (11) (2012 Nov) 792–802, <https://doi.org/10.5966/sctm.2012-0088>. Available from.
- [19] M. Albanna, K.W. Binder, S.V. Murphy, J. Kim, S.A. Qasem, W. Zhao, et al., In situ bioprinting of autologous skin cells accelerates wound healing of extensive excisional full-thickness wounds [Internet], *Sci. Rep.* 9 (1) (2019) 1–15, <https://doi.org/10.1038/s41598-018-38366-w>. Available from.
- [20] K. Derr, J. Zou, K. Luo, M.J. Song, G.S. Sittampalam, C. Zhou, et al., Fully three-dimensional bioprinted skin equivalent constructs with validated morphology and barrier function, *Tissue Eng. C Methods* 25 (6) (2019) 334–343.
- [21] L.J. Pourchet, A. Thepot, M. Albouy, E.J. Courtial, A. Boher, L.J. Blum, et al., Human skin 3D bioprinting using scaffold-free approach [Internet], *Adv. Healthc. Mater.* 6 (4) (2017 Feb 22). Available from, <http://www.ncbi.nlm.nih.gov/pubmed/27976537>.
- [22] F. Kreimendahl, M. Köpf, A.L. Thiebes, D.F. Duarte Campos, A. Blaeser, T. Schmitz-Rode, et al., Three-dimensional printing and angiogenesis: tailored agarose-type I collagen blends comprise three-dimensional printability and angiogenic potential for tissue-engineered substitutes, *Tissue Eng. C Methods* 23 (10) (2017) 604–615.
- [23] N. Hakimi, R. Cheng, L. Leng, M. Sotoudehfar, P.Q. Ba, N. Bakhtyar, et al., Handheld skin printer: in situ formation of planar biomaterials and tissues [Internet], *Lab Chip* 18 (10) (2018 May 21) 1440, 51, <http://www.ncbi.nlm.nih.gov/pubmed/29662977>.
- [24] Y.-J. Seol, H. Lee, J.S. Copus, H.-W. Kang, D.-W. Cho, A. Atala, et al., 3D bioprinted biomask for facial skin reconstruction [Internet], *Bioprinting* 10 (3) (2018 Jun), e00028. Available from, <https://linkinghub.elsevier.com/retrieve/pii/S2405886618300137>.
- [25] W.L. Ng, J.T.Z. Qi, W.Y. Yeong, M.W. Naing, Proof-of-concept: 3D bioprinting of pigmented human skin constructs, *Biofabrication* 10 (2) (2018).
- [26] D. Min, W. Lee, I.H. Bae, T.R. Lee, P. Croce, S.S. Yoo, Bioprinting of biomimetic skin containing melanocytes [Internet], *Exp. Dermatol.* 27 (5) (2018 May 1) 453, 9, <http://www.ncbi.nlm.nih.gov/pubmed/28453913>.
- [27] S. Michael, H. Sorg, C.T. Peck, L. Koch, A. Deiwick, B. Chichkov, et al., Tissue engineered skin substitutes created by laser-assisted bioprinting form skin-like structures in the dorsal skin fold chamber in mice, *PLoS One* 8 (3) (2013).
- [28] N. Cubo, M. Garcia, J.F. Del Cañizo, D. Velasco, J.L. Jorcano, 3D bioprinting of functional human skin: production and in vivo analysis, *Biofabrication* 9 (1) (2017).
- [29] V. Lee, G. Singh, J.P. Trasatti, C. Bjornsson, X. Xu, T.N. Tran, et al., Design and fabrication of human skin by three-dimensional bioprinting, *Tissue Eng. C Methods* 20 (6) (2014) 473–484.
- [30] B.S. Kim, J.S. Lee, G. Gao, D.W. Cho, Direct 3D cell-printing of human skin with functional transwell system, *Biofabrication* 9 (2) (2017).
- [31] T. Baltazar, J. Merola, C. Catarino, C.B. Xie, N.C. Kirkiles-Smith, V. Lee, et al., Three dimensional bioprinting of a vascularized and perfusable skin graft using human keratinocytes, fibroblasts, pericytes, and endothelial cells, *Tissue Eng. Part A* 26 (5–6) (2020) 227–238.
- [32] Y. Shi, T.L. Xing, H.B. Zhang, R.X. Yin, S.M. Yang, J. Wei, et al., Tyrosinase-doped bioink for 3D bioprinting of living skin constructs, *Biomed. Mater.* 13 (3) (2018).
- [33] P. Liu, H. Shen, Y. Zhi, J. Si, J. Shi, L. Guo, et al., 3D bioprinting and in vitro study of bilayered membranous construct with human cells-laden alginate/gelatin composite hydrogels, *Colloids Surf. B Biointerfaces* 181 (2019) 1026, <https://doi.org/10.1016/j.colsurfb.2019.06.069>. Available from.
- [34] L. Cheng, B. Yao, T. Hu, X. Cui, X. Shu, S. Tang, et al., Properties of an alginate-gelatin-based bioink and its potential impact on cell migration, proliferation, and differentiation [Internet], *Int. J. Biol. Macromol.* 135 (2019) 1107–1113, <https://doi.org/10.1016/j.ijbiomac.2019.06.017>. Available from.

- [35] Lothar Koch, Andrea Deiwick, Sabrina Schlie, Stefanie Michael, Martin Gruene, Vincent Coger, Daniela Zychlinski, Axel Schambach, Kerstin Reimers, Peter M. Vogt, Skin tissue generation by laser cell printing, *Biotechnol. Bioeng.* 109 (7) (2012) 1855–1863, <https://doi.org/10.1002/bit.24455>. Wiley.
- [36] G. Ahn, K.H. Min, C. Kim, J.S. Lee, D. Kang, J.Y. Won, et al., Precise stacking of decellularized extracellular matrix based 3D cell-laden constructs by a 3D cell printing system equipped with heating modules, *Sci. Rep.* 7 (1) (2017 Dec 1).
- [37] J.Y. Won, M.H. Lee, M.J. Kim, K.H. Min, G. Ahn, J.S. Han, et al., A potential dermal substitute using decellularized dermis extracellular matrix derived bio-ink [Internet], *Artif Cells, Nanomed. Biotechnol.* 47 (1) (2019) 644–649, <https://doi.org/10.1080/21691401.2019.1575842>. Available from.
- [38] G.F. Muschler, C. Nakamoto, L.G. Griffith, Engineering principles of clinical cell-based tissue engineering, *J. Bone Jt Surg. - Ser A* 86 (7) (2004) 1541–1558.
- [39] R. Attalla, E. Puersten, N. Jain, P.R. Selvaganapathy, 3D bioprinting of heterogeneous bi- and tri-layered hollow channels within gel scaffolds using scalable multi-axial microfluidic extrusion nozzle [Internet], *Biofabrication* 11 (1) (2018 Dec 27), 015012. Available from, <https://iopscience.iop.org/article/10.1088/1758-5090/aaf7c7>.
- [40] H. Cui, W. Zhu, Y. Huang, C. Liu, Z.X. Yu, M. Nowicki, et al., In vitro and in vivo evaluation of 3D bioprinted small-diameter vasculature with smooth muscle and endothelium, *Biofabrication* 12 (1) (2020).
- [41] S. Krishnamoorthy, Z. Zhang, C. Xu, Biofabrication of three-dimensional cellular structures based on gelatin methacrylate–alginate interpenetrating network hydrogel, *J. Biomater. Appl.* 33 (8) (2019) 1105–1117.
- [42] G. Zhang, M. Varkey, Z. Wang, B. Xie, R. Hou, A. Atala, ECM concentration and cell-mediated traction forces play a role in vascular network assembly in 3D bioprinted tissue, *Biotechnol. Bioeng.* 117 (4) (2020) 1148–1158.
- [43] L.H. Solis, Y. Ayala, S. Portillo, A. Varela-Ramirez, R. Aguilera, T. Boland, Thermal inkjet bioprinting triggers the activation of the VEGF pathway in human microvascular endothelial cells in vitro, *Biofabrication* 11 (4) (2019).
- [44] W. Wu, A. Deconinck, J.A. Lewis, Omnidirectional printing of 3D microvascular networks, *Adv. Mater.* 23 (24) (2011) 178–183.
- [45] A.R. Armiento, M.J. Stoddart, M. Alini, D. Eglin, Biomaterials for articular cartilage tissue engineering: learning from biology, *Acta Biomater.* 65 (2018) 1–20, <https://doi.org/10.1016/j.actbio.2017.11.021>. Available from.
- [46] R.S. Tuan, A.F. Chen, B.A. Klatt, Cartilage Regeneration [Internet] vol. 21, *Journal of the American Academy of Orthopaedic Surgeons*, 2013, p. 303. Available from, <http://www.ncbi.nlm.nih.gov/pubmed/23637149>.
- [47] C. Antich, J. de Vicente, G. Jiménez, C. Chocarro, E. Carrillo, E. Montañez, et al., Bio-inspired hydrogel composed of hyaluronic acid and alginate as a potential bioink for 3D bioprinting of articular cartilage engineering constructs [Internet], *Acta Biomater.* 106 (2020) 114–123, <https://doi.org/10.1016/j.actbio.2020.01.046>. Available from.
- [48] J.H. Gallarraga, M.Y. Kwon, J.A. Burdick, 3D bioprinting via an in situ crosslinking technique towards engineering cartilage tissue, *Sci. Rep.* 9 (1) (2019) 1–12.
- [49] S. Duchi, C. Onofrillo, C.D. O'Connell, R. Blanchard, C. Augustine, A.F. Quigley, et al., Handheld Co-Axial Bioprinting: application to in situ surgical cartilage repair, *Sci. Rep.* 7 (1) (2017) 1–12.
- [50] C.D. O'Connell, C. Di Bella, F. Thompson, C. Augustine, S. Beirne, R. Cornock, et al., Development of the Biopen: a handheld device for surgical printing of adipose stem cells at a chondral wound site [Internet], *Biofabrication* 8 (1) (2016) 0, <https://doi.org/10.1088/1758-5090/8/1/015019>. Available from.
- [51] L. Trachsel, C. Johnbosco, T. Lang, E.M. Benetti, M. Zenobi-Wong, Double-network hydrogels including enzymatically crosslinked poly-(2-alkyl-2-oxazoline)s for 3D bioprinting of cartilage-engineering constructs, *Biomacromolecules* 20 (12) (2019) 4502–4511.
- [52] N. Diamantides, C. Dugopolski, E. Blahut, S. Kennedy, L.J. Bonassar, High density cell seeding affects the rheology and printability of collagen bioinks, *Biofabrication* 11 (4) (2019).
- [53] T. Xu, K.W. Binder, M.Z. Albanna, D. Dice, W. Zhao, J.J. Yoo, et al., Hybrid printing of mechanically and biologically improved constructs for cartilage tissue engineering applications, *Biofabrication* 5 (1) (2013).
- [54] J. Idaszek, M. Costantini, T.A. Karslen, J. Jaroszewicz, C. Colosi, S. Testa, et al., 3D bioprinting of hydrogel constructs with cell and material gradients for the regeneration of full-thickness chondral defect using a microfluidic printing head, *Biofabrication* 11 (4) (2019).
- [55] A. Kosik-Kozioł, M. Costantini, A. Mróz, J. Idaszek, M. Heljak, J. Jaroszewicz, et al., 3D bioprinted hydrogel model incorporating β -tricalcium phosphate for calcified cartilage tissue engineering [Internet], *Biofabrication* 11 (3) (2019 May 3), 035016. Available from, <https://iopscience.iop.org/article/10.1088/1758-5090/ab15cb>.
- [56] K. Markstedt, A. Mantas, I. Tournier, H. Martínez Ávila, D. Hägg, P. Gatenholm, 3D bioprinting human chondrocytes with nanocellulose-alginate bioink for cartilage tissue engineering applications, *Biomacromolecules* 16 (5) (2015) 1489–1496.
- [57] S. Rathan, L. Dejob, R. Schipani, B. Haffner, M.E. Möbius, D.J. Kelly, Fiber reinforced cartilage ECM functionalized bioinks for functional cartilage tissue engineering, *Adv. Healthc. Mater.* 8 (7) (2019) 1–11.
- [58] R. Levato, W.R. Webb, I.A. Otto, A. Mensinga, Y. Zhang, M. van Rijen, et al., The bio in the ink: cartilage regeneration with bioprintable hydrogels and articular cartilage-derived progenitor cells [Internet], *Acta Biomater.* 61 (2017) 41–53, <https://doi.org/10.1016/j.actbio.2017.08.005>. Available from.
- [59] W. Zhu, H. Cui, B. Boudalam, F. Masood, E. Flynn, R.D. Rao, et al., 3D bioprinting mesenchymal stem cell-laden construct with core-shell nanospheres for cartilage tissue engineering, *Nanotechnology* 29 (18) (2018).
- [60] Q. Wang, Y. Huang, Z. Qian, Nanostructured surface modification to bone implants for bone regeneration, *J. Biomed. Nanotechnol.* 14 (4) (2018) 628–648.
- [61] T. Ahlfeld, F. Doberenz, D. Kilian, C. Vater, P. Korn, G. Lauer, et al., Bioprinting of mineralized constructs utilizing multichannel plotting of a self-setting calcium phosphate cement and a cell-laden bioink, *Biofabrication* 10 (4) (2018).
- [62] S.T. Bendtsen, S.P. Quinnell, M. Wei, Development of a novel alginate-polyvinyl alcohol-hydroxyapatite hydrogel for 3D bioprinting bone tissue engineered scaffolds, *J. Biomed. Mater. Res.* 105 (5) (2017) 1457–1468.
- [63] B. Byambaa, N. Annabi, K. Yue, G. Trujillo-de Santiago, M.M. Alvarez, W. Jia, et al., Bioprinted osteogenic and vasculogenic patterns for engineering 3D bone tissue, *Adv. Healthc. Mater.* 6 (16) (2017) 1–15.
- [64] D. Chimene, L. Miller, L.M. Cross, M.K. Jaiswal, I. Singh, A.K. Gaharwar, Nanoengineered osteoinductive bioink for 3D bioprinting bone tissue, *ACS Appl. Mater. Interfaces* 12 (14) (2020).
- [65] G. Cidonio, C.R. Alcalá-Orozco, K.S. Lim, M. Glinka, I. Mutreja, Y.H. Kim, et al., Osteogenic and angiogenic tissue formation in high fidelity nanocomposite Laponite-gelatin bioinks, *Biofabrication* 11 (3) (2019).
- [66] A.C. Daly, P. Pitacco, J. Nulty, G.M. Cunniffe, D.J. Kelly, 3D printed microchannel networks to direct vascularisation during endochondral bone repair [Internet], *Biomaterials* 162 (2018) 34–46, <https://doi.org/10.1016/j.biomaterials.2018.01.057>. Available from.
- [67] M. Neufurth, X. Wang, H.C. Schröder, Q. Feng, B. Diehl-Seifert, T. Ziebart, et al., Engineering a morphogenetically active hydrogel for bioprinting of bioartificial tissue derived from human osteoblast-like SaOS-2 cells, *Biomaterials* 35 (31) (2014) 8810–8819.
- [68] R. da Conceicao Ribeiro, D. Pal, A.M. Ferreira, P. Gentile, M. Benning, K. Dalgarno, Reactive jet impingement bioprinting of high cell density gels for bone microtissue fabrication [Internet], *Biofabrication* 11 (1) (2018 Dec 27), 015014. Available from, <https://iopscience.iop.org/article/10.1088/1758-5090/aaf625>.
- [69] D.F. Duarte Campos, A. Blaeser, K. Buellesbach, K.S. Sen, W. Xun, W. Tillmann, et al., Bioprinting organotypic hydrogels with improved mesenchymal stem cell remodeling and mineralization properties for bone tissue engineering, *Adv. Healthc. Mater.* 5 (11) (2016) 1336–1345.
- [70] G. Gao, T. Yonezawa, K. Hubbell, G. Dai, X. Cui, Inkjet-bioprinted acrylated peptides and PEG hydrogel with human mesenchymal stem cells promote robust bone and cartilage formation with minimal printhead clogging, *Biotechnol. J.* 10 (10) (2015) 1568–1577.
- [71] M.J. Sawkins, P. Mistry, B.N. Brown, K.M. Shakesheff, L.J. Bonassar, J. Yang, Cell and protein compatible 3D bioprinting of mechanically strong constructs for bone repair [Internet], *Biofabrication* 7 (3) (2015) 35004, <https://doi.org/10.1088/1758-5090/7/3/035004>. Available from.
- [72] M.A. Kuss, R. Harms, S. Wu, Y. Wang, J.B. Untrauer, M.A. Carlson, et al., Short-term hypoxic preconditioning promotes prevascularization in 3D bioprinted bone constructs with stromal vascular fraction derived cells, *RSC Adv.* 7 (47) (2017) 29312–29320.
- [73] J.L. Song, X.Y. Fu, A. Raza, N.A. Shen, Y.Q. Xue, H.J. Wang, et al., Enhancement of mechanical strength of TCP-alginate based bioprinted constructs, *J. Mech. Behav. Biomed. Mater.* (2020) 103, <https://doi.org/10.1016/j.jmbbm.2019.103533>. Available from.
- [74] B.F. Grogan, J.R. Hsu, Volumetric muscle loss [Internet], *Am. Acad. Orthop. Surg.* 19 (1) (2011 Feb) S35, 7. Available from, <http://content.wkhealth.com/linkback/openurl?sid=WKPILP:landingpage&an=00124635-201102001-00007>.
- [75] G. Cittadella Vigodarzere, S. Mantero, Skeletal muscle tissue engineering: strategies for volumetric constructs [Internet], *Front. Physiol.* 5 (2014 Sep 22) 362. Available from, <http://www.ncbi.nlm.nih.gov/pubmed/25295011>.
- [76] J.H. Kim, Y.J. Seol, I.K. Ko, H.W. Kang, Y.K. Lee, J.J. Yoo, et al., 3D bioprinted human skeletal muscle constructs for muscle function restoration [Internet], *Sci. Rep.* 8 (1) (2018) 1–15, <https://doi.org/10.1038/s41598-018-29968-5>. Available from.
- [77] Y.J. Choi, Y.J. Jun, D.Y. Kim, H.G. Yi, S.H. Chae, J. Kang, et al., A 3D cell printed muscle construct with tissue-derived bioink for the treatment of volumetric muscle loss [Internet], *Biomaterials* 206 (2019) 160, <https://doi.org/10.1016/j.biomaterials.2019.03.036>. Available from.
- [78] Y.J. Choi, T.G. Kim, J. Jeong, H.G. Yi, J.W. Park, W. Hwang, et al., 3D cell printing of functional skeletal muscle constructs using skeletal muscle-derived bioink, *Adv. Healthc. Mater.* 5 (20) (2016) 2636–2645.
- [79] J.H. Kim, I. Kim, Y.J. Seol, I.K. Ko, J.J. Yoo, A. Atala, et al., Neural cell integration into 3D bioprinted skeletal muscle constructs accelerates restoration of muscle function [Internet], *Nat. Commun.* 11 (1) (2020) 1–12, <https://doi.org/10.1038/s41467-020-14930-9>. Available from.
- [80] T.K. Merceron, M. Burt, Y.J. Seol, H.W. Kang, S.J. Lee, J.J. Yoo, et al., A 3D bioprinted complex structure for engineering the muscle-tendon unit [Internet], *Biofabrication* 7 (3) (2015) 35003, <https://doi.org/10.1088/1758-5090/7/3/035003>. Available from.
- [81] M. Costantini, S. Testa, P. Mozetic, A. Barbetta, C. Fuoco, E. Fornetti, et al., Microfluidic-enhanced 3D bioprinting of aligned myoblast-laden hydrogels leads to functionally organized myofibers in vitro and in vivo [Internet], *Biomaterials* 131 (2017) 98–110, <https://doi.org/10.1016/j.biomaterials.2017.03.026>. Available from.
- [82] M. Yeo, H. Lee, G.H. Kim, Combining a micro/nano-hierarchical scaffold with cell-printing of myoblasts induces cell alignment and differentiation favorable to skeletal muscle tissue regeneration [Internet], *Biofabrication* 8 (3) (2016) 1–12, <https://doi.org/10.1088/1758-5090/8/3/035021>. Available from.
- [83] A. García-Lizarribar, X. Fernández-Garibay, F. Velasco-Mallorquí, A.G. Castaño, J. Samitier, J. Ramon-Azcon, Composite biomaterials as long-lasting scaffolds for 3D bioprinting of highly aligned muscle tissue, *Macromol. Biosci.* 18 (10) (2018) 1–13.

- [84] C.K. Bektas, V. Hasirci, Cell loaded 3D bioprinted GelMA hydrogels for corneal stroma engineering, *Biomater. Sci.* 8 (2020).
- [85] A. Sorkio, L. Koch, L. Koivusalo, A. Deiwick, S. Miettinen, B. Chichkov, H. Skottman, Human stem cell based corneal tissue mimicking structures using laser-assisted 3D bioprinting and functional bioinks, *Biomaterials*, 2018, p. 171.
- [86] E. Goulart, L.C. Caires-Junior, K.A. Telles-Silva, B.H.S. Araújo, S.A. Rocco, M. Sforca, I.L. Sousa, G.S. Kobayashi, C.M. Musso, A.F. Assoni, D. Oliveira, E. Caldini, S. Raia, L.I. Lelkes, M. Zatz, 3D bioprinting of liver spheroids derived from human induced pluripotent stem cells sustain liver function and viability in vitro, *Biofabrication* 12 (1) (2020).
- [87] Y. Wu, A. Wenger, H. Golzar, X. Tang, 3D bioprinting of bicellular liver lobule-mimetic structures via microextrusion of cellulose nanocrystal-incorporated shear-thinning bioink, *Sci. Rep.* 10 (2020).
- [88] Q. Mao, Y. Wang, Y. Li, S. Juengpanich, W. Li, M. Chen, J. Yin, J. Fu, X. Cai, Fabrication of liver microtissue with liver decellularized extracellular matrix (dECM) bioink by digital light processing (DLP) bioprinting, *Mater. Sci. Eng. Part C* 109 (2020).
- [89] N. Noor, A. Shapira, R. Edri, I. Gal, L. Wertheim, T. Dvir, 3D printing of personalized thick and perfusable cardiac patches and hearts, *Adv. Sci.* 6 (11) (2019).